This is to certify that the

thesis entitled

Geometric Analysis and Kinematics of Folding
Associated with Overthrusting, Blue Ridge Province, Tennessee

presented by

William R. Sack

has been accepted towards fulfillment
of the requirements for

Masters degree in Geology

Major professor

Date Feb. 24th 1988

GEOMETRIC ANALYSIS AND KINEMATICS OF FOLDING ASSOCIATED WITH OVERTHRUSTING: BLUE RIDGE PROVINCE, TENNESSEE

By

William R. Sack

A THESIS

Submitted to
Michigan State University
in partial fulfillment of the requirements
for the degree of

MASTER OF SCIENCE

Department of Geological Sciences

1988

ABSTRACT

GEOMETRIC ANALYSIS AND KINEMATICS OF FOLDING ASSOCIATED WITH OVERTHRUSTING: BLUE RIDGE PROVINCE, TENNESSEE

By

William R. Sack

Mesoscopic structures within the Miller Cove Thrust sheet of the Southern Appalachian Blue Ridge Province record the superposition of simple shear upon preexisting folds during overthrusting. The succession of structures record a complex progressive deformation involving both folding and thrusting which is inconsistent with formation by a rigid ramp-flat thrust system. The geometric interrelations of mesoscopic structures (e.g., folds, faults, cleavage) were evaluated with respect to the kinematics predicted by various models of thrust or nappe sheet emplacement.

The geometries and succession of structures were studied along three cross-strike transects through the Miller Cove Thrust sheet. A transition exists from upright/open to inclined or overturned/close folds as a function of distance from minor thrusts. Structural successions are consistent with the modification of footwall structures by the superposition of a simple shear or transpressive deformation due to overthrusting. The observed variation in cleavage style across modified folds reflects the superposed strain. Observed microfabrics are interpreted to record the reuse of preexisting spaced cleavage as planes of shear to facilitate limb extension during fold modification.

ACKNOWLEDGMENTS

I would like to acknowledge and thank my advisor Bill Cambray for his guidance, encouragement, and patience during what proved to be a very rewarding experience. I have benefited greatly from his knowledge and expertise in both the classroom and the field. I will take with me much more than a degree.

I would also like to thank my committee members Duncan Sibley and Michael Velbel for their interest, advice, and critical review. I am indebted, as are many students in the department, to John Wilband for his assistance with computer software and the numerous program modifications he has provided. John is also to be commended for his uncanny ability to repeatedly locate and consume the last "barley malt" hidden in the bowels of our office refrigerator. I greatly appreciate the assistance provided by Loretta, Cathy, and Mona from the geology office and Diane from the library.

I acknowledge my fellow students in the department who have in one way or another contributed to my degree but will doubtfully read beyond these acknowledgments. Paul Carter, Dave Westjohn, and Bob Cuniff are thanked for their discussions on various aspects of structural geology, especially on the subjects of tube folds and field relationships. Jim Guentert is thanked both for his friendship and for sharing a common perspective on the time and effort expended while at MSU. Tim Flood, John Nelson, Jim Mills, Kim Elias, Mike and Beth Miller, Jerry and Laura Grantham, and many others are thanked for their friendship over the years.

I would also like to acknowledge those geologists I have had the pleasure of associating with along the way. Dennis Wood, John Diggins, Steve Matthews, Graham Potts, Sue Hippler, and an inexhaustible list of others have helped to provide for many unforgettable summers in Scotland. I am especially grateful to Dennis Wood of Robertson Research for his interest and assistance in my education. His enthusiastic and insightful discussions first sparked my interest in structural geology and have provided me with continued inspiration.

Research was made possible by a generous grant to study footwall deformation by Texaco, USA. Additional financial support for fieldwork was provided by MSU/Chevron grants. Rhonda Findley is thanked for her field assistance.

Finally, the sincere thanks I wish to extend to my parents, family, and friends in Minnesota is immeasurable. They have provided unending encouragement and unconditional love and support.

TABLE OF CONTENTS

Table of Contents (continued)

Table of Contents (continued)

List of Tables

LIST OF FIGURES

LIST OF FIGURES (continued)

LIST OF FIGURES (continued)

LIST OF FIGURES (continued)

LIST OF FIGURES (continued)

INTRODUCTION

Internal deformation of thrust and nappe sheets has largely been attributed to stress imposed during emplacement. Various models of structural development have been proposed to account for the geometry of observed structures. These models of deformation range from the more brittle ramping of thrust sheets characterized by hangingwall deformation to the more ductile shearing of nappe sheets involving both footwall and hangingwall deformation. Thrust sheet deformation, commonly in the form of open fold pairs, has been attributed to a relatively brittle response of the hangingwall to movement over footwall ramps and subsurface irregularities during emplacement (Boyer and Elliot 1982, Rich 1934). Nappe sheet deformation, characterized by recumbent/tight folding, has been related to the ductile shearing of the sheet during emplacement (Ramsay, et al., 1983; Sanderson, 1979).

In addition to these two basic models of deformation, polyphase or progressive deformation within thrust sheets can also be modeled. Such models consider the effect of thrust-related shear on preexisting structures. One such model, referred to here as the "modified ductile shear" model, involves buckling followed by thrusting which in turn imposes a ductile shear upon preexisting folds in the footwall of the thrust or nappe sheet. The modification of existing structures by simple shear has been addressed experimentally by Gosh (1966) and applied to field examples by Ellen (1976), Ramberg and Johnson (1976), Sanderson (1979), Lloyd and Whalley (1986).

Hypothesis:

This study will attempt to characterize the observed Taconic deformation, internal to the Miller Cove Thrust sheet within the Blue Ridge Province of Tennessee, and determine if it is consistent with the deformation predicted by one of the above models of thrust sheet deformation. The geometric interrelations of mesoscopic structures inherent in each of the three models allows them to be distinguished by structural analysis. If any of the three models are applicable to the study area, then the observed structural relationships should be consistent with those predicted by that model. In general these include;

(1) the geometric interrelations of mesoscopic and regional structures (e.g., fold, fault, and cleavage relationships),

(2) the succession or kinematics of structural development (e.g, fold-fault timing, refolding, timing of fabric development, and incremental strain history).

It is here proposed that ductile shearing in some form is largely responsible for the observed deformation in the Miller Cove thrust sheet. This is evident by both the rotation of mesoscopic fold axes and the decrease in axial plane dip and interlimb angles of these folds near the base of the thrust sheet. The structural relationships noted above are indicative of deformations involving a component of ductile shear (Lloyd and Whalley, 1986; Ramberg and Johnson, 1976; Sanderson, 1973, 1979; Williams, 1978).

It is further suggested in this study that the observed structures are most consistent with the modified ductile shear model involving the superposition of shear upon preexisting structures as depicted in Figure 1. It is proposed that on the mesoscopic scale an initial sub-horizontal layer-parallel shortening resulted in the formation of upright/open folds with an axial planar cleavage. Upon local overthrusting the folds nearest the thrusts were modified by a superposed simple shear resulting in the formation of overturned/close folds with a modified and fanned cleavage. This transition in fold style reflects a shear strain gradient which decreases with distance from the thrust.

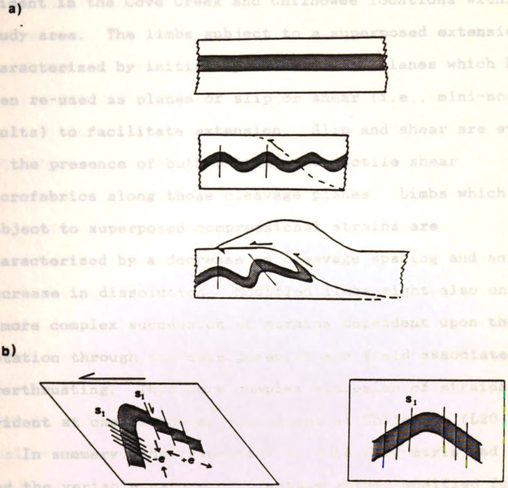

Figure 1. Sequence of events depicting the footwall modification of preexisting folds by ductile shear due to overthrusting,
b) Structural relationships observed within the Miller Cove thrust sheet (shear along cleavage due to superposed limb extension, decreased cleavage spacing due to superposed limb compression).

As depicted in Figure 1b, modified fold limbs can undergo a superposed extensional or compressional strain as evident in the Cove Creek and Chilhowee locations within the study area. The limbs subject to a superposed extension are characterized by initial spaced cleavage planes which have been re-used as planes of slip or shear (i.e., mini-normal faults) to facilitate extension. Slip and shear are evident by the presence of both brittle and ductile shear microfabrics along those cleavage planes. Limbs which are subject to superposed compressional strains are characterized by a decrease in cleavage spacing and an increase in dissolution. Modified limbs might also undergo a more complex succession of strains dependent upon their rotation through the superposed strain field associated with overthrusting. This more complex succesion of strains is evident at one of the sub-locations at Chilhowee (L20).

In summary, the transition in both fold style and trend, and the variable nature of cleavage across modified folds are consistent with the modification of preexisting structures by superposed shear. It is proposed that the mechanism of deformation for the Miller Cove thrust sheet is that of the modified ductile shear model. The models are discussed and evidence for superposed shear presented on the macroscopic to microscopic scale.

Models:

The following models outline the regional structural development associated with thrust or nappe sheet emplacement, in turn restricting the orientation and succession of mesoscopic structures.

(1) Rigid Thrust Sheet Ramping (Boyer and Elliot, 1982)

In this model, internal deformation is associated with the movement of a "rigid" thrust sheet along footwall ramps and flats. Hangingwall deformation is attributed to the gentle folding and unfolding of the hangingwall sheet as it moves over footwall ramps, flats, and irregularities on the underlying surface. A series of imbricated sheets may result from the development of a duplex system between roof and floor thrusts.

Duplex formation is a mechanism by which slip is transferred from one glide horizon at depth to another at a shallower level (see Fig. 2). As slip is transferred from one horizon to the next a portion of the major thrust is deactivated and rides passively within the growing thrust sheet. The new horse, the inactive portion of the major thrust, and the rest of the overlying thrust sheet are folded as they move into the ramp, and to some degree, unfolded as they move out of the ramp and onto the flat.

Hangingwall deformation is characterized by the gentle folding of entire sheets and in general produces little internal deformation. Ramp associated synform-antiform pairs are common. Additional deformation

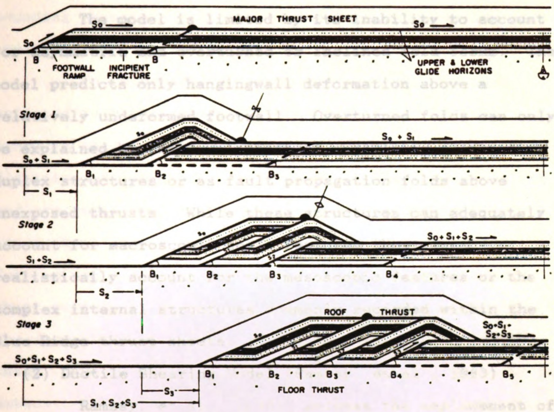

Figure 2. Rigid Ramping Model:

Geometric development of thrust sheets and duplex system. The thrust sheets undergo a series of folding and unfolding events (after Boyer and Elliot, 1982).

of similar style may result from the reactivation of thrusts or the formation of antiformal culminations due to variable horse length within a duplex system.

The model is limited by its inability to account for asymmetric and overturned or inclined fold forms. The model predicts only hangingwall deformation above a relatively undeformed footwall. Overturned folds can only be explained by the development of underlying culminating duplex structures or as fault propagation folds above unexposed thrusts. While these structures can adequately account for macroscopic scale features they cannot realistically account for the mesoscopic features or the complex internal structures commonly recorded within the Blue Ridge thrust sheets.

(2) Ductile Shearing Model (Ramsay, et al., 1983)

Ramsay, et al., (1983) address the emplacement of ductile nappe sheets and contrast the deformation to that of rigid thrust sheet ramping. With reference to the Helvetic Nappes of Europe, they attribute only minor amounts of deformation to ramping and suggest the majority of deformation is due to the ductile shearing of the nappe sheet during emplacement. They suggest some macroscopic folds, of low amplitude-wavelength ratio, develop due to ramping and are subsequently modified into asymmetric folds by simple shear. The formation of inclined asymmetric folds by simple shear sub-parallel to the enveloping surface of developing folds has been demonstrated by Gosh (1966).

Ramsay, et al., (1983) attribute the majority of mesoscopic folding to the effect of shortening and simple shear on bedding which is oblique to the nappe boundaries. These bounding thrusts act as shear zone boundaries during nappe emplacement (see Fig. 3a).

In this model the incremental strain ellipse is oriented such that the maximum shortening direction, λ_3, makes an angle of 45° with the shear zone boundary, in the direction of transport (see Fig. 3b). The folds initiate and are subsequently modified within this constant incremental strain field associated with simple shear. Contraction along competent layers obliquely inclined to the shear surface results in the formation of buckle folds. As the geometries of these folds are modified by continued shear, their limbs may rotate from the compressional to the extensional fields of the incremental strain ellipse for simple shear.

Once in the extensional field, the limbs will remain in that field for the duration of the deformation as they rotate towards the XY-plane of deformation. The resultant succession of structures is a function of the rotation of the fold limbs through the fields of strain and in this model is limited to compressional structures followed by extensional structures.

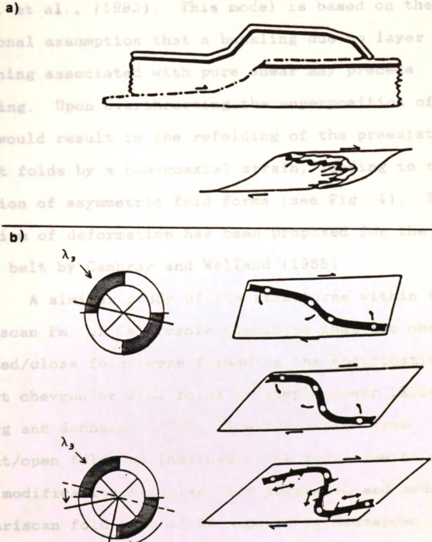

Figure 3. Ductile Shear Model:

a) Geometric development of nappe sheet.
b) Incremental strain history of developing folds. Fold limb rotation, from compressional field (shaded) to extensional field, is depicted within the associated incremental strain ellipse (after Ramsay et al., 1983).

(3) Modified Ductile Shear Model

This third model is a variation of that proposed by Ramsay, et al., (1983). This model is based on the additional assumption that a buckling due to layer parallel shortening associated with pure shear may precede thrusting. Upon overthrusting the superposition of simple shear would result in the refolding of the preexisting upright folds by a non-coaxial strain, leading to the formation of asymmetric fold forms (see Fig. 4). This mechanism of deformation has been proposed for the Ouachita thrust belt by Cambray and Welland (1985).

A similar study of the structures within the Fransiscan Fm. of California concluded that the observed inclined/close folds were formed by the modification of upright chevron or kink folds by simple shear (Ellen, 1976; Ramberg and Johnson, 1976). The transition from upright/open folds to inclined/close folds due to simple shear modification has also been suggested and modeled for the Variscan fold belt of SW England by Sanderson (1979) and Lloyd and Whalley (1986). This transition represents a decreasing shear strain gradient with distance from the thrust. Ramberg and Johnson (1976) have demonstrated experimentally that inclined/close folds can be produced by the passive rotation of fold limbs in response to the superposition of simple shear upon preexisting upright/open folds.

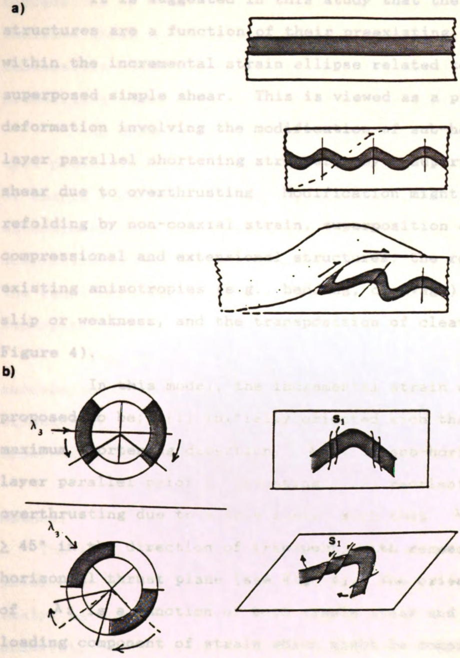

Figure 4. Modified Ductile Shear Model:

a) Geometric development of thrust or nappe sheet. Initial layer parallel shortening followed by the modification of existing structures by ductile shear upon overthrusting.
b) Incremental strain history marked by the superposition of a non-coaxial strain and fold modification.

It is suggested in this study that the resultant structures are a function of their preexisting orientations within the incremental strain ellipse related to the superposed simple shear. This is viewed as a progressive deformation involving the modification of sub-horizontal layer parallel shortening structures by a superposed simple shear due to overthrusting. Modification might include refolding by non-coaxial strain, superposition of compressional and extensional structures, the reuse of existing anisotropies (e.g., bedding, cleavage) as planes of slip or weakness, and the transposition of cleavage (see Figure 4).

In this model, the incremental strain ellipse is proposed to be; (1) initially oriented such that the maximum shortening direction, λ_3 , is sub-horizontal and layer parallel prior to thrusting; (2) reoriented upon overthrusting due to simple shear, such that λ_3 dips $\geq$ 45° in the direction of transport, with respect to a horizontal thrust plane (see Fig. 4). The orientation of λ_3 is a function of both simple shear and any loading component of strain which might be considered.

The kinematics predicted here differ from those predicted in the ductile shearing model in that the superposition of simple shear and the resultant succession of structures is a function of the orientation of the preexisting fold limbs with in the superposed strain field. While the ductile shearing model restricts the structural successions to compression followed by extension, the modified shear model allows for more complex structural successions which are dependent upon the orientation of the preexisting structures at the time of the superposed strain.

An example of the superposition of simple shear upon preexisting structures might include the superposition of simple shear upon first stage compressional and extensional structures resulting in second stage compressional and eventually extensional strains (Fig. 5). The reuse of preexisting structures to accommodate superposed strains during overthrusting is also predicted.

The modified ductile shear model predicts a complex succession of strains which is dependent upon the orientation of the preexisting structures within the superposed strain fields related to overthrusting.

Methods:

The aim of the study is to determine the geometric interrelations of mesoscopic structures by measuring and analyzing any available structural data and using these observations to determine the sequence of structural development. The orientation, succession, and type of observed structures (i.e., compressional vs extensional) are used to determine the kinematics of deformation on the mesoscopic scale.

Within the study area, footwall deformation in the form of modified folds is clearly evident. The modification of

Figure 5. Example of an incremental strain history predicted in Modified Ductile Shear model (Compressional strain fields shaded).

a) First stage compression followed by extension (folding followed by boudinage),
b) Left limb undergoes second stage compression followed by second extension (contractional folding followed by extensional faulting), Right limb undergoes second stage extension only.

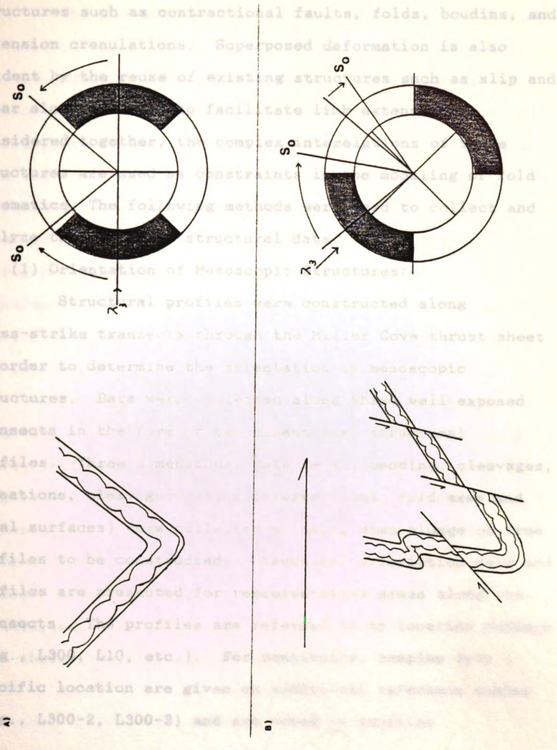
S_o
S_o
λ_3
S_o
S_o
λ_3
A
B

mesoscopic folds is recorded by the superposition of structures such as contractional faults, folds, boudins, and extension crenulations. Superposed deformation is also evident by the reuse of existing structures such as slip and shear along cleavage to facilitate limb extension. Considered together, the complex interelations of these structures are used as constraints in the modeling of fold kinematics. The following methods were used to collect and analyze the available structural data.

(1) Orientation of Mesoscopic Structures:

Structural profiles were constructed along cross-strike transects through the Miller Cove thrust sheet in order to determine the orientation of mesoscopic structures. Data were collected along three well exposed transects in the form of two dimensional structural profiles. Three dimensional data (e.g., bedding, cleavages, lineations, cleavage-bedding intersections, fold axes and axial surfaces) were collected allowing down-plunge or true profiles to be constructed. Structural orientation data and profiles are presented for representative areas along the transects. The profiles are referred to by location numbers (e.g., L300, L10, etc.). For continuity, samples from a specific location are given an additional reference number (e.g., L300-2, L300-3) and are noted on profiles.

(2) Succession of Structures:

The succession of local structures was determined and used to infer the kinematics of deformation for each profile locality. The superimposition of structures and fabrics were documented using both field relationships and petrographic analysis. Fabric development was determined from the analysis of oriented samples collected from representative structures along the transects. The reuse of cleavage planes during fold modification is evaluated by microfabric analysis. Techniques used in strain measurements varied depending upon available strain markers and are discussed in detail where used.

(3) Incremental Strain Ellipse:

Structural succession also provided information which was used to determine changes in the orientation of incremental strain fields as discussed by Ramsay (1967, Chapter 3). The succession and orientation of structures was used to interpret and restrict the orientations of inferred incremental strain axes. The orientations of deduced incremental strain ellipses are related to the style of deformation and can be judged consistent or inconsistent with those predicted in each model.

AREA OF STUDY

Regional Geologic Setting:

The Miller Cove thrust sheet is located in the Southern Appalachian Blue Ridge Province of Tennessee (see Fig. 6). This frontal portion of the Blue Ridge is dominated by complexly deformed thrust sheets of early Paleozoic (470-430mya) Taconic age which have later been transported up to 140km along major regional decollements during Alleghenian deformation (Witherspoon, 1981). The Alleghenian movements have emplaced the more internal Taconic thrust or nappe zone out on top of the more external Paleozoic sediments of the Valley and Ridge fold and thrust belt to the west. Structural windows within the Blue Ridge thrust sheets expose these Paleozoic sediments beneath a major decollement which is locally exposed as the Great Smoky Thrust.

Stratigraphic and structural relationships indicate the Great Smoky Thrust was active during both Taconic and early Alleghenian deformational events (Witherspoon, 1981). The Great Smoky Fault may have acted as a basal decollement or floor thrust to a major duplex system during Taconic deformation and been reactivated and possibly utilized as a

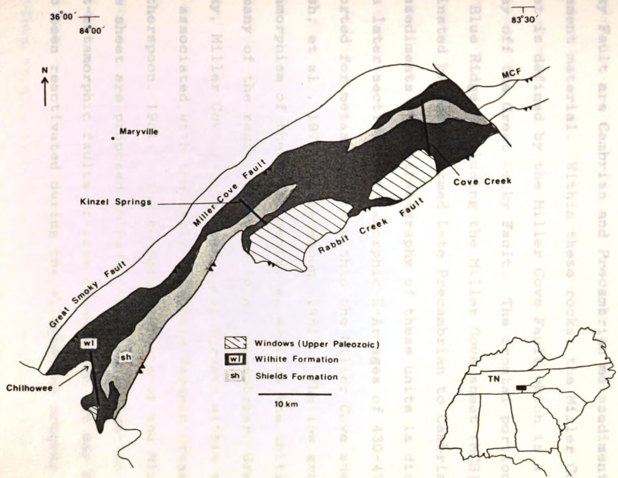

Figure 6. Geologic map of study area, location map inset (geology after Hadley and Nelson, 1971; Witherspoon, 1981). Transect localities noted.

regional roof thrust to the Valley and Ridge thrust system during early Alleghenian deformation.

Exposed to the east and structurally above the Great Smoky Fault are Cambrian and Precambrian metasediments and basement material. Within these rocks, the Miller Cove sheet is defined by the Miller Cove Fault which is a major splay off the Great Smoky Fault. The frontal portions of the Blue Ridge, including the Miller Cove sheet (MCS), are dominated by polydeformed Late Precambrian to Cambrian metasediments (the stratigraphy of these units is discussed in a later section). Metamorphic K-Ar ages of 430-470my are reported for metasediments within the Miller Cove sheet (Kish, et al., 1975; Witherspoon, 1981). The low grade metamorphism of these sediments, as well as the initiation of many of the regional faults (e.g., Greenbriar, Great Smoky, Miller Cove Faults) and minor thrusts within the MCS, are associated with the early Paleozoic Taconic Orogeny (Witherspoon, 1981). The bounding thrusts of the Miller Cove sheet are proposed to have initiated as syn- to post-metamorphic faults of late Taconic age but may have also been reactivated during the Alleghenian orogeny.

Regional Deformation:

The semi-ductile style of Taconic deformation which involved both folding and thrusting is the subject of this study. The structures reported within the study area by Witherspoon (1981) appear to be inconsistent with simple rigid ramping models of deformation. The inability of Witherspoon (1981) to accurately balance sections within this portion of the Blue Ridge attests to the structural complexity of the Taconic deformation. In contrast, the Alleghenian deformation in the Valley and Ridge Province has been shown to conform to a rigid ramping style of deformation in various studies (Harris, 1970; Milici, 1970; Rich, 1934; Witherspoon, 1981). The more ductile Taconic deformation recorded in the Blue Ridge Province must be viewed separately, in kinematic terms, from the later Alleghenian deformation.

Alleghanian deformation is recorded within the Miller Cove sheet by the macroscopic upwarping of the sheet in the areas marked by structural windows. These windows are the erosional expression of Alleghanian age duplex structures formed within the underlying Cambrian to Ordovician sediments. Based on earlier work (King, 1964; Livingston, 1977; Witherspoon, 1981) the Alleghenian deformation recorded within the MCS is restricted to the gentle bending of the sheet on a macroscopic scale and its effects are negligible on the mesoscopic scale.

This study attempts to document and model the style of Taconic deformation within this portion of the Blue Ridge Province. The polyphase deformation appears to record a progression in time and/or space from an internal nappe like deformation to an external fold and thrust belt deformation during a progression from Taconic to Alleghenian orogenic events.

Local Geologic Setting; Miller Cove Sheet:

The Miller Cove sheet is bound by the underlying Miller Cove Fault and the overlying Rabbit Creek Fault. In the study area it is physiographically delineated to the south by the trace of the Little Tennessee River and to the north by TN Hwy 341 (see Figure 6). The Miller Cove structural sheet may extend to the north of the Pigeon River fault which is interpreted to be a major SW dipping lateral ramp. The delineation of the sheet to the north is beyond the scope of this study but discussed by Witherspoon (1981).

Stratigraphy:

The regional Taconic thrust sheets are composed of Late Precambrian to Early Ordovician metasediments. The Miller Cove sheet is known to include Precambrian Ocoee Series strata and exposures are dominantly those of Walden Creek Group metasediments (King, 1961).

The Wilhite Formation of the Walden Creek Group is dominated by a thick member of dark interbedded calcareous siltstones and slates. The formation also includes thinner members of coarse sandstones, pebble conglomerates, limestones. The Wilhite Formation is a minimum of 1100m thick in the Miller Cove sheet and up to 3000m thick in overlying thrust sheets (King 1964; King, et al., 1968; Neuman and Nelson, 1965; Witherspoon, 1981).

The Wilhite Formation is overlain by the coarser, less calcareous feldspathic sandstones and siltstones of the Sandsuck Formation which is a minimum of 1100m thick in the Richardson Cove area to the northwest (Witherspoon, 1981). Underlying the Wilhite is the 700m thick Shields Formation which is dominated by coarse sandstones and conglomerates, but which also contains laminated siltstones and slates similar to that of the Wilhite Formation. Exposures within the Miller Cove sheet are dominated by the Wilhite Formation.

Structural Setting:

The Miller Cove sheet is dominated by a major sub-horizontal anticline whose axial trace trends approximately N60E (see Figure 6). Bedding attitudes of Witherspoon (1981), stratigraphic boundary assignments of Hadley and Nelson (1971), and fold envelopes determined in this study define a major northwest facing asymmetric anticline. The shallow SE dipping limb of the anticline dominates the eastern exposures of the sheet while the steep NW dipping limb near the base of the thrust sheet fills the western portion of the study area.

This macroscopic fold is inferred by Witherspoon (1981) to be of syn-metamorphic Taconic age based on the presence of associated metamorphic foliations. The limbs of this fold contain mesoscopic second- and third-order folds which are commonly cut by numerous minor thrust faults.

These folds with sub-axial planar foliations are also interpreted as broadly syn-metamorphic in age. The minor thrusts which cut and modify the folds and metamorphic foliations are proposed to be relatively late-stage Taconic structures based on their near-fold-concordent NE-SW trends.

Mesoscopic fold axes show an ordered variation in orientation from ENE to NNE from the upper portions to the base of the thrust sheet (Figure 7). This variation from regional trend is proposed to reflect the rotation of fold axes during modification by simple shear as demonstrated by Sanderson (1973) and Rattey and Sanderson (1982).

Structural Nomenclature:

FOLDS

In general mesoscopic folding is transitional from upright/open to overturned/close. Upright folds will be referred to as "unmodified" or F_1 folds and inclined or overturned folds as "modified" or F_2 folds. Although the subscripts change, the "later" refolding (F_2) is best described in terms of fold modification during a single progressive deformation as opposed to two separate unrelated stages of deformation. F_2 folds are characterized by the reuse of F_1 hinge lines resulting in the modification of upright/open folds into inclined/close folds about the same axis. In some cases fold modification has resulted in the formation of a new hinge line which is parallel to but non-coincidental with the existing F_1 hinge. This folding

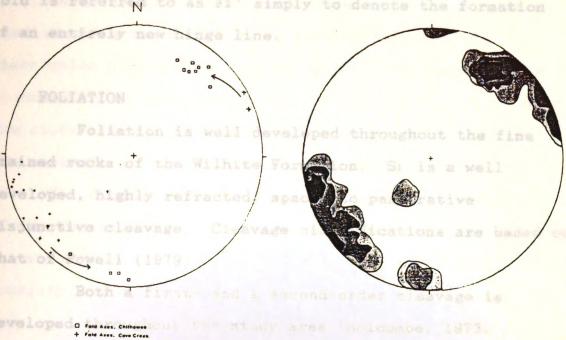

+ Fold Axes, Cove Creek Transect
□ Fold Axes, Chilhowee Transect

Figure 7. a) Equal-area projection of mesoscopic F_1 and F_2 fold axes within the Miller Cove sheet (30 total). Proposed axes rotations depicted by arrows. b) Contoured plot of fold axis data depicting partial girdle. Contour intervals of 2%, 6%, 12%, and 20%.

results in the rolling of that F_1 hinge to a point along one of the limbs of the new fold. Where this occurs the new fold is referred to as F_2' simply to denote the formation of an entirely new hinge line.

FOLIATION

Foliation is well developed throughout the fine grained rocks of the Wilhite Formation. S_1 is a well developed, highly refracted, spaced to penetrative disjunctive cleavage. Cleavage classifications are based on that of Powell (1979).

Both a first- and a second-order cleavage is developed throughout the study area (Holcombe, 1973; Witherspoon, 1981). The first order cleavage, S_{1p}, is a weak anastomosing disjunctive cleavage spaced on the order of grain size. While S_{1p} is strongly developed and highly refracted in fine grained units, it is weak to absent and shows little sign of refraction in coarser siltstone units.

S_{1p} is defined by the presence of fine opaque insoluble residue films and the preferred orientation of white mica and quartz growths (i.e. beards) between detrital grains. Holcombe (1973) mapped chemical distributions across S_{1p} cleavage films and found them enriched in K, Al, and Ti with respect to the adjacent material. They are depleted in Si, Ca, and Mn, indicating the removal of quartz and ankerite. This suggests cleavage was formed by a process involving a component of solution transfer.

The second order spaced cleavage, S_{1sp}, is a zonal to discrete crenulation cleavage, spaced on the order of 0.5cm to 2.5cm. In the study area, S_{1sp} zones commonly consists of a concentration of very closely spaced dissolution planes or a zone of ductile deformation bound by a concentration of discrete dissolution planes. Throughout the study area S_{1sp} is present but the internal fabric of the cleavage is highly variable (see Figures 19, 22, 32, and 34). The variable nature of S_{1sp} appears to be a function of the degree of fold modification at each locality. The nature of S_{1sp} will be described separately for each locality throughout the study area.

A clearly defined S_2 fabric is not present although a weak fabric appears incipient in some F_2 folds. A late stage extension crenulation cleavage associated with fold modification deforms both bedding and S_1 and is referred to here as S*.

Structural Transects:

Mesoscopic structures were examined along three transects which expose various portions of the major anticline (Figure 6). The northernmost transect is the "Cove Creek transect" which runs along TN Hwy 341 to the NW of Wears Cove. Exposed along it are the mesoscopic folds which define the gently SE dipping limb of the macroscopic anticline. The southernmost transect is located along TN Hwy 72 and the banks of the Little Tennessee River and is referred to as the "Chilhowee transect". Exposed along it is the steeply NW dipping limb of the anticline. A central transect located west of Tuckaleechee Cove along TN Hwy 73 near Kinzel Springs also exposes upright folds on the southeast limb of the anticline and is referred to as the "Kinzel Springs transect". The use of the Kinzel Springs transect, with respect to Taconic deformation, is limited due to the presence of intense Alleghenian deformation in that area. Mesoscopic structures are described for each transect in the following sections.

Northeast Transect; Cove Creek:

Geologic Setting:

The Cove Creek transect exposes the northern portion of the MCS and the shallow SE dipping limb of the macroscopic anticline. The regional transect extends along Hwy 341 from the Happy Hollow Fault northwest for some 3 miles to Walden Creek and the Miller Cove Fault (Figure 6). The transect is sub-perpendicular to the trend of mesoscopic folds and faults, and consists of nearly continuous outcrop. This portion of the sheet is dominated by the interbedded siltstones and mudstones of the Wilhite Formation beneath the Happy Hollow Fault which brings up the underlying Shields Formation.

Figure 8 is a schematic structural profile of the Cove Creek Cascades area which is presented as a representative portion of this transect along its SE end. The upright to overturned mesoscopic folds along the transect form an enveloping surface which dips gently to the SE. A structural profile at location 300 (L300) from the center of the Cascades profile is shown in Figure 9. The profile is nearly perpendicular to local mesoscopic fold axis which are sub-horizontal and trend approximately 260°.

Mesoscopic Structures: (Location L300)

The dominant mesoscopic structures are sub-horizontal upright/open to overturned/close folds. Structural orientation data from the profile is plotted

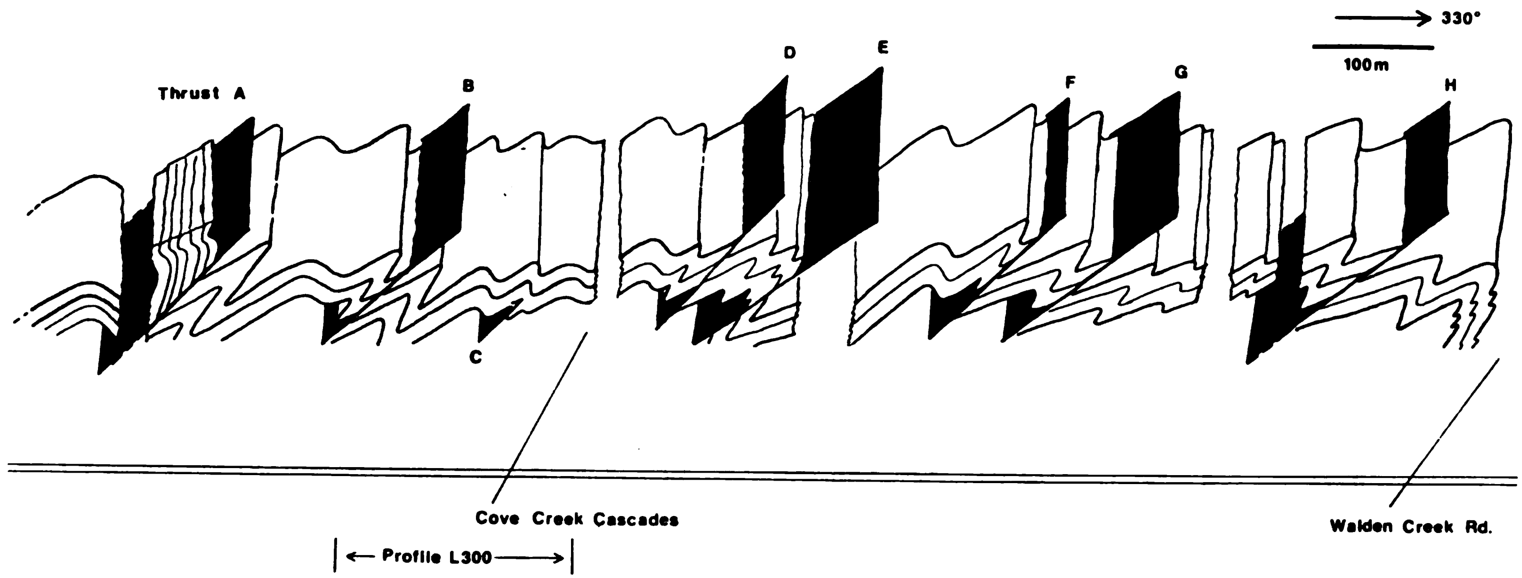

Figure 8. Schematic profile of Cove Creek transect (minor thrusts shaded).

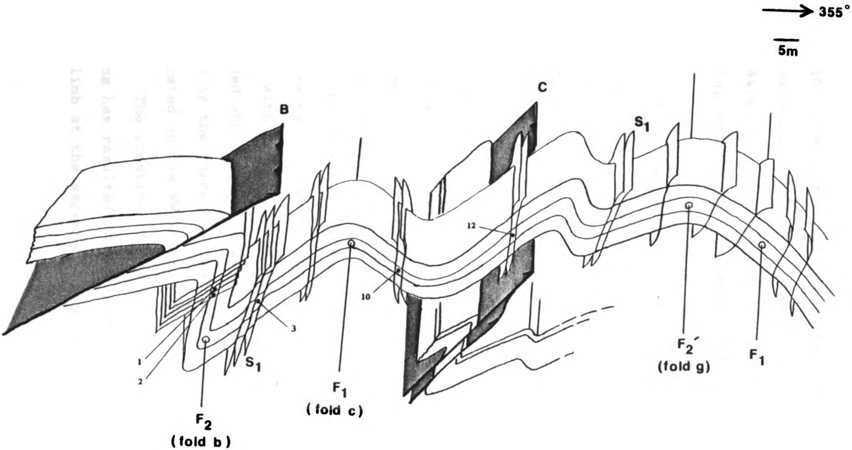

Figure 9. a) 3-D structural profile of location L300 along the Cove Creek transect. Sample locations numbered.

in Figure 10. Local mesoscopic fold axes are sub-horizontal, trend approximately 260°, and range in wavelength from 10m to 100m. Axial plane dips range from 90° to 45°, and interlimb angles from 140° in unmodified F_1 folds to 30° in modified F_2 folds (see Figure 11). Minor thrust faults strike 250°, dip moderately to gently towards the south, and are spaced on the order of 150m. Offsets along such faults range from a few centimeters to more than several meters. One such thrust (thrust C, Figure 9) shows offset of ~0.5m which quickly decreases to zero within less than 10m and eventually dies out into the core of an asymmetric fault propogation fold.

A transition exists between upright/open F_1 folds and inclined/close F_2 folds (Figure 9). Cleavage appears axial planar to unmodified F_1 folds. In F_1 folds the refraction and offset along bedding planes of early extension veins oriented at high angles to bedding are consistent with flexural slip type folding. In F_2' folds, S_1 is folded about a new hinge line and the old F_1 hinge is defined by the change in the refraction direction of S_1 and is located on the NW limb of the F_2' folds (fold "g", Figure 9). The location of the old hinge indicates that the F_2' folding has resulted in the growth of the overturned or steep limb at the expense of the upright limb.

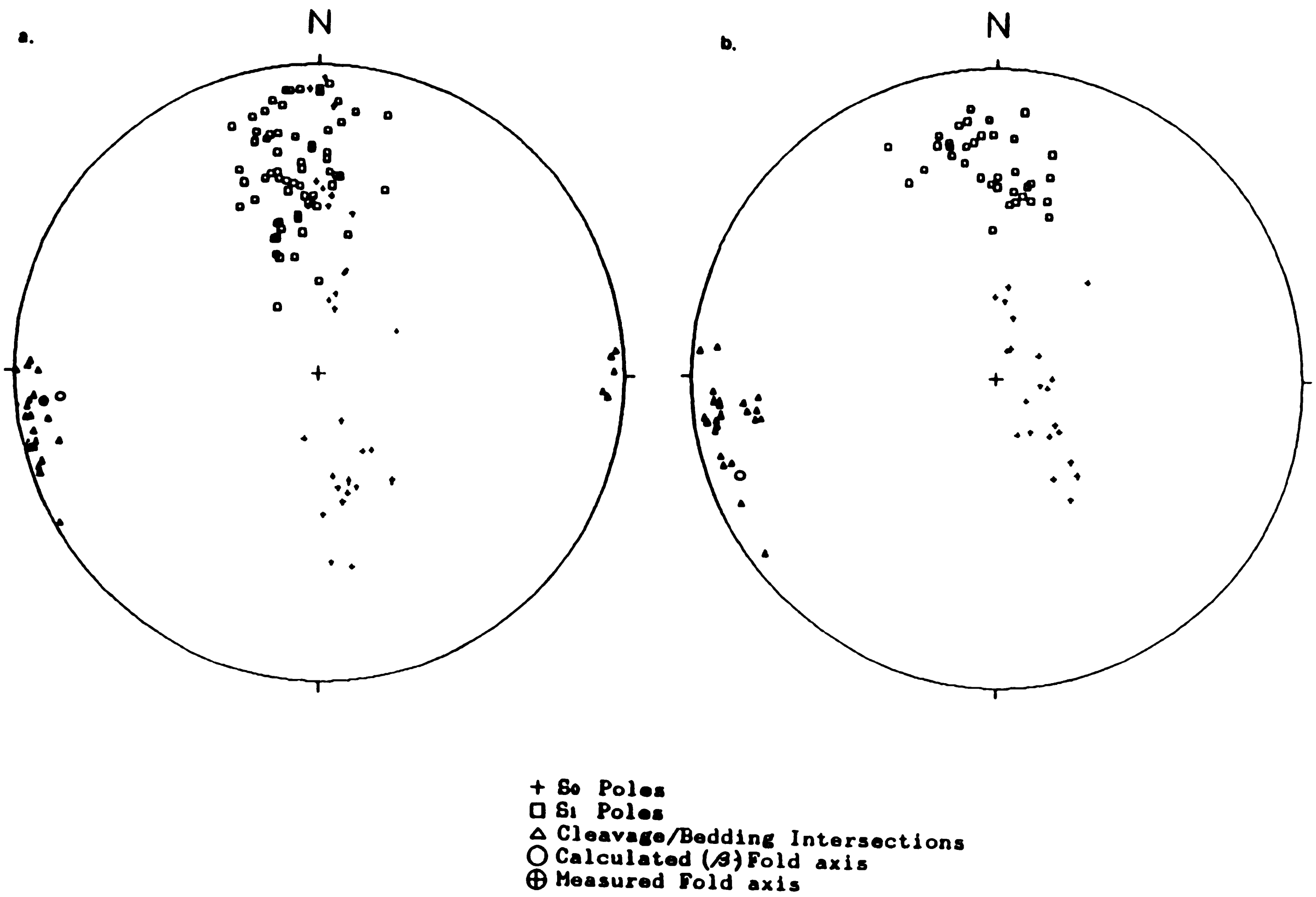

Figure 10. Equal-area lower hemisphere projections of mesoscopic structural data for location L300.
a) F_2 data (fold "b", L300),
b) $F_{2'}$ data (fold "g", L300).

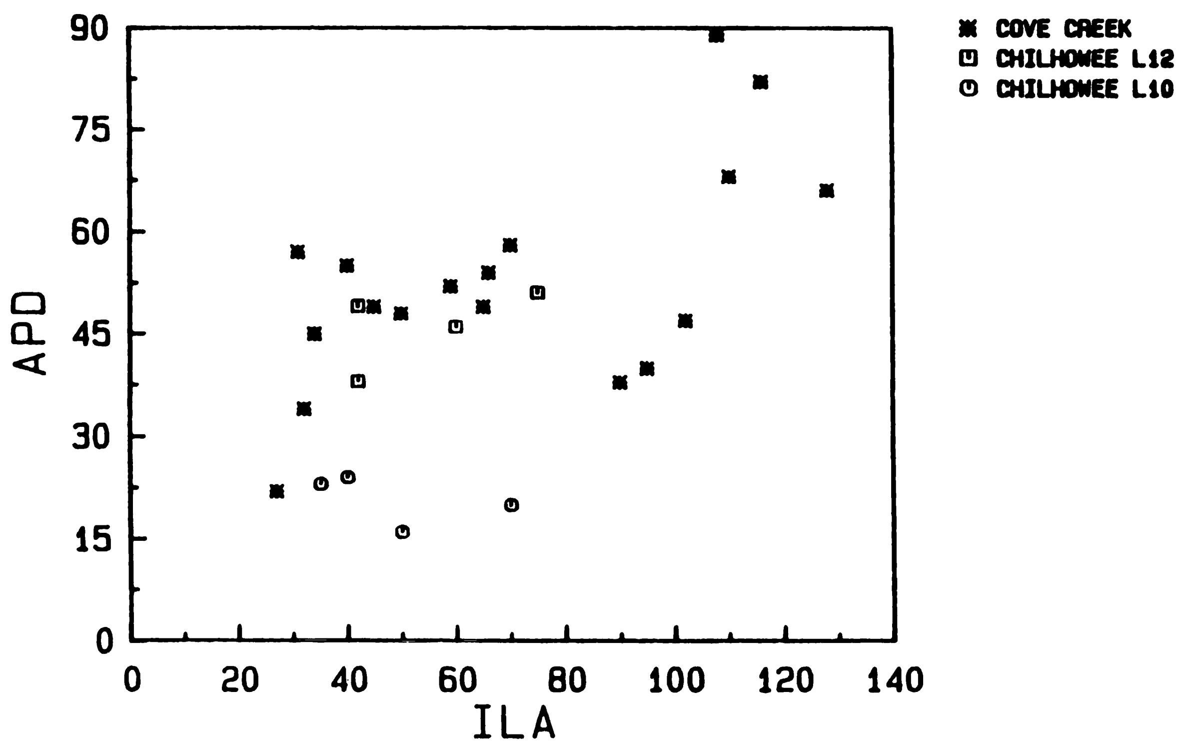

Figure 11. Plot of Axial Plane Dip vs Interlimb Angle for mesoscopic folds in the Miller Cove sheet.

Foliation:

Along L300, S_{1p} is defined by weak anastomosing insoluble residue films spaced on the order of grain size. S_{1sp} is defined by a concentration of S_{1p} films defining zones 1mm-3mm wide. In hand specimens S_{1sp} appears as dark bands located along micro folds or offsets in bedding (see Figure 12). The microfolds commonly demonstrate the offset of bedding (S_0) across S_{1sp} planes. It is proposed that the offset of S_0 across S_{1sp} is accomplished by an actual slip and ductile shear across the cleavage zone during fold modification rather than simply by an apparent displacement due solution transfer mechanisms during cleavage formation. Evidence for this includes sheared and displaced porphyroblasts within the cleavage zones. These features are evaluated and discussed in the later section on microfabrics, and the mesoscopic variation in cleavage orientation and style is discussed below.

S_{1sp} Cleavage Variation:

S_{1sp} is a weakly developed zonal crenulation cleavage in unmodified regions and a strongly developed zonal to discrete crenulation cleavage in modified regions. Within unmodified F_1 folds, S_{1sp} is near axial planar and little or no offset of S_0 across S_{1sp} is evident.

In F_2 folds, S_{1sp} becomes strongly developed and convergently fanned (see fold "b" in L300, Figure 9). The mean cleavage spacing decreases to 0.5cm on the overturned limb of fold "b" as compared to a mean

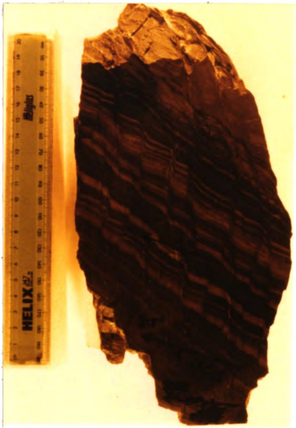

Figure 12. Photograph of hand specimen from location L300.

spacing of 2.3cm within the same units on the shallow right limb (see Figure 13). Offset of S_0 across S_{1sp} is nearly undetectable on the overturned limb of fold "b" but pronounced on the shallow limb. Offset is related to shear along S_{1sp} and is here evident by locally offset and thinned bedding S_0 across the cleavage zone, sheared mica "fish", and deformed calcite "porphyroblasts" (Figure 14). These structures are evaluated in detail in the later section on microfabrics.

S_{1sp} is proposed to have initially formed as a refracted spaced cleavage, axial planar to F_1 folds. S_{1sp} is deflected and folded within thrust plane slip zones indicating a pre-thrust formation. Shear, slip, and offset along S_{1sp} zones are proposed to be associated with the modification of structures due to the formation of local thrust or shear zones.

In general, the nature of S_1 within F_2' folds is variable. Although S_{1sp} is clearly developed, the penetrative S_{1p} is the dominant foliation. In fold "g" (Figure 9), normal offset of S_0 across S_{1sp} (i.e., extending S_0) occurs on the shallow SE limb but both normal and reverse offsets are apparent on the steep NW limb. This may reflect the complex rolling or unfolding of the preexisting hinge during fold modification.

In addition, the following evidence suggests complex deformation of the rolled section of this F_2' fold. The portion of the F_2' limb which has been unfolded

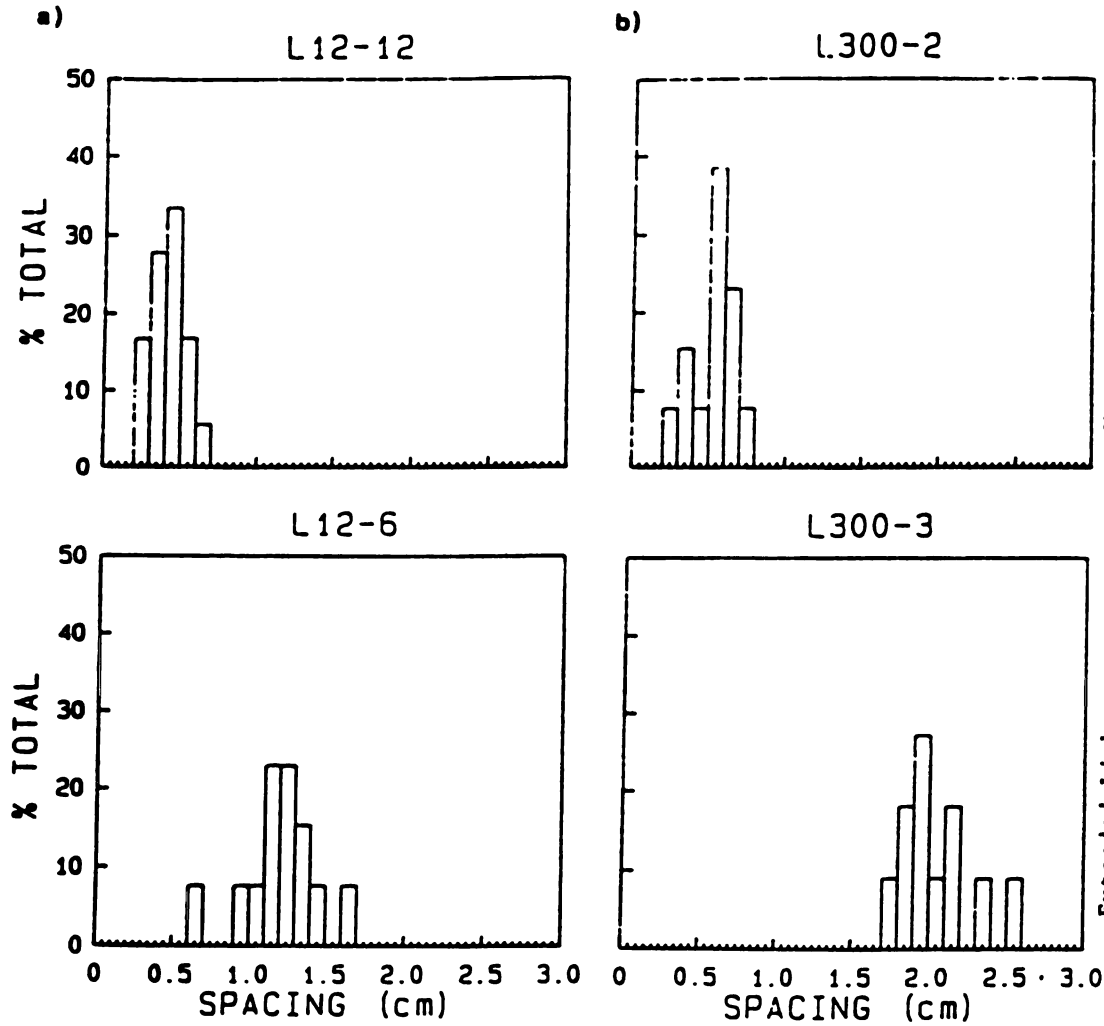

Figure 13. Histogram plot of cleavge spacing across folds. a) Location L12. b) Location L300, fold "b"

a)

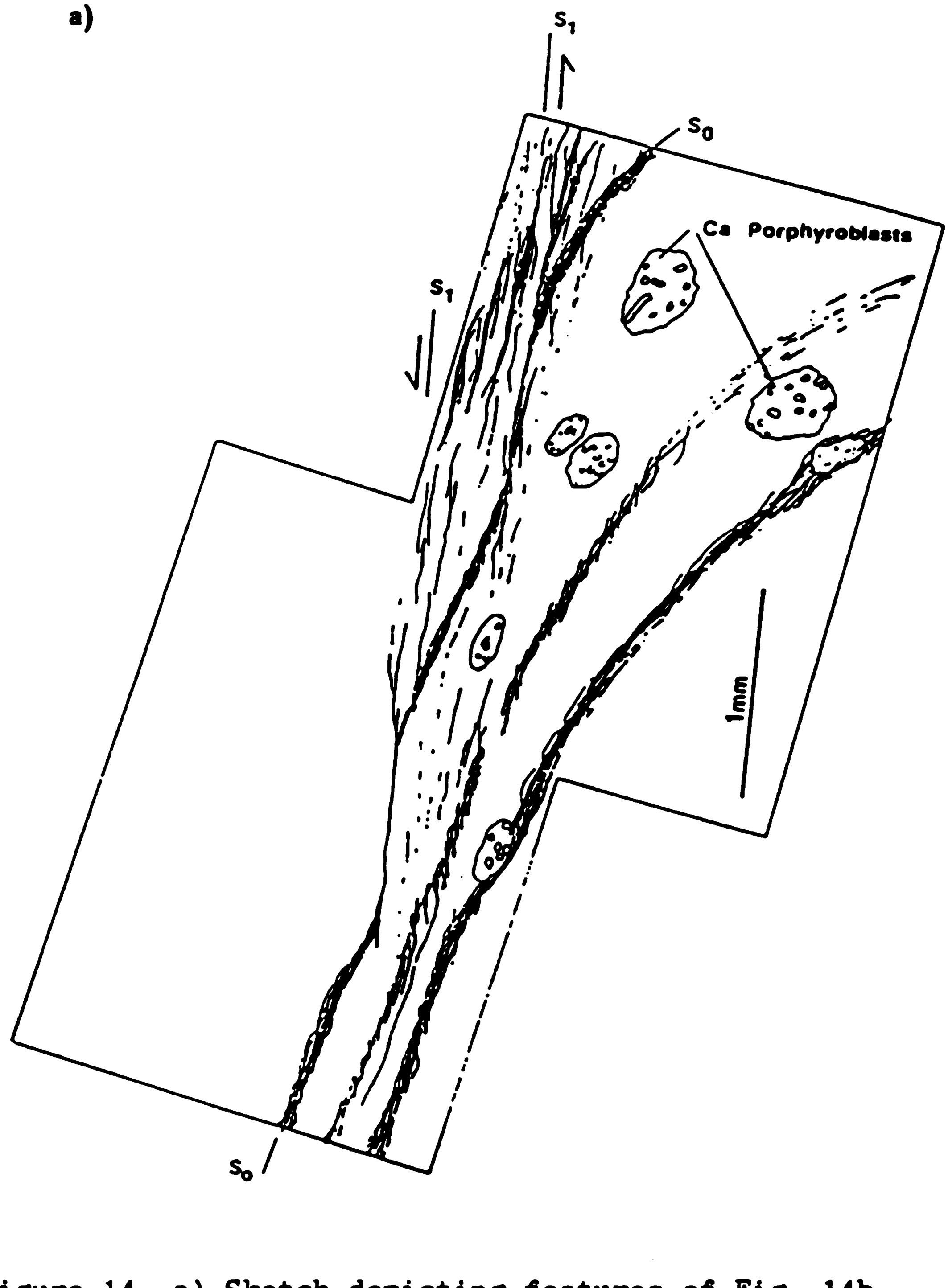

Figure 14. a) Sketch depicting features of Fig. 14b.
b) Photomicrographs of deflected bedding and sheared calcite porphyroblasts across S_{1sp} zone (sample L300-3). Scale bar = 1mm.

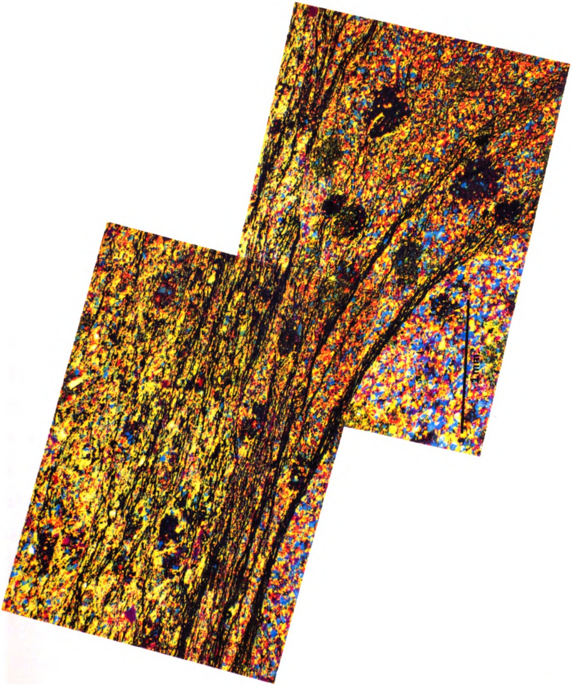

Figure 14.

and/or rolled through the new hinge contains refracted extension veins at high angles to bedding. These veins are refracted with a sense of dextral shear and are consistent with formation by flexural shear during initial F_1 folding. In addition, these same veins record a post-refraction sinistral offset along bedding planes due to flexural slip. This sinistral component of offset recorded on the rolled section of the fold is consistent with the modification of that limb by sinistral flexural slip along bedding during F_2' folding.

Succession of Structures:

Upright/open F_1 folds, with axial planar, penetrative to spaced S_1 cleavage, represent the earliest formed and unmodified folds observed in the MCS. F_1 is commonly modified to form inclined/close F_2 folds with fanned S_1 planes. S_{1sp} planes, where modified, are often planes of shear or slip, reflecting extension or compression of the fold limbs. In some locations folds with entirely new hinge lines are formed by the modification of F_1 folds along new fold axis (fold "g", Figure 9). These F_2' folds are marked by the broad open folding of S_1 planes. It is proposed that the modification of F_1 folds is spatially related to the formation and propagation of local thrust or shear planes.

Discussion of L300:

Transitions from upright/open to inclined/close folds along the section appear to be related to local thrusting. This is apparent when the axial plane dip (APD) of each fold and the location of local thrust planes are plotted with respect to distance along the transect, as shown in Figure 15a. From the figure it is apparent that the orientation of the folds are a function of the distance from each thrust plane. This may reflect modification of upright folds by simple shear (Ramberg and Johnson, 1976; Sanderson, 1979; Lloyd and Whalley, 1986) and the transition thus reflect a shear strain gradient. The possible shear strain gradient is calculated in Appendix B, and the resultant gradient is shown in Figure 15b.

In summary, F_1 folds are defined by upright/open folds which show no signs of modification. F_2 folding is defined by the non-coaxial modification of upright/open folds to inclined/close folds with reused hinge lines and fanned cleavage. F_2' folding is characterized by the broad open folding of S_1 around new hinge lines. Fold modification appears to be a function of distance from thrust planes and can be described by a shear gradient suggesting modification by a mechanism of simple shear. The evaluation of fold modification with respect to the various models of deformation will be addressed in the kinematic interpretation section.

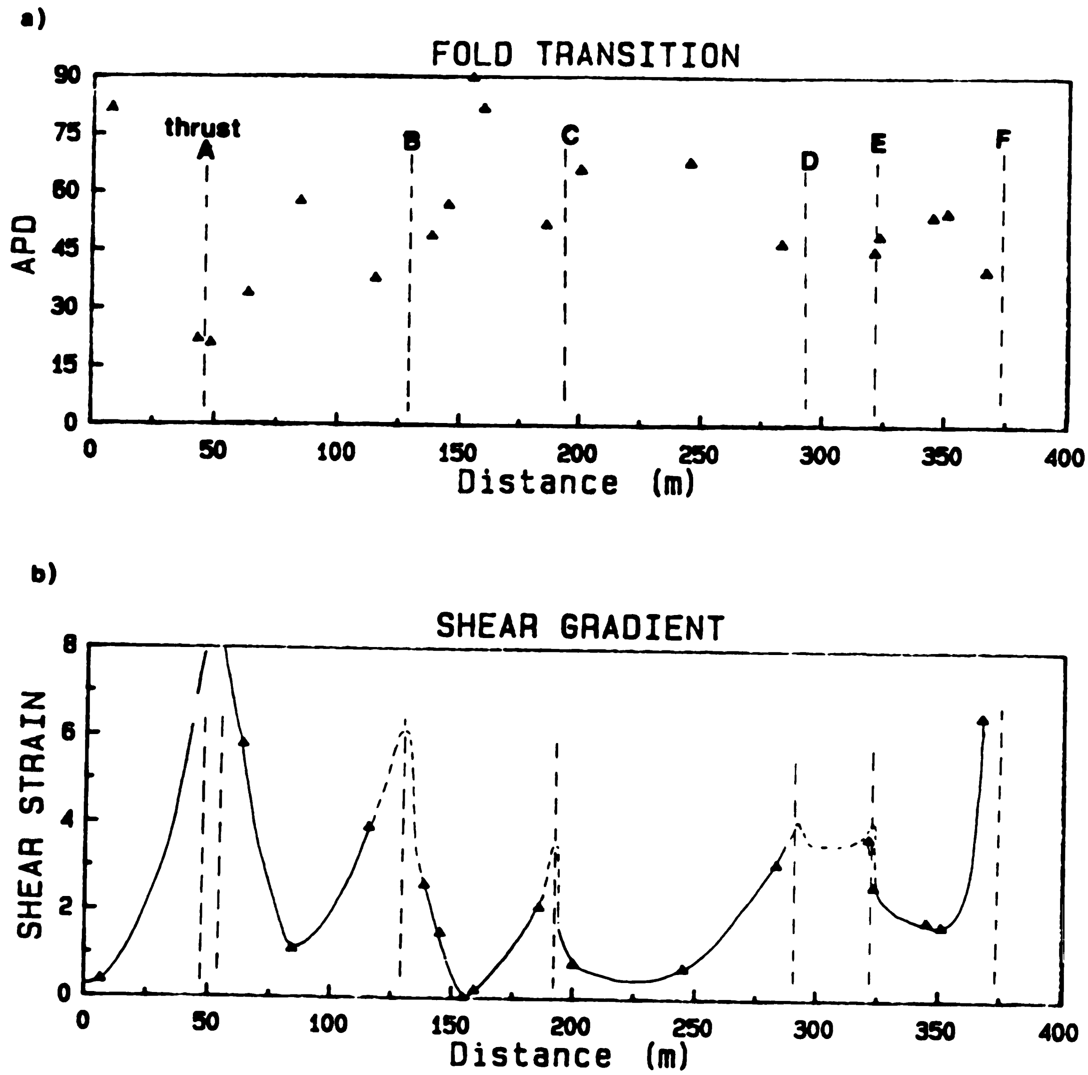

Figure 15. a) Transition of APD with distance along Cove Creek transect.
b) Derived shear strain gradient (see Appendix B).

Southern Transect; Chilhowee:

Geologic Setting:

The regional transect along the Little Tennessee River extends along Hwy 72 from the Calderwood Window northwest to the Miller Cove Fault for some 2 miles with nearly complete exposure (see Figure 6). The regional transect is taken from Livingston (1977) with modifications (see Figure 16). Structural profiles of representative structures were constructed and their locations along the transect are shown in Figures 6 and 16. The Wilhite Formation fills nearly the entire southwest portion of the sheet as the steeply NW dipping limb of the major anticline. Small inliers of the underlying Shields Formation mapped by King (1961), and Hadley and Nelson (1971) mark minor thrust faulting or parasitic folding on this limb.

Mesoscopic hinge lines on this steep limb are sub-horizontal and trend between 008° and 040° notably oblique to regional trend (see Figure 7). Axial planes dip gently to the SE and interlimb angles define close to tight folds (Figure 11). Minor SE dipping thrusts and NW dipping backthrusts are also present. The amount of offset along most thrusts is undetermined due to the lack of sufficient marker beds but movement is indicated by the deflection and offset of cleavage and appears to range upward from a few meters. As in the northern transect, early folds (F_1) with axial planar cleavage (S_1) are modified by local thrust

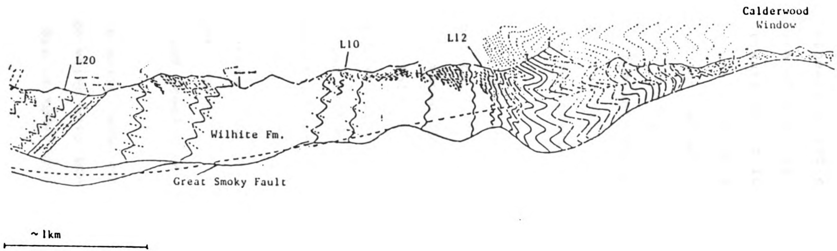

Figure 16. Schematic crossection along Chilhowee transect demonstrating steeply dipping fold envelope (from Livingston, 1977). Profile locations noted.

faults. The style of folding (i.e., tight to close) recorded along the transect appears to reflect the high strains expected near the base of a thrust sheet (Wojtal, 1983). The more N-S trending orientation of fold axes compared to those of the Cove Creek transect, which are located in the upper portion of the sheet, may reflect the rotation of fold axes due to high strains at the base of the sheet or at a lateral ramp or surge zone. The interrelations of faults, folds, and fabrics are discussed for each of the profile localities (L10, L12, L20) along the transect.

L10:

Mesoscopic Structures:

The profile, shown in Figure 17, is representative of the numerous tight fold trains whose enveloping surfaces delineate the steep limbs of second order folds on the steeply dipping NW limb of the macroscopic anticline. The basic structural data for the L10 profile are plotted in Figure 18. These F_2 folds are near recumbent with small interlimb angles. Axial plane dips range from 15° to 25°, and interlimb angles from 35° to 67° (Figure 11). Fold axes are sub-horizontal and trend approximately 008°.

Foliation:

S_1 is once again developed as both a penetrative and spaced cleavage which dips gently to the SE and is commonly fanned. S_{1p} is again defined by the preferred

Figure 17. True structural profile, location L10.
Sample locations numbered.

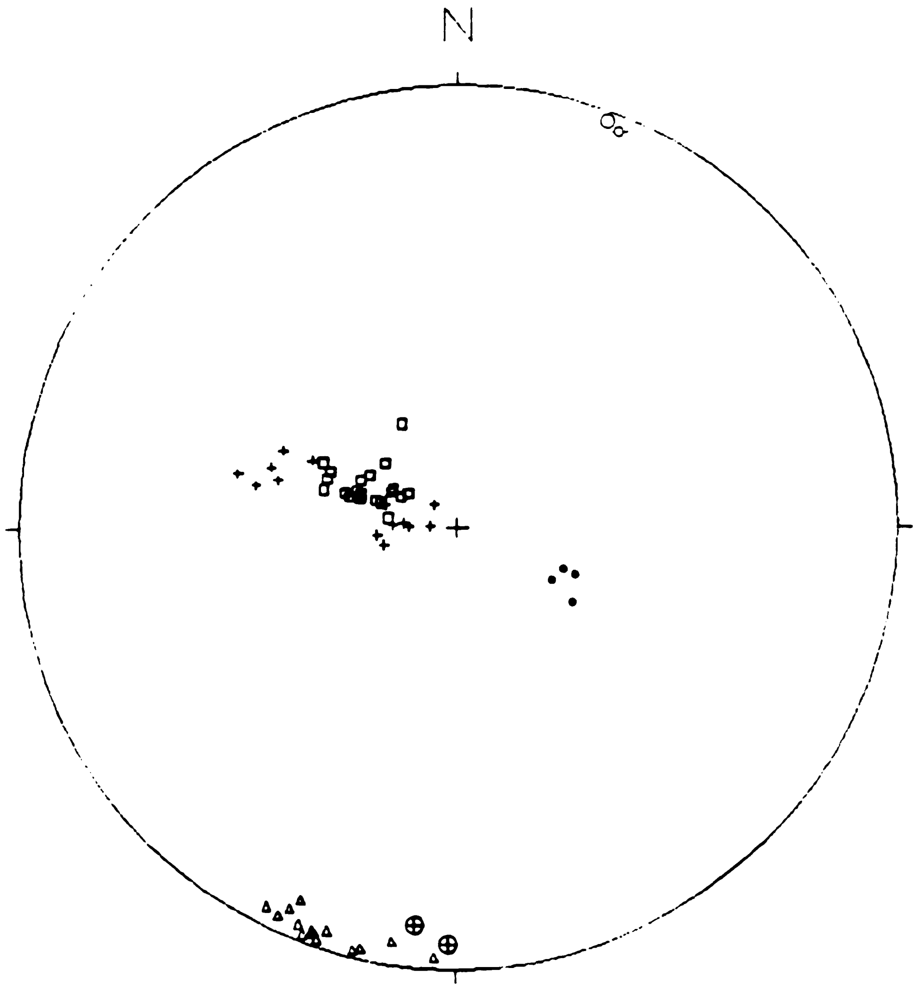

+ S_0 Poles (15)
□ S_1 Poles (22)
△ Cleavage/Bedding Intersections (15)
● S_* Poles (4)
○ Calculated F_2 axis
⊕ Measured F_2 axis

Figure 18. Equal-area lower hemisphere projection of mesoscopic structural data for location L10.

orientation of weak anastomosing insoluble residue films and the formation of mica and quartz beards. S_{1sp} is a spaced zonal cleavage with zonal boundaries defined by a high concentration of dissolution films. S_{1sp} is very strongly developed, zones are up to 2mm wide and are commonly spaced on the order of 5mm. Bedding is again offset across S_{1sp} zones.

S_{1sp} zonal fabric is extremely complex. The zonal nature is defined by an internal fabric, consisting of irregular planar surfaces of opaque material which cut obliquely across the zone (see Figure 19a). These planes form a fabric similar to that described by Platt (1984) as extension crenulation cleavage or "ecc" (see Figure 19b). Internal to the S_{1sp} zones, S_{1p} is evident by the presence of quartz and mica beards but is transected and deformed by these microscopic extension crenulations. The extension crenulations everywhere dip to the NW, regardless of the apparent sense of shear suggested by the offset of bedding across the cleavage zone. This is true on both limbs of the fold in the profile.

The formation of extension crenulations can be associated with the extension of the foliation during the progressive deformation of fabric internal to a shear zone. The shear zone is here defined by the S_{1sp} zone boundaries and shear might be reflected in the offset of bedding. Alternatively the crenulations may be related to a continued flattening in the plane of the developing foliation with no a)

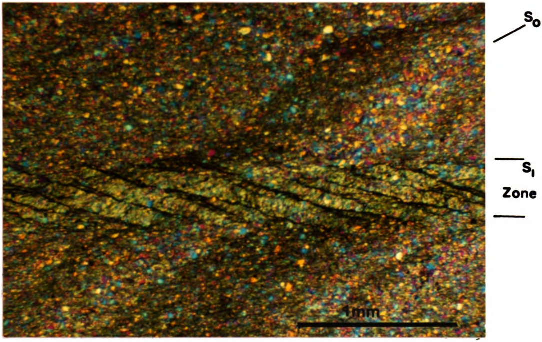

b)

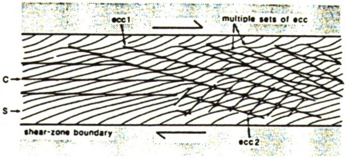

Figure 19. a) Photomicrograph of extension crenulation subfabric within S_{1sp} cleavage zones (L10-1). b) Extension crenulation geometry (Platt, 1984).

component of shear involved. These fabrics indicate the modification of cleavage during the latest stages of cleavage formation possibly related to a superposed shear or flattening of the fold.

A mesoscopic extension crenulation cleavage, here referred to as S*, is also present. S* dips to the NW and its formation marks the extension of both S_{1sp} and S_0 (see Figure 17). The orientation and offset directions of the extension crenulation, S*, are consistent with the extension of the shallow dipping fold limb and its cleavage planes during the relatively late stages of the deformation.

Succession of Structures: (L10)

The proposed succession of structures includes the initial F_1 folding and the development of an axial planar S_{1sp} cleavage which has been fanned during F_2 fold modification. The involvement of S_{1sp} in fold modification appears to be recorded in the development of a microscopic extension crenulation fabric internal to the cleavage zones. It remains undetermined whether these fabrics indicate extreme flattening or shear. The formation of mesoscopic S* extension crenulations during fold modification is also evident.

L12:

Mesoscopic Structures:

The profile in Figure 20 is representative of the less commonly observed upright folds whose fold envelopes define the shallow limb of a second order fold on the macroscopic anticline.

Structural data are plotted in Figure 21. Measured fold axes are sub-horizontal and trend approximately 040°. The average axial plane dip is 50° with interlimb angles of 35° to 80° (Figure 11). A minor thrust is present and dips ~50° to the SE. Offset along the fault is speculative due to the monotonous nature of the finely interbedded units but appears to be on the order of one to several meters and no more than 10 meters. A backthrust is also present and dips ~30° to the NW. Backthrust movement of several meters is indicated by the deflection and folding of S_1 and S_0 as depicted in the L12 profile (Figure 20).

The main anticlinal F_2 fold in the profile is treated in detail. The overturned limb dips approximately 79° to the SE and faces the NW and the upright shallow limb dips approximately 15° to the SE.

Foliation:

S_{1p} and S_{1sp} are both well developed across the fold. S_{1sp} is once again defined as a zonal to discrete cleavage made up of numerous residue films. Offset of S_0 across S_{1sp} is common on the overturned limb but not observed on the shallow limb. As seen in the Cove Creek

Figure 20. a) 3-D structural profile of location L12.
Sample locations numbered.
b) True structural profile of L12.

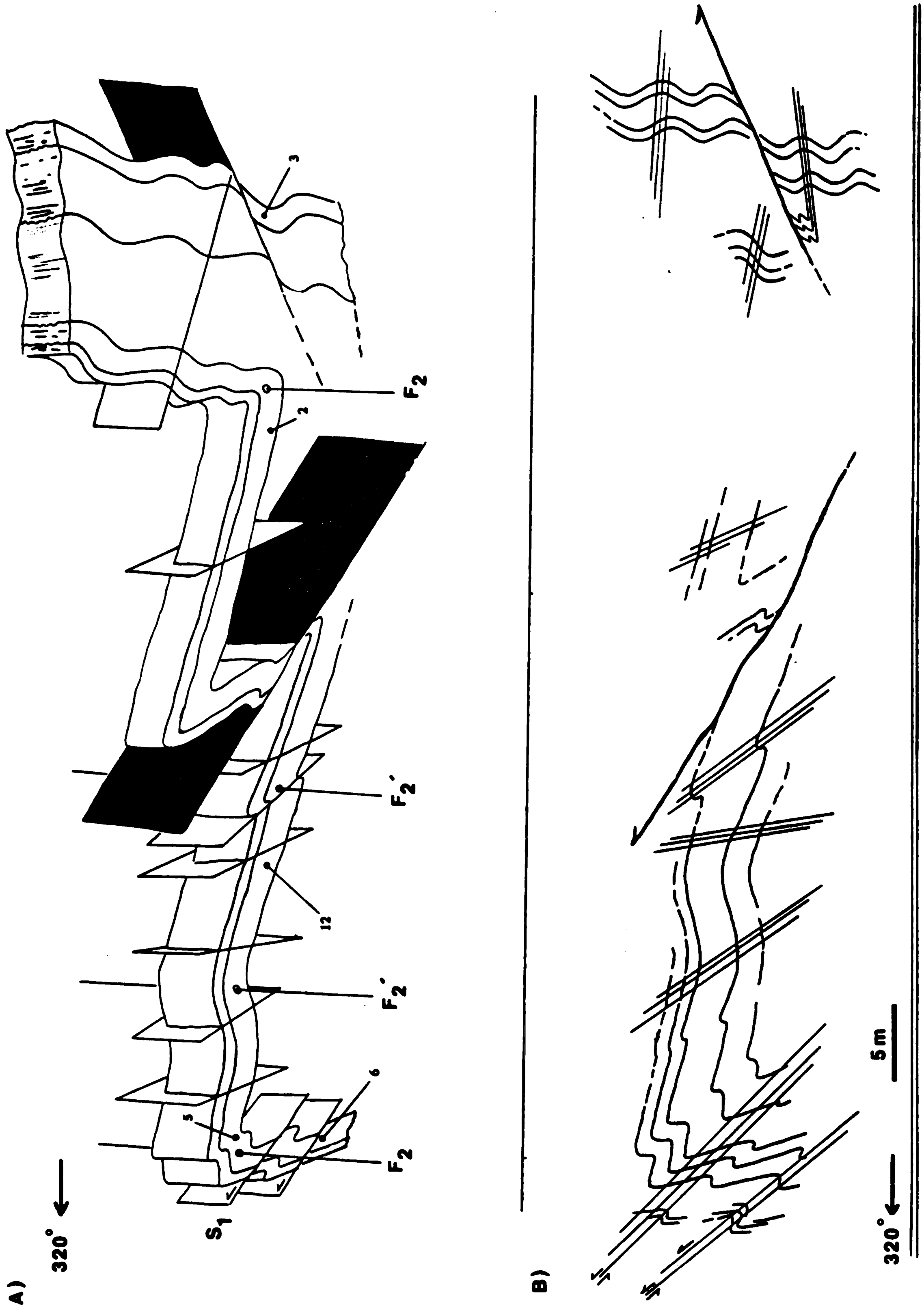

Figure 20.

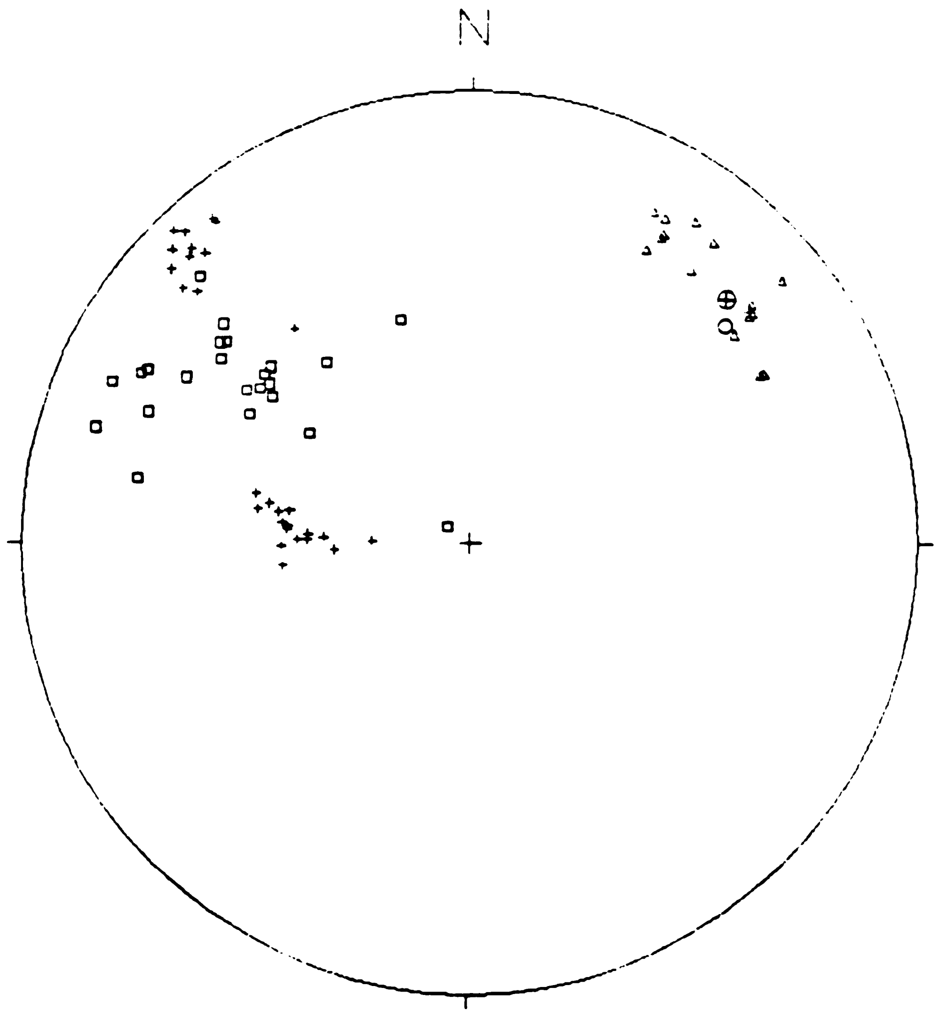

+ S_0 Poles (30)
□ S_1 Poles (23)
△ Cleavage/Bedding Intersections (18)
○ Calculated F_2 axis (β-axis)
⊕ Measured F_2 axis

Figure 21. Equal-area lower hemisphere projection of structural data for location L12.

profile, discrete S_{1sp} planes are commonly the site of shear and slip resulting in the offset of S_0. It is proposed that the offset of S_0 across S_{1sp} is most commonly accomplished by slip along discrete planes or by ductile shear offset across zonal cleavage.

Ductile shear is recorded by the deflection of fabric elements across cleavage zones. Elongate quartz grains define a recrystallized fabric which is asymptotically deflected into cleavage zones at a low to moderate angle, consistent with formation by ductile shear. In addition, bedding is also deflected and thinned as it enters the cleavage zones.

Slip is indicated by fibrous growths and slickensides present on S_{1sp} planes. Slip directions inferred from slickenside surfaces are consistent with offset directions of S_0 across S_{1sp} planes and nearly perpendicular to the F_2 axis (Figure 21). In cross section these appear as stepped fibre growths or micro pull-apart structures (Figure 22a) with step orientations consistent with slip directions indicated by offset bedding (Figure 22b). The fabrics mentioned above are evaluated in detail in the later section on microfabrics.

Offset of S_0 has effectively extended the length of the overturned limb. The shallow limb shows no sign of extension by slip along S_{1sp} but instead records additional shortening. Shortening of this limb is evident by the formation of F_2 folds which fold S_{1sp} and S_0 into

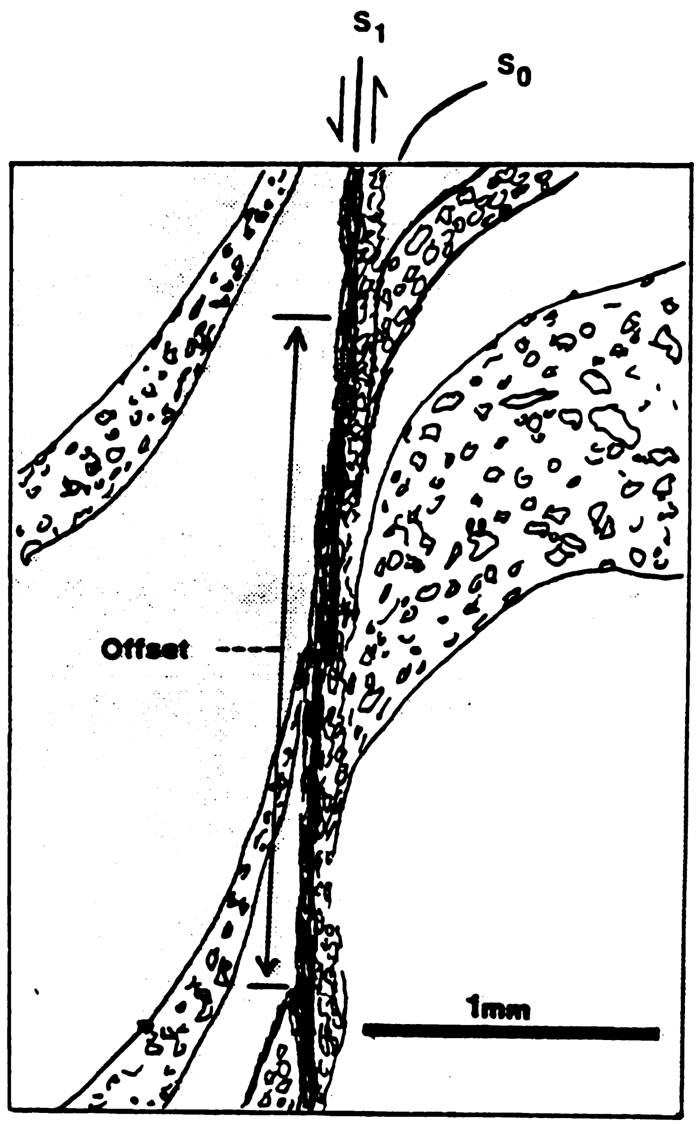

Figure 22a. Photomicrograph (facing page) and sketch of bedding deflection and offset across S_{1sp} cleavage plane (sample L12-6). Scale bar = 1mm.

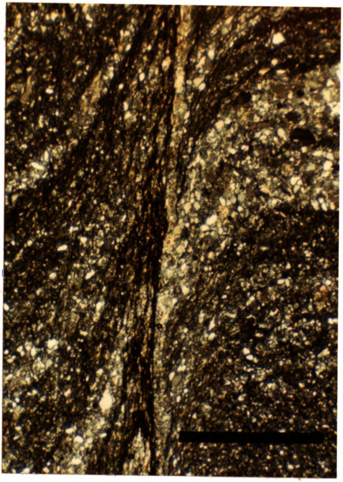

Figure 22a.

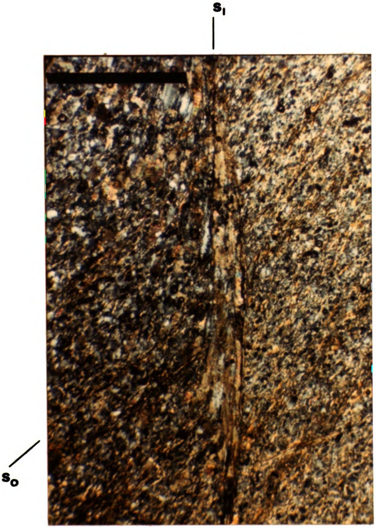

Figure 22b. Photomicrograph of micro pull-apart structure along S_{1sp} recording bedding offset (sample L12-6). Scale bar = 1mm.

gentle upright folds (see Figure 20). Shortening is also accomplished by a decrease in S_{1sp} spacing from 1.2cm on the overturned limb to 0.4cm on the shallow limb (Figure 13).

Succession of Structures: (L12)

F_2 folding at locality L12 appears to be the result of the modification of an initial F_1 fold with axial planar S_{1sp} cleavage. S_{1sp} has since been fanned by continued fold tightening. This modification is also recorded in the F_2' folding of S_0 and S_{1sp} along the shallow limb and the extension of S_0 on the overturned limb accomplished by shear across S_{1sp} cleavage planes.

L20:

Mesoscopic Structure:

Figure 23 is a schematic profile of the NW end of the transect. These overturned units dip approximately 50° to the SE and represent the overturned limb of a first- or second-order fold. A younging direction which indicates overturned beds is indicated by graded bedding and cross ripple erosional surfaces. A large thrust fault surface crops out structurally above the overturned strata approximately 150m to the SE and dips approximately 32° to the SE. Deflection of S_1 indicates an offset to the NW which post-dates cleavage formation.

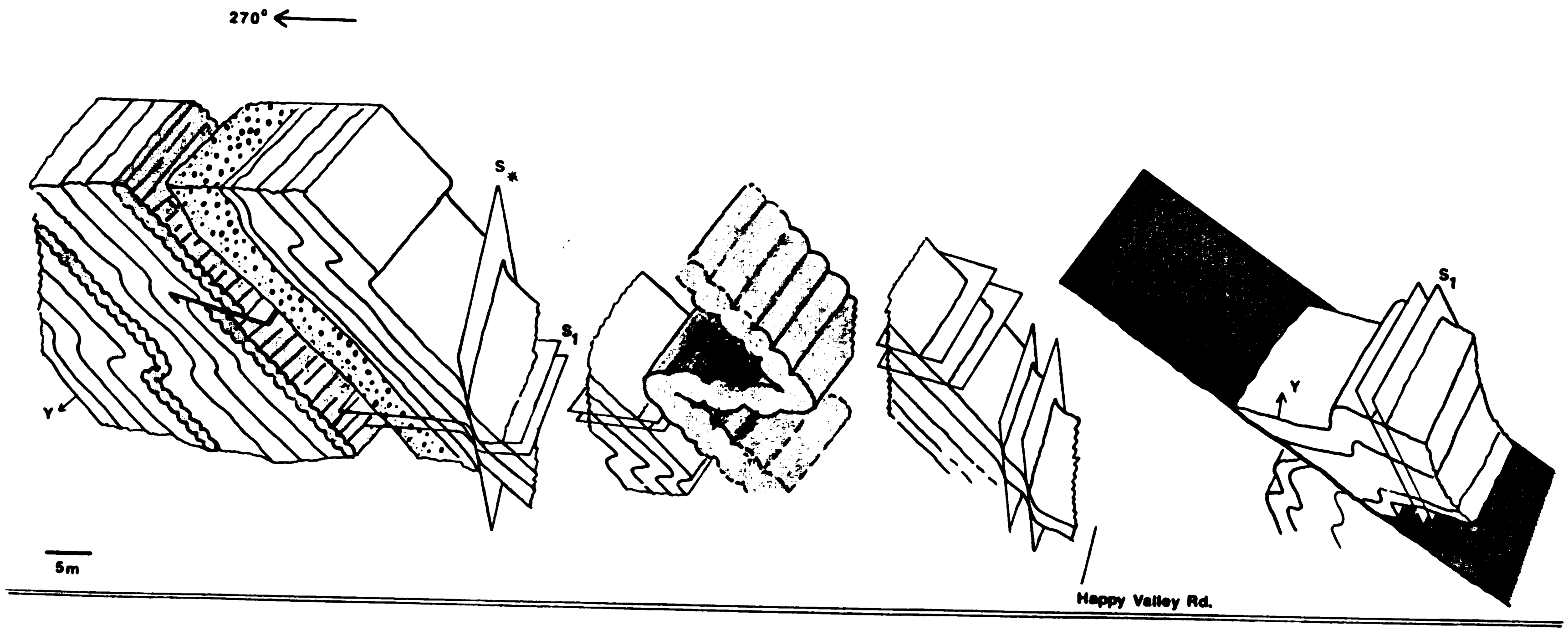

Figure 23. Schematic profile of location L20.

Structural data are plotted in Figure 24. S_1 is a penetrative to spaced cleavage which is commonly refracted, consistent with flexural shear folding. Local minor folds trend approximately 040°. Offset of S_0 across S_1 is nowhere observed, although it would not be easily identified in these slaty units. Thin (<30cm) carbonate layers are commonly boudinaged. Cleavage appears to be deflected and folded into boudin necks suggesting post-cleavage formation. Boudin long axes roughly parallel the fold axis (Figure 24). These boudined layers are folded and cut by minor contractional faults. Large extension crenulations, S*, with crosscutting extensional veins are also present in slaty units and cut both bedding and cleavage indicating a post S_1 formation. Their relative timing with respect to other structures is unclear.

Succession of Structures: (L20)

The interrelation of structures indicates the formation of S_1 during the initial F_1 folding. This folding was followed by or accompanied with the boudinage of more competent carbonate layers during extensional deformation of the limb, possibly during the late stages of the initial folding. These boudined units were then folded and faulted in response to a superposed shortening of the limb. It is proposed that this shortening is related to a superposed deformation associated with fold modification and F_2 folding due to overthrusting along the observed fault

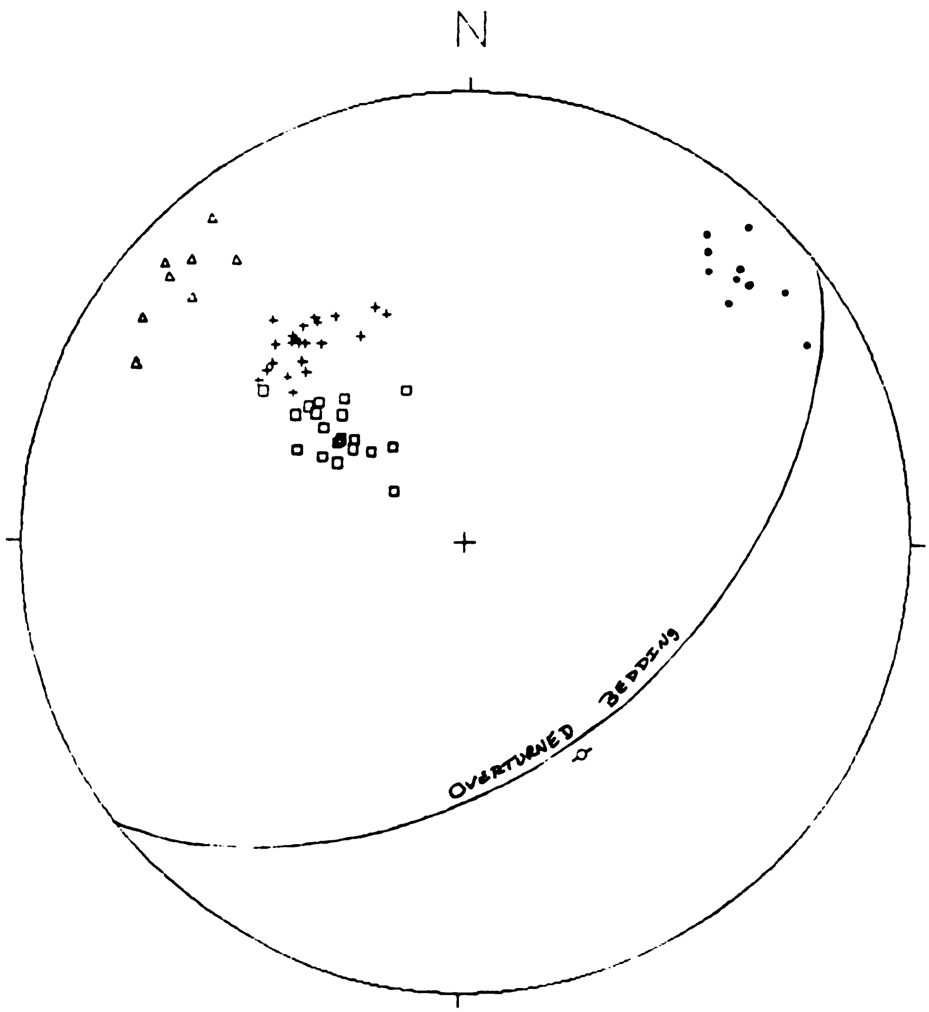

+ S_0 Poles (22)
□ S_1 Poles (21)
△ S* Poles (8)
-o- Mean pole to S* extension veins
● Boudin long axes

Figure 24. Equal-area lower hemisphere projection of mesoscopic structural data for location L20.

zone to the SE.

The extensional crenulations which effect both S_0 and S_1 may be related to either the first extensional stage during initial folding or possibly a second extensional stage of limb deformation during fold modification.

Summary of Chilhowee Transect:

The transect is characterized by inclined/close folds which commonly exhibit modification structures. Unmodified folds are nowhere recognized along the transect. The observed succession of structures appears to record a progressive or superposed deformation. The variability of structural successions along the transect may reflect the local strain histories related to fold modification.

In summary, the deformations recorded in the rocks of the southern transect are much more intense than those of the northern area, as might be expected in rocks near the base of a thrust sheet. The more northerly fold trends together with the more inclined/closed nature of these folds are proposed to reflect a greater degree of fold modification along the base of the sheet. It is proposed that the modification included the rotation of fold axes due to shear.

Central Transect; Kinzel Springs:

The Kinzel Springs transect is located along Hwy. 73 and extends from Kinzel Springs towards the NW for approximately 1.5 miles. The Taconic deformation along this transect is similar to that recorded along the Cove Creek transect but is complicated by the presence of Alleghenian deformation. A schematic profile along the transect is shown in Figure 25. The profile is dominated by open to close folds which have been externally rotated and cut by numerous high angle faults during Alleghenian deformation. These fold trains are interpreted as having been located on the shallow SE dipping limb of the macroscopic anticline in the MCS prior to Alleghanian deformation. The folds are interpreted as F_2 or F_2' folds based on the fanned and folded nature of S_1.

The local Alleghenian upwarping of the MCS is marked by the formation of erosional windows. The upwarping of the plate is apparently the result of the development of underlying culminating duplex structures. These duplex structures are exposed within the Lower Ordovician Limestones in the Tuckaleechee Cove window located just to the SE of the transect.

The external rotation of the MCS and the accompanying normal faulting have complicated the geometrical interrelations of the Taconic folds. While the local Alleghenian structures prevent the determination of Taconic kinematics, the transect does provide a means to correlate general macroscopic structures across the MCS.

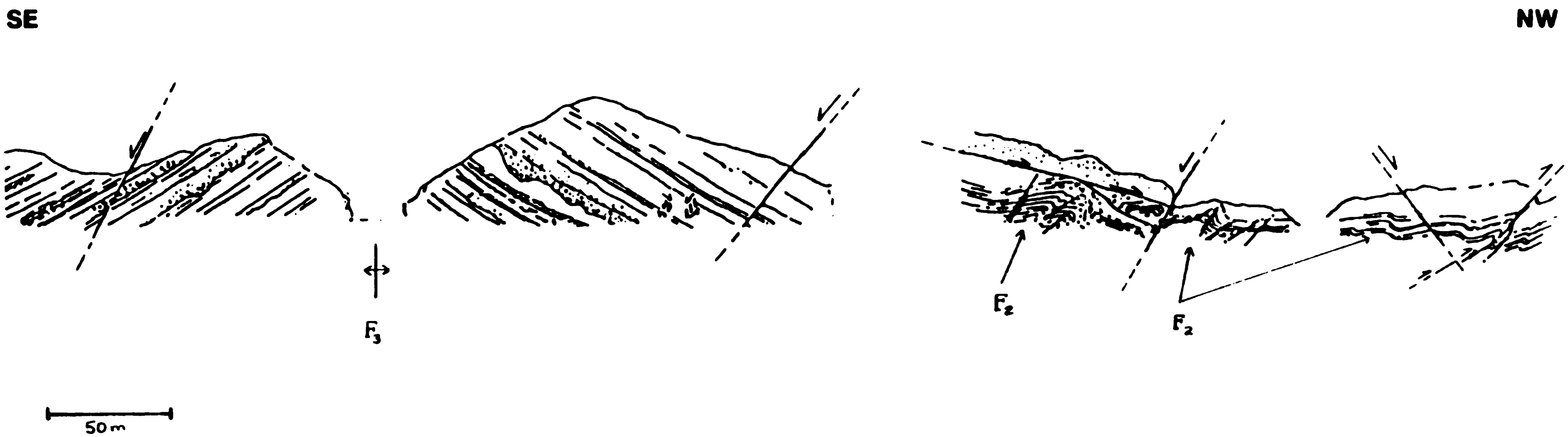

Figure 25. Schematic profile of Kinzel Springs transect.

Discussion:

Mesoscopic structures throughout the study area record a progressive deformation involving the modification of early structures during later stages of the deformation evnt. As evident along profile L300, a transition exists from unmodified upright/open F_1 folds to modified overturned/close F_2 folds as minor thrusts are approached. In addition, a transition from an unmodified axial planar cleavage to a modified fanned cleavage exists. These modified spaced cleavage planes record a superposed deformation associated with simple shear due to the development of local thrust or shear zones.

If the superposition of strain did occur during this progressive deformation, this strain may be recorded by the development of a second cleavage or the deformation of the existing fabric (cleavage). If the existing cleavage lies parallel to the superposed shortening, the cleavage may buckle or be transected by the formation of a second cleavage. If the existing cleavage lies at a low or moderate angle to the superposed shortening and acts as an anisotropic plane, the cleavage may be used as a plane of shear. Cleavage oriented at a high angle to a superposed shortening may simply facilitate the continued dissolution of material along that plane.

The variability of cleavage style and the microfabrics associated with cleavage development are outlined in the following chapter. The observed structures are consistent with the modification of existing fabrics during a superposed deformation.

MICROFABRICS

Microfabrics related to the formation and reuse of cleavage planes are used to evaluate the kinematics associated with fold modification. Whereas the nature of S_{1p} is relatively consistent throughout the Miller Cove sheet, the nature of S_{1sp} and the amount of bedding offset across S_{1sp} is variable. While one limb of a fold may demonstrate the offset of bedding across cleavage, the opposite limb is commonly characterized by a lack of offset and a decrease in cleavage spacing. It is proposed that offset across cleavage is the result of a superposed shear along cleavage due to limb extension during fold modification and that the decrease in cleavage spacing is the result of continued shortening of a limb during modification. The variation of cleavage style across folds is proposed to be a function of fold modification and is later used to characterize those modifications.

Offset of S_0 across S_{1sp}:

Two aspects of bedding offsets across S_{1sp} are relevant to this study. First, the mechanism by which offset has occurred; second, the spatial relationship of offset to mesoscopic fold modification. The importance of offset is; what function, if any, does it serve during the modification of folds? It is proposed that cleavage was initiated by solution transfer mechanisms and developed normal to sub-horizontal layer parallel strains during upright F_1 folding and that upon fold modification the cleavage planes have been reused as planes of shear to facilitate limb extension. An attempt is made to first, determine the mechanism of offset along cleavage planes by evaluating the observed microfabrics and second, relate the mechanism to the local fold kinematics.

Offset Mechanisms:

Two possible mechanisms of offset are evaluated: 1) a solution transfer offset due to shortening normal to the cleavage plane; 2) a transpressive offset due to an initial or superposed shortening oblique to the cleavage plane.

The offset of layering across crenulation cleavage is commonly referred to as an "apparent displacement", attributed to the solution transfer of material due to shortening normal to the cleavage plane. Alternately, offset can be the result of actual displacement along the cleavage plane due to oblique shortening and shear. While the first mechanism is widely accepted, the formation of crenulation cleavage by initial or superposed shear has not been clearly demonstrated.

Solution Transfer Offset:

Gray (1979) suggests that the offset of layering across crenulation cleavage forms as a result of shortening normal to the cleavage plane and the associated solution transfer removal of material (see Figure 26a). The formation of elongate fabric within the cleavage zone should theoretically record the orientation of λ_1 parallel to cleavage. Solution transfer offset can occur if bedding is inclined at some angle to the developing cleavage plane or zone (i.e., the xy-plane). The dissolution of material from within the cleavage zone results in the offset of bedding across cleavage and an apparent displacement along the dissolution plane. The shortening required to accomplish a given offset can be calculated as shown in Figure 26.

Gray (1979) demonstrates that the offset of layering can be accomplished by solution transfer mechanisms alone. He suggests minor shear or slip might occur but that concrete evidence is lacking. The evidence which he considered would indicate actual shear or slip includes cataclastic fabrics such as microfaults and broken or sheared grains, or ductile fabrics (i.e., plastic deformation) within the cleavage zone indicating the maximum elongation direction λ_1 oblique to cleavage.

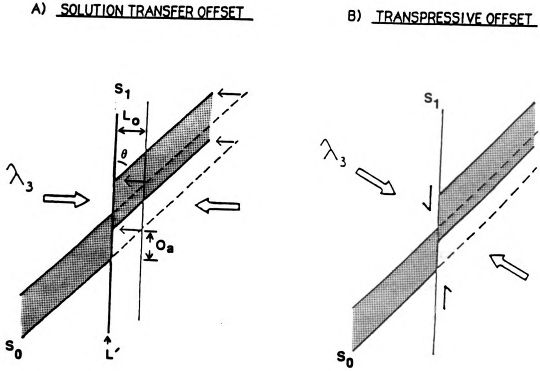

$$\% \text{ Shortening} = 100 \times \frac{L' - L_o}{L_o}$$

$$\text{where } L = \frac{O_a}{\tan\theta}$$

Figure 26. Offset Mechanisms:
a) Solution transfer,
b) Transpressive offset.

The structures predicted in solution-transfer cleavage formation are summarized in Figure 28 (p.77). In general these structures indicate dissolution and shortening normal to the cleavage plane, and lack the microfabrics indicative of shear.

Transpressive Offset:

The offset of layering across discrete cleavage planes by a process of shear or slip has been proposed by several workers (e.g., Sorby, 1880; Hobbs, Means, and Williams, 1976; Williams, 1972). This hypothesis was discounted by Gray (1979) due to the lack of evidence of microfaulting or shear along such planes within the samples he studied from numerous locations throughout the world.

Knipe and White (1979), in a study of spaced cleavage within a low-grade shear zone, identify solution transfer fabrics as well as ductile and brittle shear fabrics along crenulation cleavage planes. They attribute these shear fabrics to a component of shear along the cleavage planes in response to the rotation of those planes within the shear zone.

Together, the processes of shortening across and simple shear along the cleavage zone might best be described as a transpressive deformation (see Figure 26b). Transpression is the combination of simple shear and shortening across a shear zone bound by rigid blocks (Harland, 1971; Sanderson and Marchini, 1984).

In this particular case the blocks are the microlithons and the shear zones are the cleavage zones. In a transpressive mechanism the orientation of the maximum extension direction λ_1 would be $\leq 45°$ to the zone due to the oblique shortening.

A transpressive deformation might result from the rotation of a developing cleavage plane within the constant strain field during a single stage of folding or from the external rotation of the strain field with respect to the cleavage plane due to a superposed strain (see Figure 27).

Segall and Simpson (1986) have demonstrated that both brittle and ductile fabrics can result from a single shear deformation across planar fractures. A component of shear along a discrete cleavage plane can result in brittle microfaulting along that plane and/or the ductile shearing of the bounding microlithons. Shear along a zonal cleavage could conceivably involve movement along a series of brittle microfaults or the ductile shearing of material within the cleavage zone or bounding microlithons.

The structures predicted in a transpressive mechanism are summarized in Figure 28. In general these are structures which indicate oblique shortening and record a ductile or brittle shear.

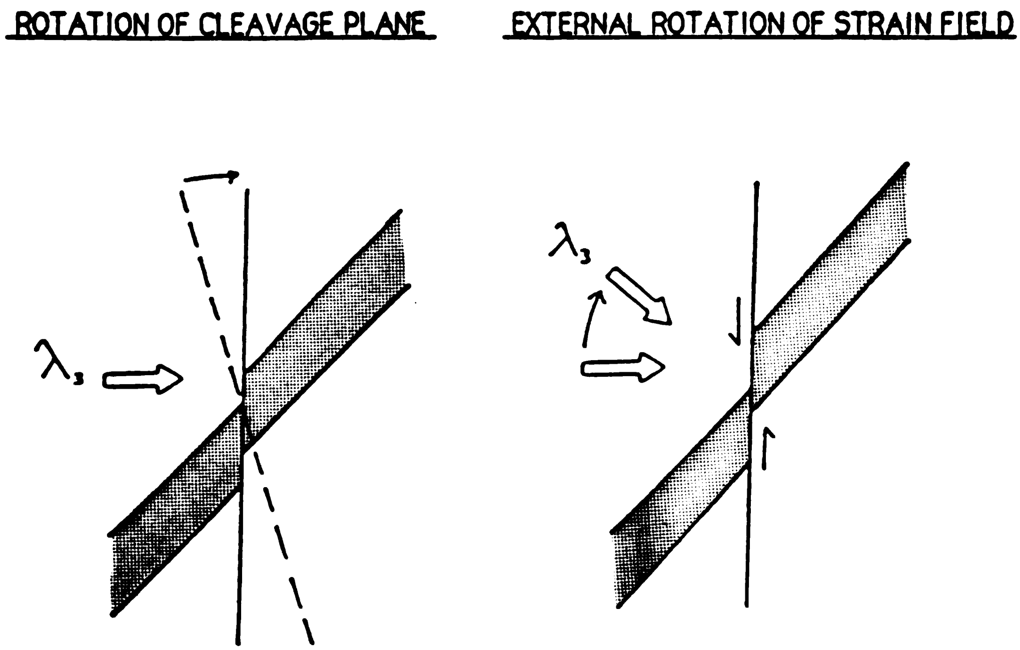

Figure 27. Processes resulting in transpressive offset.

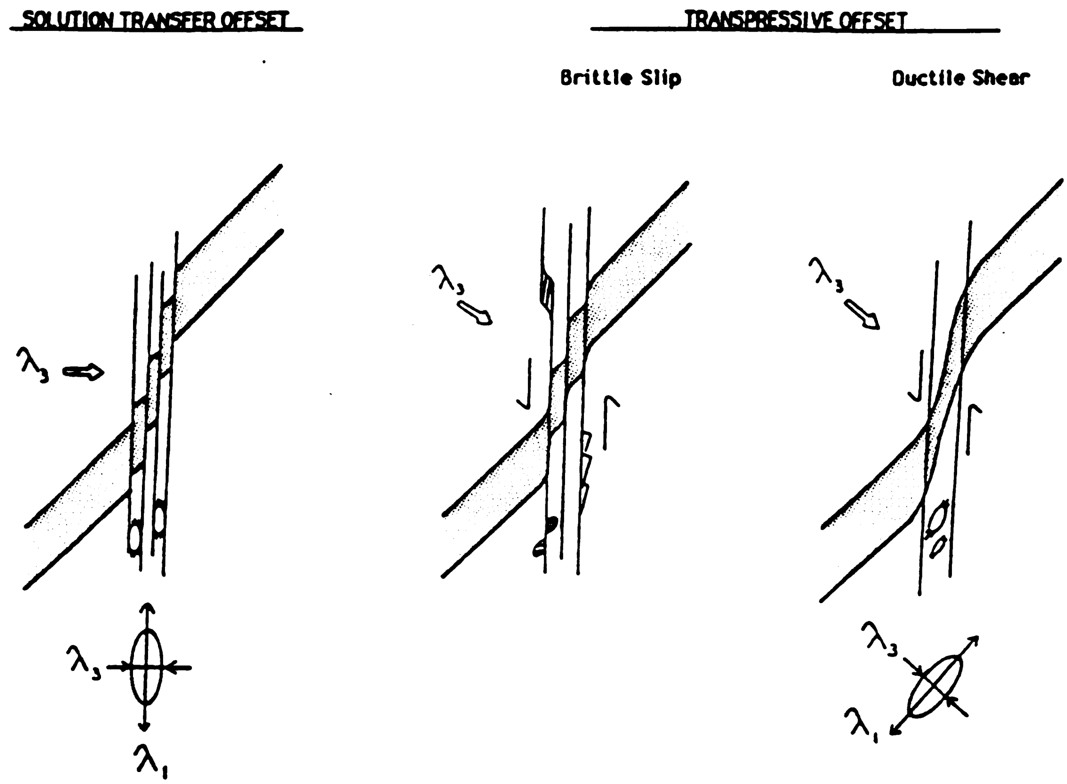

PREDICTED STRUCTURES	
1. Chemical differentiation across zone	1. Chemical differentiation
2. λ_1 orientation **parallel** to zone	2. λ_1 orientation **oblique** to zone
3. **Non-shear** microfabrics (i.e.dissolution truncation)	3. **Shear** microfabrics (i.e.micro faulting, micro pull-aparts, mica "fish", sheared & broken grains

Figure 28. Structures predicted by each offset mechanism.

Evaluation of Cleavage Zones:

Methods:

Microfabrics associated with S_{1sp} cleavage zones are evaluated within folds along the Cove Creek and Chilhowee transects at locations L300 and L12, respectively.

The orientation of various deformational fabrics were measured in order to determine the orientation of λ_1 within the cleavage zones. Deformational fabrics were determined by the measurement of aspect ratios (i.e., ellipticities) of quartz grains and calcite porphyroblasts within individual bedding laminations as they crossed cleavage planes. The measurement of grain aspect ratio is based on the R_f/Phi technique as described by Lisle (1984) and was used in a similar manner by Knipe and White (1979).

The long and short axes of the grains were measured from photomicrographs, ratios (R) obtained and plotted against the orientation (Phi) of the long axis with respect to the cleavage plane. The orientation of the maximum extension direction, λ_1, was determined within the assumed xz-plane (i.e., the plane perpendicular to the "xy"-cleavage plane which contains the x-axis) using the vector mean of the Phi data.

The deviation of the λ_1 orientation from the theoretical xy-plane (i.e., cleavage plane) is taken to indicate oblique shortening and therefore a component of shear. The symmetry value (I_{sym}) of the R_f/PHI data distribution, and the fluctuation value (F) of the Phi data distribution provides additional information which is used to infer original fabric orientations (Lisle 1984).

Symmetry refers to the distribution of data points with respect to the mean R and Phi values and is determined by the equations given in Appendix A. Fabrics with no initial preferred orientation demonstrate a symmetric distribution about λ_1, while those with an initial preferred orientation result in asymmetric distributions. Fluctuation refers to the spread of Phi values (i.e., long axis orientations). Fluctuation decreases from 180° in a fabric with no preferred orientation to <90° in a fabric with a preferred orientation. The determination of fluctuation is further discussed in Appendix A.

Other microfabric shear indicators such as broken and sheared porphyroblasts, mica "fish", and micro pull-aparts are also used to evaluate offset mechanisms (Simpson and Schmid, 1983; Lister and Snoke, 1984).

It is shown that the oblique orientation of λ_1 with respect to cleavage, the presence of shear microfabrics, and the high fluctuation and strong symmetry of the data are consistent with a deformational mechanism involving a component of shear along the cleavage planes. The observed microfabrics are summarized below.

Cove Creek Transect; Location L300:

Cleavage zones within sample L300-3 from the shallow limb of fold "b" (Figure 9) and cleavage zones within samples L300-1 and L300-2 from the overturned limb were studied using photomicrographs and petrographic observations.

Quartz grain fabrics from samples L300-1 and L300-3, representing both limbs of the fold, record little or no plastic deformation of quartz grains within the cleavage zones (see Figure 29). Aspect ratios show no increase within the zones although fluctuation values appear to decrease slightly. It is proposed that the weak preferred orientation of quartz grains within the zones, indicated by a decrease in fluctuation, is the result of particulate flow as described by Borradaile (1981). In this case, grain boundary sliding was accomplished by the rotation of quartz grains within the more ductile calcite and micaceous rich matrix. The quartz grain fabrics are not inconsistent with either mechanism of offset.

Figure 29. Rf/phi plots of quartz grain fabrics. Sketch of data location with respect to bedding and cleavage; mean ellipse axes depicted.
a) sample L300-1 (overturned limb);
b) sample L300-3 (upright limb).

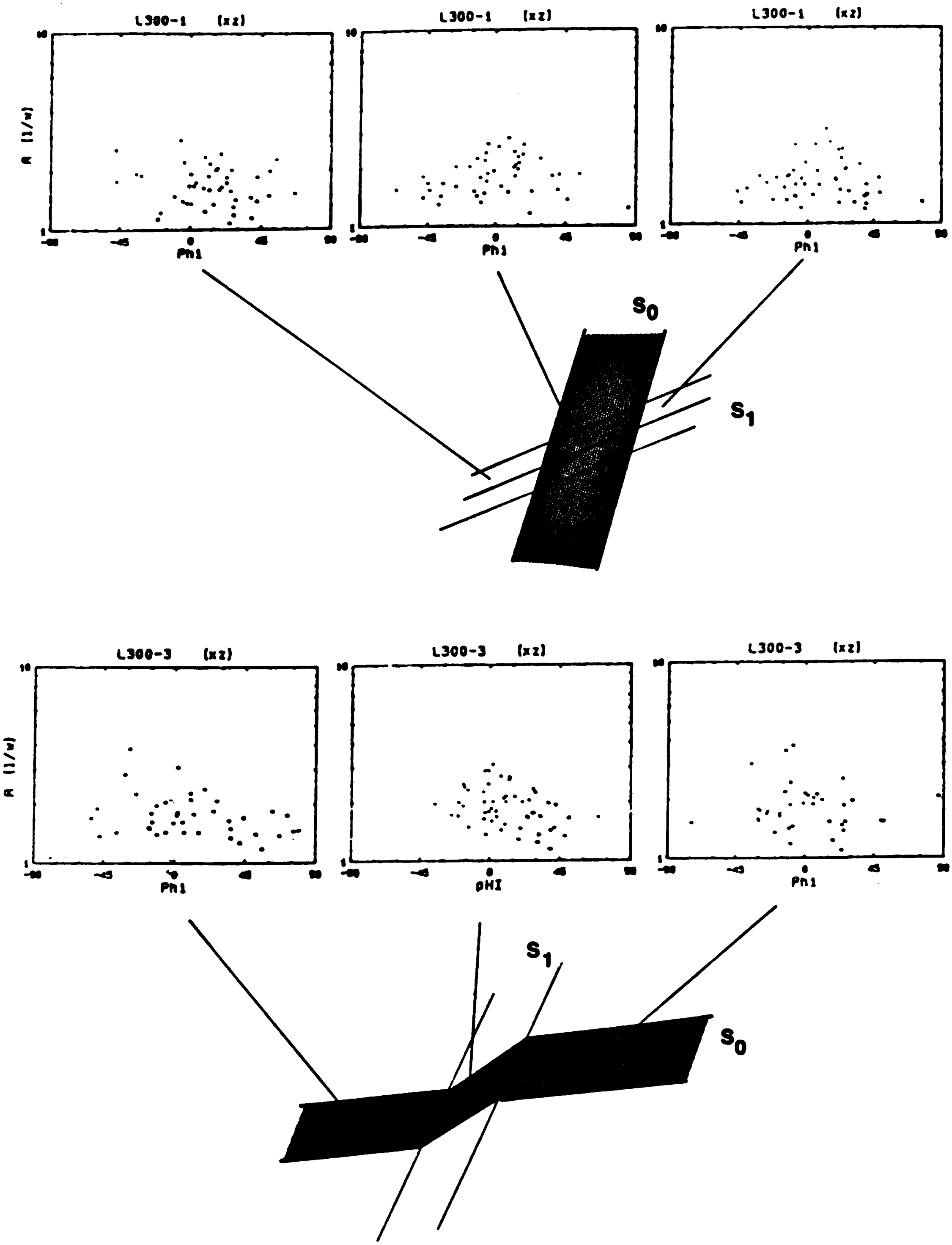
L300-1 (xz)
L300-1 (xz)
L300-1 (xz)
R (1/w)
Phi
S0
S1
L300-3 (xz)
L300-3 (xz)
L300-3 (xz)
R (1/w)
Phi
pHI
S1
S0

Figure 29.

The presence of deformed calcite porphyroblasts and other microfabrics are consistent with a component of shear or oblique shortening across the cleavage zones in sample L300-3 from the shallow limb. The observed fabrics include:

1) sheared and micro faulted mica (see Figure 30a);
2) sheared and broken calcite porphyroblasts connected by fibrous mica growths oriented at a moderate angle to the cleavage zone (~25°, see Figure 30b);
3) deformed calcite porphyroblasts indicating λ_1 oriented at moderate angle to the cleavage zone ($\lambda_1 = 18° \pm 4°$, F= 45°, Figure 31).

Aspect ratios of 282 calcite porphyroblasts from sample L300-3 were measured from photomicrographs across cleavage zones. Porphyroblast R_f/Phi data are summarized in Figure 31. The vector mean orientation of λ_1, derived from R_f/Phi data, is 18° with respect to the orientation of cleavage. Fluctuation values of F= ~45° within the cleavage zone and F= ~180° in the bounding microlithons, indicate that no preexisting porphyroblast fabric was present and attests to the higher strains within the zone. Symmetry test values for the separate data groups also indicate that no preexisting fabric was present (see Appendix A, Table A-2).

In addition, the highly asymmetric distribution of ellipse long axes with respect to cleavage within the zone is inconsistent with shortening normal to the zone (Fig. 31)

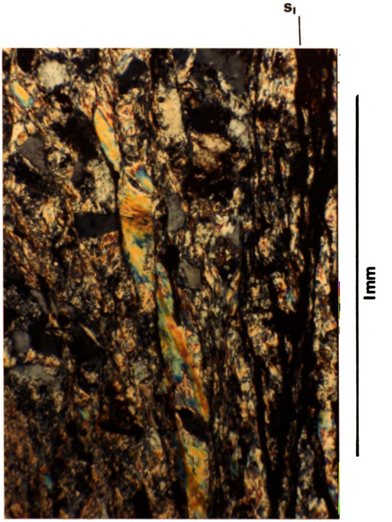

Figure 30a. Photomicrograph of micro-faulted Mica (sample L300-3). Scale bar = 1mm.

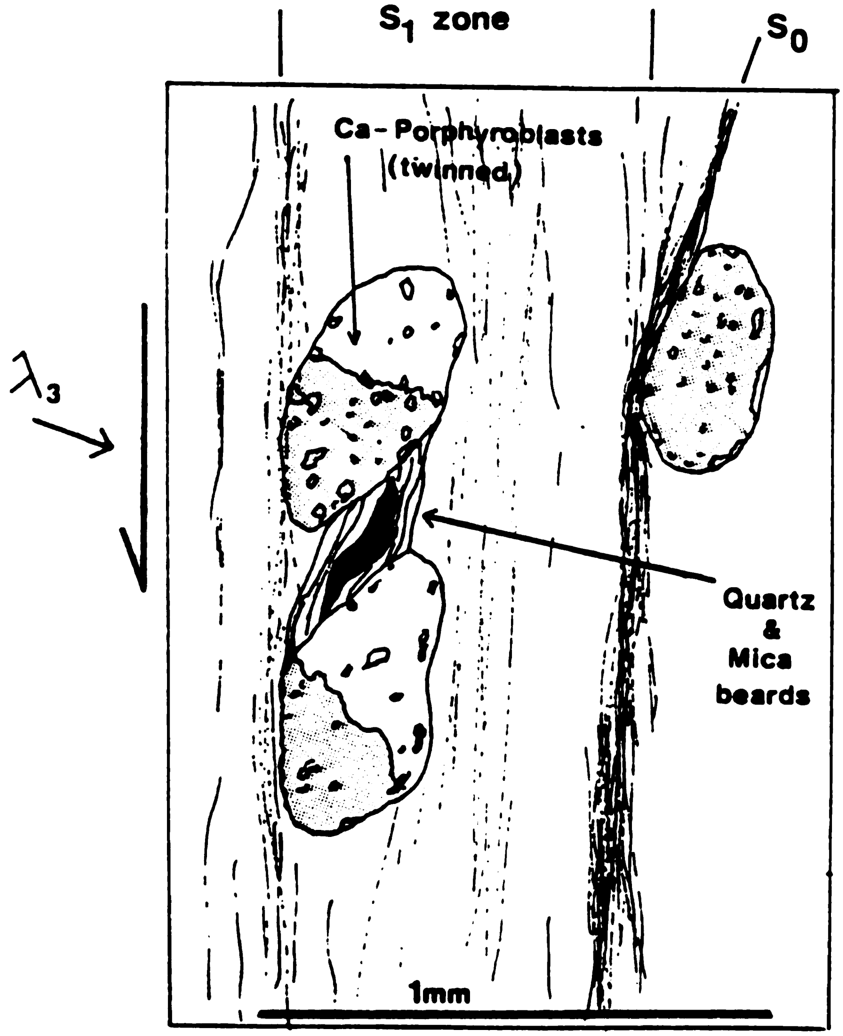

Figure 30b. Photomicrograph (facing page) and sketch of sheared calcite porphyroblasts (sample L300-3). Scale bar = 1mm.

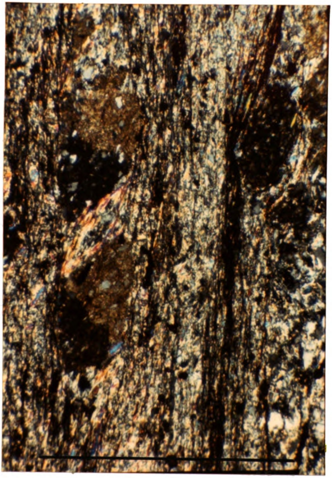

Figure 30b.

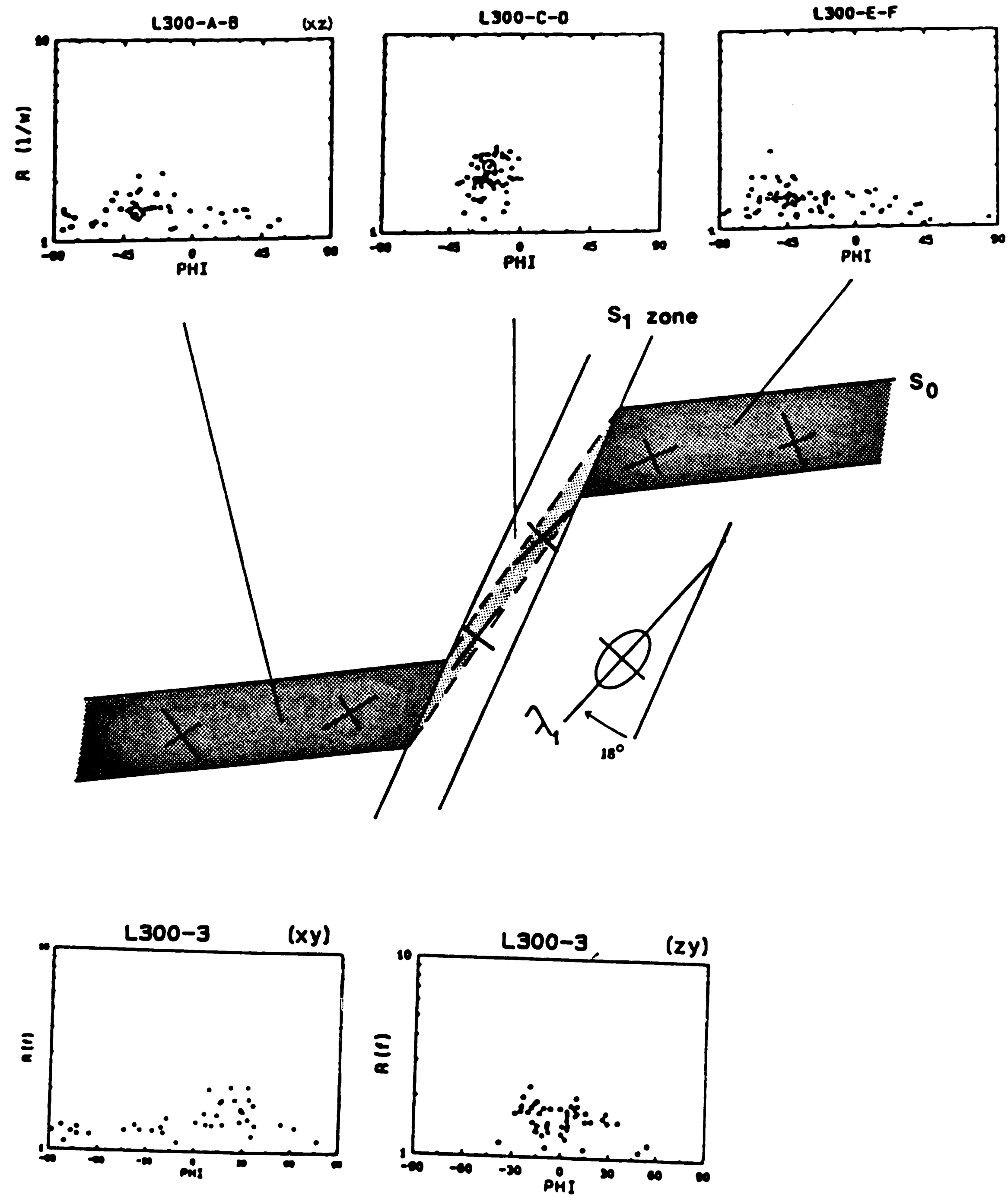

Figure 31. Rf/Phi data for calcite porphyroblasts (sample L300-3). Sketch showing data location.

Given the high fluctuation values within the undeformed microlithons, if deformation took place by shortening normal to cleavage then long axis distribution within the cleavage zone should lie to both sides of the cleavage plane (i.e., a distribution semi-symmetric about cleavage, the "xy"-plane). The asymmetric distribution of data is indicative of simple shear strain (Choukroune et al., 1987).

A component of shear across the cleavage zone is supported by the presence of mica fish, and broken/sheared porphyroblasts within the zone which indicate shear consistent with the observed bedding offsets. Broken porphyroblasts are connected by linear white mica and quartz fibrous growths, which mark the offsets and lie at a moderate angle (~25°) to the shear zone boundaries. The fact that these fibres are linear rather than curved suggests they were formed during the late stages of shear deformation and have undergone little if any subsequent rotation. Assuming these formed parallel to the maximum elongation direction, then λ_1 must have been oriented at approximately 25° to the cleavage zone during the latest increments of deformation.

The amount of shortening normal to the cleavage zone needed to accomplish the observed offset of bedding by solution transfer in sample L300-3, as determined by palinspastic reconstruction, has a mean value of 83%. This value is extremely high and mechanically unreasonable considering the abundance of shear indicators and lack of dissolution textures. While 83% volume loss may be possible it is notably higher than the maximum values of ~50% volume loss for the Martinsville slates of the Central Appalachians reported by Wright and Platt (1982). The microfabrics noted above are consistent with a component of shear or slip across those cleavage zones on the shallow limb of the fold.

In contrast, microfabrics observed in sample L300-1 and L300-2 from the overturned limb indicate a lack of shear offset (Figure 32). No shear microfabrics are observed and the porphyroblast fabric analysis in sample L300-1 is inconsistent with shear offset (Figure 33). The λ_1 orientation determined from calcite porphyroblast aspect ratios lacks a preferred orientation which is limited to cleavage zones. A very weak fabric, which is reflected in the R_f/Phi data, is unaffected as it crosses cleavage and lies sub-parallel to bedding. This weak bedding-parallel fabric may reflect the initiation of a second cleavage S_2 in response to modification strains. A decrease of cleavage spacing is also recorded along the overturned limb (Figure 13).

Offset Mechanisms:

Offset by solution transfer is consistent only with the observed fabrics in samples L300-1 and L300-2 from the overturned limb. The amount of offset or presence of shear in these samples appears negligible on this overturned limb.

Figure 32. Photomicrographs of non-sheared S_{1sp} cleavage.
a,b) L300-1, c) L300-12, d) L12-12
Scale bar = 1mm.

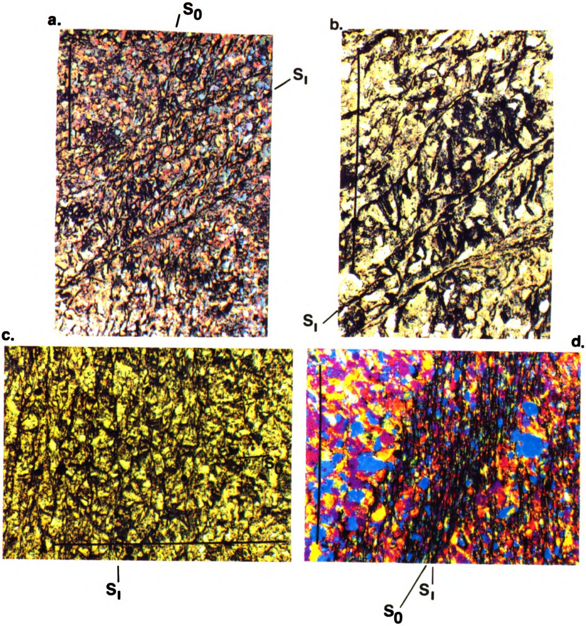

Figure 32.

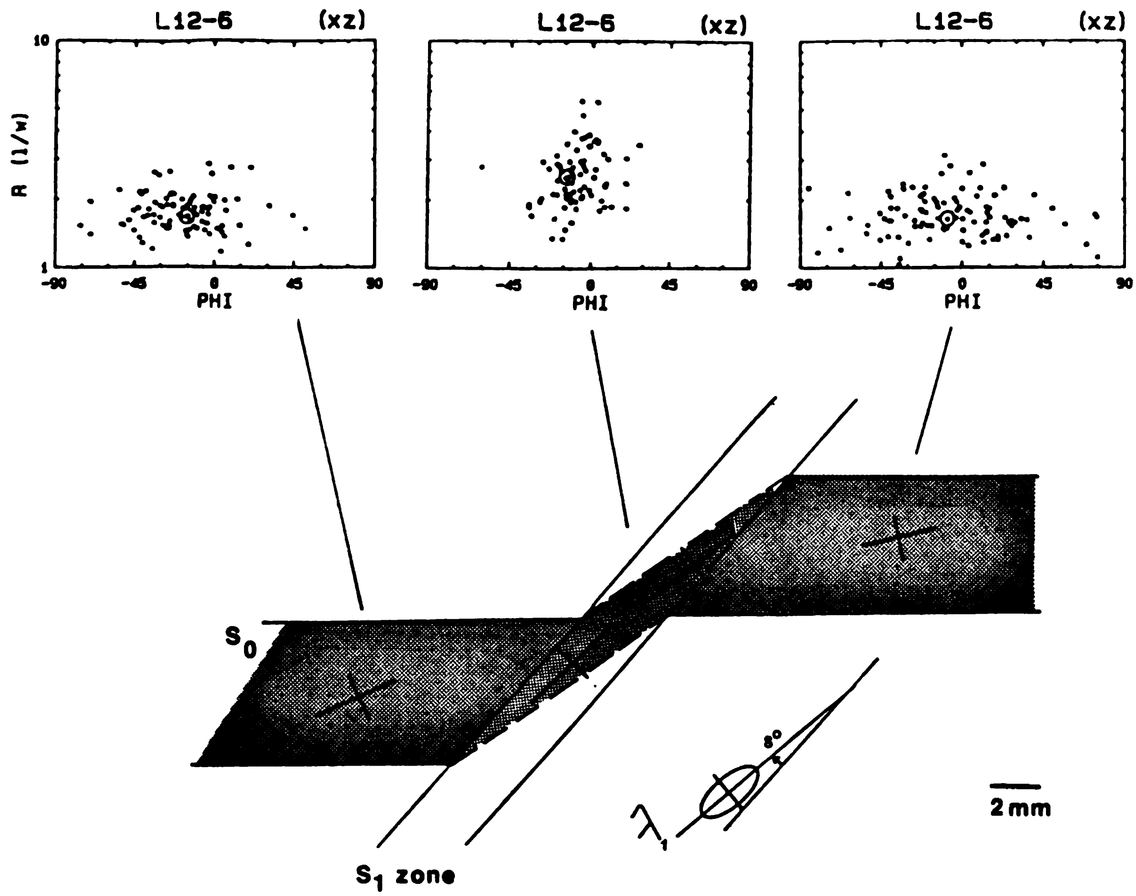

Figure 33. Rf/Phi data of calcite porphyroblasts fabric (sample L300-1). Sketch showing data location.

Offset by solution transfer alone on the shallow upright limb is inconsistent with the observed fabrics and is rejected for this limb. The oblique orientation of λ_1 and the presence of mica "fish", sheared porphyroblasts, and oblique mica/quartz beards within the cleavage zones of sample L300-3 indicate that some component of shear accompanied offset. A transpressive deformation best describes the observed structures on the shallow limb. The fact that the microlithons remained relatively undeformed may indicate that preexisting anisotropies existed along the present cleavage zone, possibly as early dissolution planes, and were reused during subsequent shear.

Discussion of L300:

In summary, it is the shallow limb which records transpressive offset while the overturned limb records no such offset. The variation in offset mechanisms from the shallow limb to the overturned limb of the fold may reflect the effects of a superposed strain. Transpressive offset along the shallow limb may record a superposed limb extension while the fabrics on the overturned limb simply record continued limb shortening. This variability is proposed to be a function of limb orientation within the superposed strain fields associated with fold modification and is discussed further in the later section on kinematics.

Chilhowee Transect; Location L12:

Unlike the fold at location L300, the asymmetric fold at L12 is characterized by shear offset on the overturned limb rather than on the shallow limb (Figure 20). Cleavage zones from samples L12-11,-12 from the shallow limb and L12-6 from the overturned limb were studied using photomicrograph mosaics and petrographic observations. Transpressive offset occurs across both discrete and zonal crenulation cleavage in sample L12-6, from the overturned limb. Discrete planes record brittle microfaulting (Figure 22), while zonal cleavage records the ductile shearing of quartz grains (Figure 34). The observed microfabrics include:

Discrete cleavage:

1) brittle microfaulting (Figure 22a);
2) slickenside or micro pull-apart structures with steps consistent with observed offset directions and offsets ~1-2mm. (Fig. 22b);

Zonal cleavage:

1) elongate quartz grain fabric indicating the orientation of λ_1 oblique to S_{1sp} zone boundaries (λ_1=~8°$\pm$4°, F=65°, see Figure 34);
2) calcite filled brittle fractures within S_{1sp} zones which transected the fabric and indicate a late incremental λ_1 oriented at ~20° to the zone (see Figure 35);

Figure 34. Photomicrograph of sheared quartz grain fabric across S_{1sp} cleavage zone (mica plate inserted, sample L12-6, scale bar = 1mm).

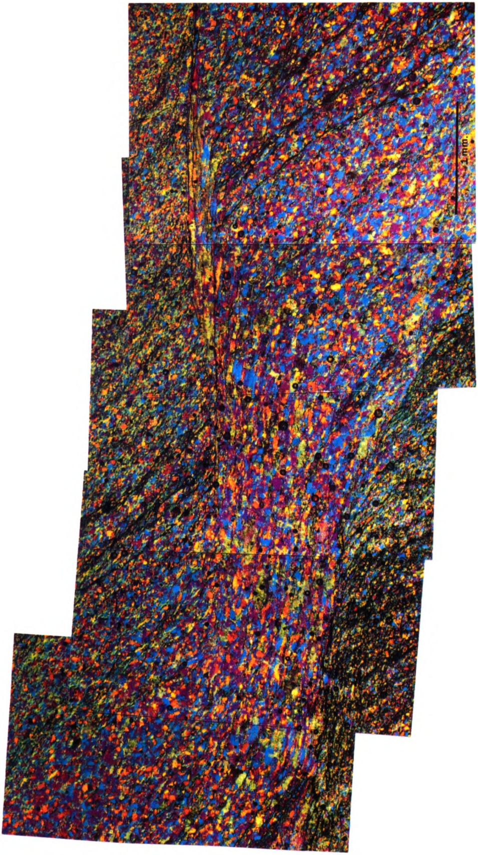

Figure 34.

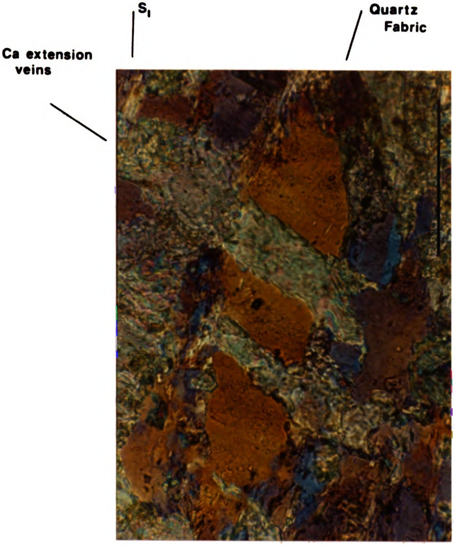

Figure 35. Photomicrograph of quartz grain fabric transected by calcite extension veins (sample L12-6). Scale bar =0.1mm.

3) shear microfabrics such as mica "fish", micro pull-apart structures or slickensides along cleavage zone boundaries (Figure 22).

In sample L12-6, cleavage varies along its trace from discrete to zonal. Brittle microfaults and micro pull-aparts along discrete cleavage planes record offsets which range between 1mm and 3mm. The orientation of λ_1 within zonal cleavage was calculated in sample L12-6 from the preferred orientation of recrystallized quartz grains.

The determined mean vector orientation of λ_1 within the cleavage zone is approximately 8° oblique to cleavage (Figure 36). The high ratio (R = 2.4) and low fluctuation value (F = 65°) record the recrystallization and preferred growth of quartz grains within the zone during deformation. Low aspect ratios (R = 1.7) and high fluctuation values (F = 180°) outside the cleavage zone indicate little or no quartz grain fabric within the microlithons.

The late increment λ_1 orientation of ~20°, determined from calcite fractures, is probably the best estimate of an incremental λ_1 orientation related to offset. The 8° value determined from quartz fabric is likely to reflect the finite λ_1 orientation which has undergone numerous incremental rotations towards the cleavage plane during offset.

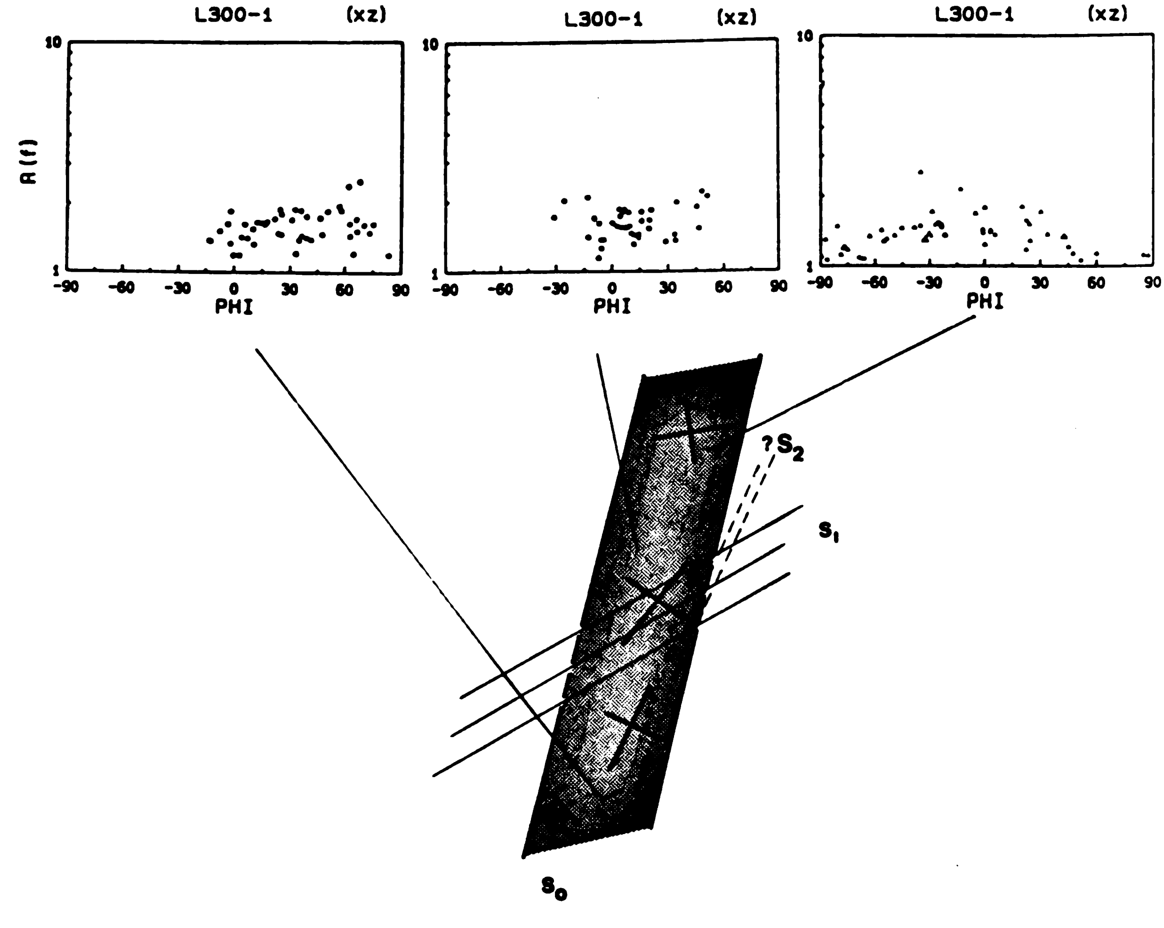

Figure 36. Rf/Phi data, quartz grain fabric (sample L12-6). Sketch showing data location.

Assuming only solution transfer removal for sample L12-6, the mean value of shortening normal to the cleavage zone needed to accomplish the observed offset of bedding is 82%. Again this value is extremely large and judged unreasonable considering the lack of dissolution features and the abundance of shear indicators within the cleavage zone. In summary the fabrics are consistent with a transpressive mechanism on the overturned limb.

Mesoscopic observations of cleavage on the shallow limb of this fold indicate that bedding is not visibly offset across cleavage. Microscopic observations from samples L12-12 and L12-11 confirm this. There are no ductile or brittle shear microfabrics observed within the samples (Figure 32). Cleavage spacing on this shallow limb is considerably smaller than that on the overturned limb (Figure 13). In addition, cleavage is folded into gentle F_2' folds on the upright limb.

Offset Mechanism:

Solution transfer offset on the shallow limb is consistent with the observed microfabrics. The microfabrics observed on the shallow limb fail to demonstrate offset by shear and are inconsistent with formation by transpression.

In contrast, microfabrics from the overturned limb are inconsistent with formation solely by solution transfer mechanisms. The transition along trace from discrete cleavage, demonstrating slip, to zonal cleavage, demonstrating ductile shear and recrystallization, clearly indicate that a component of shear accompanied the offset across cleavage. These fabrics, considered together, are consistent with formation by a transpressive mechanism.

Discussion of L12:

The presence of shear fabrics along both discrete and zonal cleavage from the overturned limb indicates that solution transfer alone cannot account for the observed deformation. As at location L300, there is a variation in offset style from the overturned limb to the shallow limb of the fold. Unlike the fold in L300, it is here the overturned limb which records transpressive offset while the shallow limb records no such offset. It is proposed that the variation in offset style is a function of the limb's orientation within a superposed strain field related to fold modification.

Discussion of Offset Mechanisms:

As shown in the above examples, cleavage spacing and offset mechanisms are variable across folds. Some cleavage planes record the offset of bedding by both brittle and ductile shear while others record no measurable offset. The noted component of shear across cleavage is consistent with either the rotation of developing cleavage within a constant strain field or the superposition of non-coaxial strain upon a preexisting or semi-developed cleavage zone (Figure 27). Rotation of cleavage within a constant strain field might occur during the modification of structures during thrust sheet deformation by a ductile shearing process. The superposition of non-coaxial strain and the external rotation of λ_3 might occur in response to overthrusting. The mesoscopic variation of the offset mechanisms noted above are used in the evaluation of fold kinematics.

Mesoscopic Variation of Offset:

The amount and style of bedding offset across S_{1sp} varies on the mesoscopic scale as a function of the degree of fold modification. Unmodified F_1 fold limbs are characterized by the development of an axial planar weak crenulation cleavage which, on the mesoscopic scale, demonstrates little or no evidence of shear offset. The nature of these cleavage zones are consistent with formation by a mechanism involving solution transfer due to shortening normal to cleavage. Modified F_2 folds are characterized by a fanned, strongly developed crenulation cleavage which clearly demonstrates bedding offset by transpression. Together, these observations suggest a correlation between shear-induced offset and fold modification.

The normal offset of bedding across cleavage suggests extension of the limb while a reverse offset, the lack of offset, or a decrease in cleavage spacing suggests the additional compression of the limb. In modified areas, the amount and style of offset appears to be a function of limb orientation within the local strain field (i.e., extensional vs compressional field) associated with fold modification.

The developing S_{1sp} cleavage planes are proposed to have acted as preexisting anisotropic planes across which slip or shear occurred in response to fold modification. On the mesoscopic scale the cleavage planes appear to have acted as small normal faults which facilitated limb extension. For limbs in which shear offset is not recognized, it is proposed that the continued shortening of the limb during modification has resulted in the formation of additional dissolution planes as reflected in the noted decrease in cleavage spacing and at location L300 the initiation of an incipient or weak S_2 fabric.

The extension or compression of a limb is a function of the strain field in which it is deformed during folding and fold modification. The orientations of limbs with respect to local thrusts and the deformation recorded across cleavage provide additional constraints on the kinematics of the deformation. Mesoscopic variations will be included in the derivation of fold kinematics.

Other Microfabrics:

Complex Microfabrics within S_{1sp} Zones (L10):

The nature and possible origin of the extension crenulations internal to S_{1sp} zones at the Chilhowee L10 location are briefly discussed. These extension crenulation cleavages, found internal to S_{1sp} zones, are comparable to the "ecc_1" and "ecc_2" fabrics as defined by Platt (1984) and shown in Figure 19.

At location L10 the kinematic significance of the microscopic extension crenulation fabric is unclear. As noted earlier these fabrics can form by either shear or flattening. They may record either a component of shear along the developing S_{1sp} zones or simply record large amounts of shortening normal to S_{1sp}. The fact that all observed eccs dip to the NW regardless of position in the fold is enigmatic. The mechanism of formation and the kinematic significance of these fabrics is unclear and requires further investigation beyond the scope of this study.

Discussion of Microfabrics:

A variation in cleavage style exists across modified folds which reflects the superposed strain associated with overthrusting. Observed microfabrics are interpreted to record the reuse of preexisting spaced cleavage as planes of shear to facilitate limb extension during fold modification. Brittle slip or shear along spaced cleavage is evident by the presence of shear microfabrics such as micro-faulted grains and micro pull-apart structures. Ductile shear zones along cleavage are evident by the presence of deformed quartz grain and calcite porphyroblast fabric. Superposed limb shortening was accomplished by the decrease of cleavage spacing (i.e., an increase in the density of dissolution planes).

While the results do not provide a unique solution they are consistent with both the modified ductile shear and the ductile shear models of deformation. The fabrics indicate the modification of early formed structures during progressive deformation. The kinematic significance of this is demonstrated in the following chapter.

KINEMATIC INTERPRETATIONS

The kinematics of structural development are inferred from the succession of mesoscopic and microscopic structures. Early Paleozoic (Taconic) deformational events are correlative across the MCS and are summarized in Table 1. Inferred events include a regional low grade metamorphism (M_1), accompanied or followed by a regional folding and faulting event (D_1).

The late stages of this folding event are characterized by the modification of early formed structures due to the development of local thrusts. As a first approximation, the modification appears to be described by the superposition of simple shear on preexisting upright folds in the footwall (see Figure 4). These deformational events are characterized and the proposed kinematics outlined below.

1.) Regional Metamorphism (M_1):

Rocks of this portion of the Blue Ridge increase in metamorphic grade to the southeast. Hadley and Nelson (1971) place the chlorite isograd near the Miller Cove Fault and the biotite isograd just southeast of the Rabbit Creek Fault. According to Witherspoon (1981), rocks internal to

Table 1. Summary of proposed deformational events.

Deformational Event	Associated Fabrics	Strain Field
M_1 **Regional Metamorphism (480-400mya)**	**Mimetic replacement of biotite by chlorite ± albite, epidote, and the growth of calcite porphyroblasts.**	
D_1 (?Taconic?) **Folding:** **F_1 (upright folding)**	**S_{1p} (penetrative)** **S_{1sp} (solution transfer only)**	$\rightarrow\ \leftarrow \lambda_3$
Thrusting and Folding: **F_2 (fold modification)**	**S_{1sp} (enhanced by additional dissolution and shear)** **S_2 (incipient, weakly developed)**	$\nearrow\ \swarrow \lambda_3$
D_2 (Alleghanian) **F_3** **Folding & Thrusting (Rigid Ramping style)**	**Gentle warping of existing thrust sheets and associated fabrics.** **S_3 kinks of S_1**	$\rightarrow\ \leftarrow \lambda_3$

the Miller Cove sheet have undergone lower greenschist facies regional metamorphism. Rocks within the MCS commonly contain the metamorphic assemblage of quartz-white mica-chlorite±albite (King, 1964). In addition to these assemblages, calcite porphyroblasts are present in samples from location L300, internal to the MCS.

Within rocks of the MCS, regional metamorphism is evident by the presence of epidote and the replacement of detrital biotite by chlorite and calcite. Chlorite is commonly oriented parallel to bedding within siltstones; this is inferred to be a mimetic preferred orientation resulting from the replacement of detrital biotite. Calcite porphyroblast growth predates the formation of S_1.

Slaty units of the Chilhowee area commonly contain pre- to syn-tectonic cubic pyrite crystals with syn-tectonic pressure shadows. Pyrite growth is assumed to be pre-cleavage formation from the deflection of S_{1p} around both pyrite and the pressure shadows. The variability of deflection around the pressure shadows suggest the formation of these fibrous growths coincided with the early stages of S_1 cleavage development and F_1 folding and possibly into the F_2 stage of modification. In general, the curved fibres appear to record the superposition of a non-coaxial strain consistent with F_2 folding during the latest increments of fibre growth.

2.) F_1 Folding:

Cove Creek Transect (Location L300):

F_1 folding is characterized by the formation of upright mesoscopic folds with sub-horizontal axes which are parasitic to the major anticline within the MCS and form its shallow dipping SE limb. F_1 folding was dominantly by flexural slip. Unmodified F_1 folds are defined by upright/open folds with a refracted axial planar, penetrative to spaced, S_1 cleavage.

S_{1sp} can be correlated from unmodified folds where it appears as a weakly developed axial planar spaced cleavage to modified folds where it appears as a strongly developed spaced crenulation cleavage which is commonly fanned or folded. This transition in the nature of S_{1sp} appears to be a function of fold modification. It is proposed that S_{1sp} formed during the initial F_1 folding but was selectively enhanced during F_2 fold modification by a mechanism involving the superposition of shear across the cleavage planes during superposed extension and by the decrease in cleavage spacing in superposed compression.

Chilhowee Transect:

The Chilhowee transect is characterized by intense F_2 folding which likely reflects the modification of F_1 folds by high strains accumulated at the base of the Miller Cove sheet. The orientation of fold axes along the base of the sheet are also oriented more nearly N-S than those along the other transects which represent structurally higher portions of the sheet. These more N-S orientations may represent the rotation of F_1 fold axes from initial ENE trends towards the direction of thrust movement as a result of high shear strains at the base of the sheet.

While unmodified F_1 folds are not recognized along this transect, F_2 folds (i.e., modified F_1 folds) are present. It is proposed that the modified nature of fabrics within F_2 folds reflects their origin as F_1 folds. The observed fold-fabric relationships are similar to those in the Cove Creek area in which both F_1 and F_2 folds are present. S_{1sp} is well developed, convergently fanned across F_2 folds, and locally varies as a function of fold modification.

3.) Kinematics of Fold Modification (F_2):

On the mesoscopic scale the complex succession of structures and fold geometries observed within the MCS is most consistent with deformation by the simple shear modification of preexisting folds due to overthrusting. On the macroscopic scale the observed deformation appears consistent with both the ductile shearing model of Ramsay, et al., (1983) and the modified ductile shear model proposed here.

Evaluation of Rigid Ramping Model:

The rigid ramping model is rejected as a possible deformation mechanism responsible for the Taconic deformation for the following reasons:
1) the inability of Witherspoon (1981) to balance cross sections within the study area assuming a rigid ramping model; 2) the inability of the model to account for the observed footwall deformation within the subsheets internal to the MCS (e.g., transitional fold trains, thrust related shear gradients, fold modification structures, near-recumbent mesoscopic fold styles); 3) the lack of observed ramp-flat fault systems in the study area. Any attempt to account for these mesoscopic structures with the ramping model results in geologically and mechanically unrealistic kinematics. The rigid ramping model is rejected due to its inability to account for the observed structures.

Evaluation of Ductile & Modified Ductile Shear Models:

In evaluating these models, the incremental strain ellipses in each model are defined and used to predict the possible succession of structures for each location. The observed structure and kinematics will then be judged consistent or inconsistent with the strain histories predicted by each model.

The orientations of incremental ellipses describing the predicted deformations in each model are based on two basic assumptions. First, that the orientation of the thrust plane is approximately parallel to the orientation of the acting shear zone. Second, that a component of load due to the overthrusting sheet is insignificant.

The first assumption is consistent with the observed structural relationships along the Cove Creek transect at L300 and is inferred to accurately reflect fault development throughout the study area. It is apparent from the fault propogation fold at location L300 (see Figure 9), that a ductile zone of deformation precedes displacement on the discrete fault plane surface. This ductile deformation can be described as an initial ductile shear zone in which displacement is eventually concentrated along a discrete fault plane parallel to the shear zone boundaries.

The second assumption, on the significance of the load component, can be treated in several ways. It is ultimately proposed that in this particular case the increase in the component of loading strain is insignificant because of the relatively small displacements along the fault planes. These possible alternatives are discussed below.

First, one can assume the component is negligible (Case A) and that simple shear parallel to the dip of the thrust plane best describes the deformation associated with overthrusting or ductile shearing. Second, one could assume that the component of load is significant and that the fault formed as either a moderately dipping imbricate or ramp fault (Case B) or a sub-horizontal fault (Case C).

Case C, assuming initially sub-horizontal faults, is rejected. It is proposed that the Miller Cove Fault formed as a major ramp or imbricate to the regional decollements and that the mesoscopic faults originated sub-parallel to the Miller Cove Fault forming minor subsheets within the MCS. The imbricate nature of these faults is evident by the moderate dip of the Miller Cove Fault with respect to the sub-horizontal major decollements at depth (e.g., Great Smoky Fault) identified in COCORP studies (Cook, et al., 1979).

In case B, assuming moderately dipping faults and load, the resultant λ_3 orientation is taken to lie half way between the two contributing components of strain. These include the component due to simple shear (λ_3 at 45° to the thrust plane), and the component due to load (λ_3 vertical). Since thrust orientation is the only variable, the resultant orientation of λ_3 is ultimately a function of the dip of the thrust.

Both Case A and B are evaluated for each model at each location (see Figure 37). The predicted kinematics for both cases indicate that the modified ductile shear model is most consistent with the observed structural successions while the ductile shear model is to various degrees inconsistent. The overthrust model is most consistent where load is considered negligible. The apparent insignificance of load in this particular case is likely the result of small displacements along the faults. It is shown in

Figure 37. Evaluation of models with assumptions regarding load. Consistency of model kinematics are compared to those observed. Incremental strain ellipses and inferred strain paths of limbs depicted for each model. C = consistent, I = inconsistent (reason footnoted), compressional strain fields shaded, and λ_3 orientations shown.

[1] Limb originates in extensional field.
[2] Observed second stage extension not predicted
[3] Limb originates in extensional field.
[4] Observed second stage extension not predicted
[5] Limb originates in extensional field.

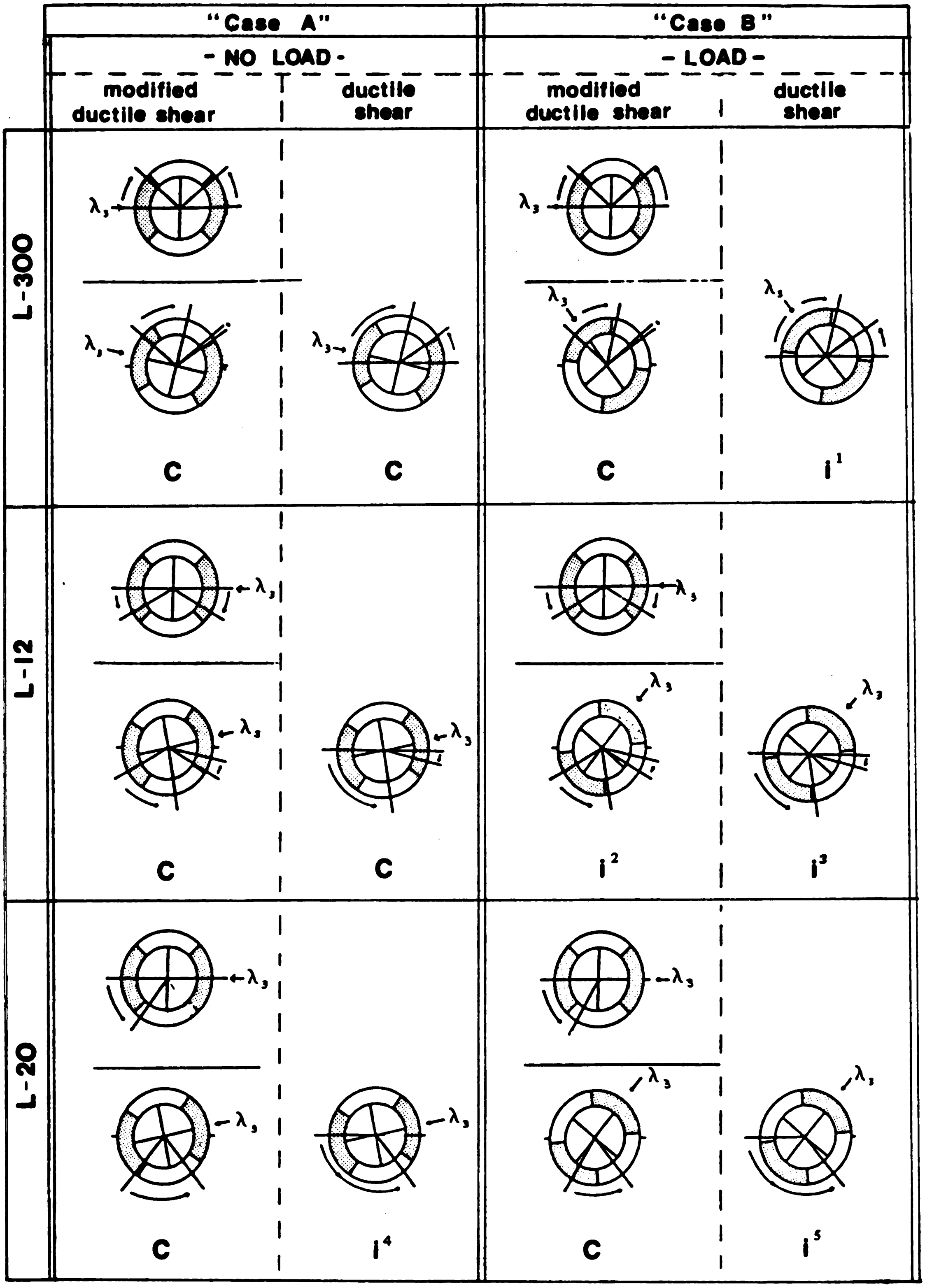
"Case A"
- NO LOAD -
modified ductile shear
ductile shear
"Case B"
- LOAD -
modified ductile shear
ductile shear
L-300
L-12
L-20
λ_3
C
C
C
i1
C
C
i2
i3
C
i4
C
i5

Figure 37

Appendix C that significant displacement is necessary in order to significantly increase load (e.g., the offset/ramp length ratio must be >.25 to accomplish an increase of 50% on a 30° fault). Small offset/ramp length ratios for the studied faults, coupled with the effect of any overlying roof material, support the evaluation of insignificant load.

For these reasons the "Case A" scenerio is proposed, in which the effect of load on the orientation of the incremental λ_3 is negligible and simple shear is assumed. Regardless of load assumptions, the modified shear model is most consistent with the observed structures while the ductile shear model is least consistent.

A detailed evaluation of the overthrusting and ductile shear models of deformation assuming a "Case A" scenerio of simple shear and insignificant load is presented for the Cove Creek and Chilhowee transects below.

Cove Creek (Location L300):

The removal of modification strains assuming modification by simple shear is attempted along location L300 and discussed in Appendix B. The resultant geometry of structures along L300 is consistent with both the ductile shearing of preexisting folds and the ductile shearing of oblique layering. The kinematics of the area are further constrained by evaluating the succession and nature of deformational structures.

MODIFIED DUCTILE SHEAR MODEL:

Fold "b" from the footwall of thrust B (Figure 9) is used in the kinematic analysis because of the excellent exposure and control. The incremental strain ellipse for initial folding by sub-horizontal layer parallel shortening is shown in Figure 38a. The predicted structures are upright folds with sub-vertical axial planar foliation parallel to the xy-plane of deformation. The structures observed within the unmodified folds at L300 are consistent with these predicted structures and include upright folds with both penetrative and spaced axial planar foliations. The open nature and the lack of observed extensional structures in unmodified F_1 folds suggest the limbs of such folds did not initially rotate beyond the compressional fields of the ellipse. The assumed limit of limb rotation of <45° (i.e., within the compression field) is consistent with the limb orientations and interlimb angles determined when fold "b" is unfolded (Appendix B).

The development of strain inhomogeneities during the late stages of this folding likely resulted in the formation of local shear zones and eventually thrust fault displacement. The incremental strain ellipse associated with the predicted superposed simple shear, as well as the observed structures are depicted in Figure 38b.

During modification the overturned left limb of the syncline continues its initial clockwise rotation and remains in the compressional strain field for a large

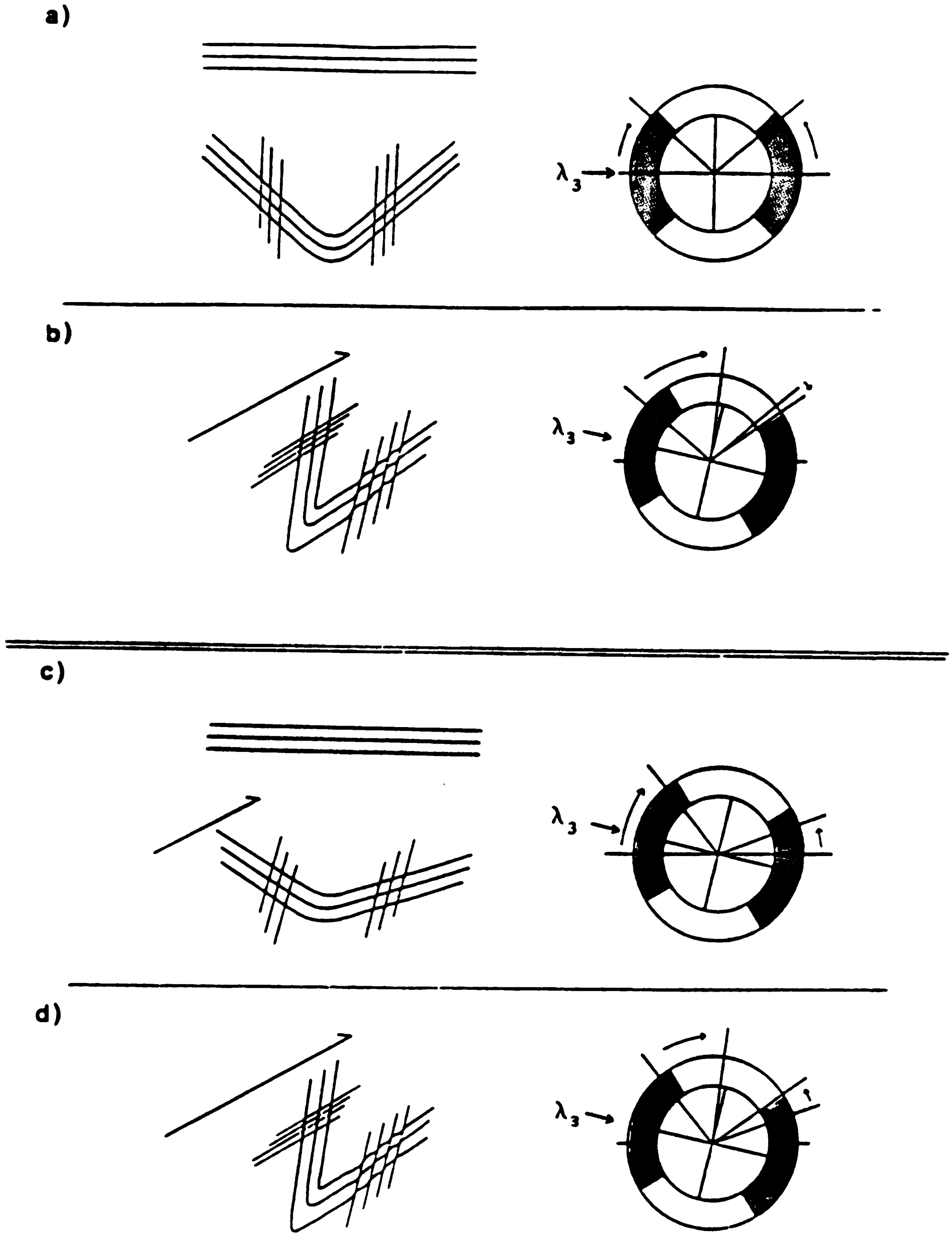

Figure 38. Evaluation of models for location L300:
a-b) Modified Ductile Shear Model depicting initial sub-horizontal shortening followed by overthrusting and superposed shear strain.
c-d) Ductile Shear Model depicting initiation and continued deformation by shear

duration of its rotation. The resulting compressional structures are expressed as a decrease in S_{1sp} spacing. The presence of shear planes nearly parallel to bedding indicate either the initiation of extensional strains along this limb or the large flexural shear strains expected by such a large amount of limb rotation. These slip planes deflect cleavage and bedding and eventually cut across the hinge in an apparent attempt to conserve space in the hinge region. Whether this slip is a response to flexural shear or extension remains undetermined.

Upon modification the shallow right limb of the syncline undergoes a reversal in rotation from counterclockwise to clockwise. Upon modification the limb also lies in a field of extensional strain rather one of compressional strain. Limb extension is accomplished by the reuse of S_{1sp} planes as mini normal faults and shear zones. As shown in the microfabric section, extension was accomplished by a process involving both oblique shortening and shear along these cleavage zones. The orientation of the cleavage planes within the superposed strain field make them favorably oriented as planes of shear.

In summary, the succession of structures of fold "b" at location L300 are consistent with a kinematic sequence involving sub-horizontal layer parallel shortening followed by the modification of existing folds by simple shear due to overthrusting.

DUCTILE SHEARING MODEL:

The formation of fold "b" by the initial simple shear of oblique layering alone is also considered. The orientation of the associated incremental strain ellipse during initial folding due to ductile shear is shown in Figure 38c,d. The succession of structures observed on each limb is consistent with the formation by ductile shearing. The overturned left limb records compression of the limb with minor evidence of a late extension. The shallow right limb clearly demonstrates a compressional stage followed by an extensional stage of deformation.

L300 Discussion:

While the kinematics derived from the observed structures are consistent with both models of deformation, the modified shear model is favored. The nature of cleavage offset suggests the superposition of strain following initial spaced cleavage formation. The presence of axial planar S_1 in upright unmodified folds in L300 is not easily resolved in the ductile shearing model since the predicted xy-plane is inclined at all stages of the deformation. While the proposed kinematics are not inconsistent with ductile shearing, the transition in fold styles form upright to overturned and the geometrical considerations of cleavage formation are. Consequently, the modified ductile shear model is favored.

Chilhowee (Location L12)

MODIFIED DUCTILE SHEAR MODEL:

Initial sub-horizontal layer-parallel shortening is depicted in Figure 39a. Initial folding, the development of S_{1p}, and the initiation of S_{1sp} record the limbs rotation within the compressive strain fields. Assuming initial upright folds and axial planar cleavage prior to modification, the observed cleavage-bedding dihedral angles of approximately 40° restrict the dip of unmodified fold limbs to $\leq$40°. This suggests the limbs remained within the compressive strain fields during initial folding. During initial folding the right limb undergoes a clockwise rotation and the left limb a counterclockwise rotation.

The orientation of the predicted incremental strain ellipse associated with the superposition of simple shear during fold modification is depicted in Figure 39b. Upon modification, the shallow dipping right limb of the anticline changes from a clockwise to a counterclockwise rotation. In doing so, the limb remains within the compressional strain field. This is expressed by the development of F_2' folds which gently fold the layering and cleavage into minor folds along the limb.

The structures of the overturned left limb of the anticline indicate a complex deformational sequence. Upon modification the limb continues its counterclockwise rotation from the compressional strain field into the extensional field.

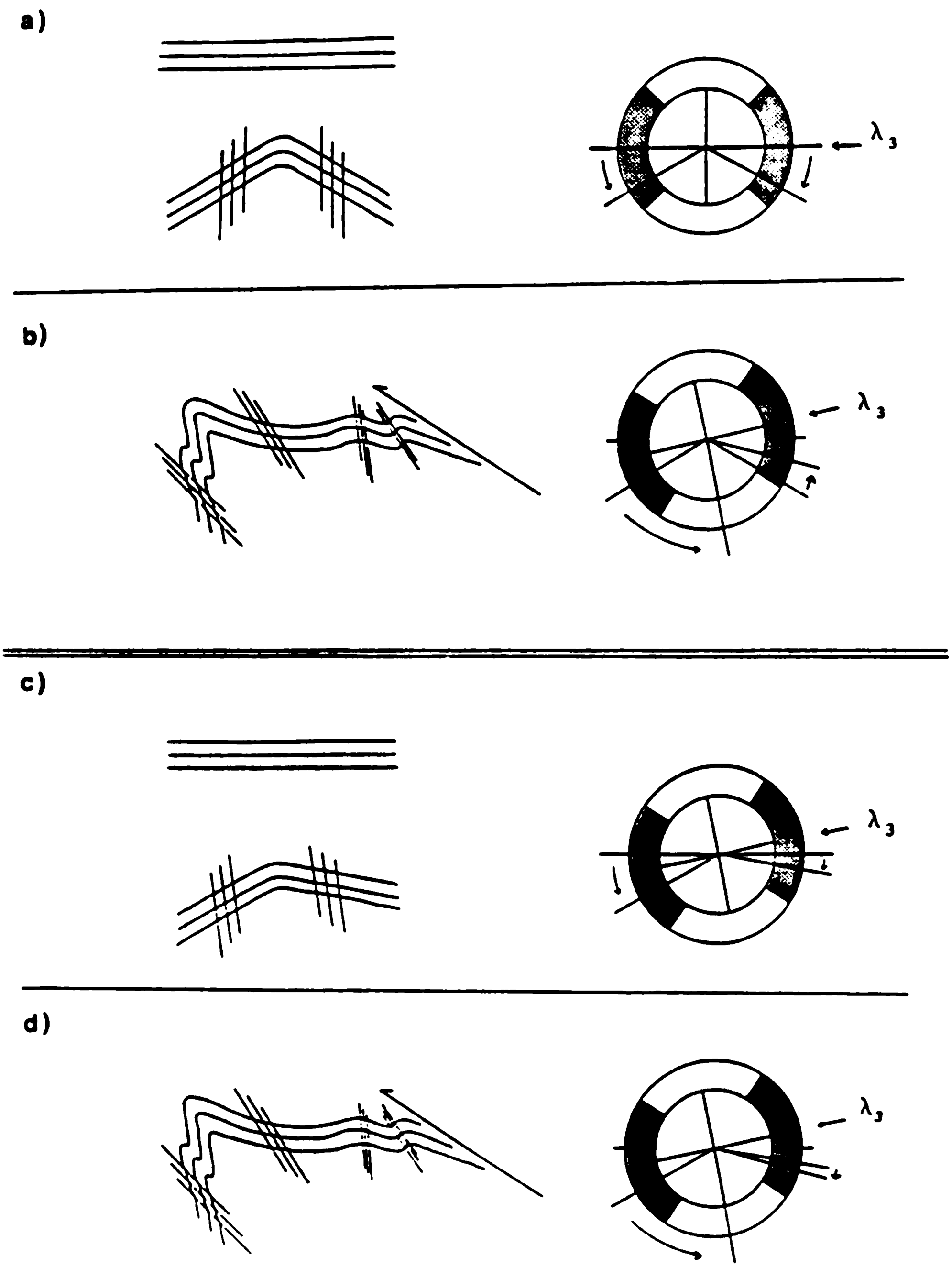

Figure 39. Evaluation of models for location L12: a-b) Modified Ductile Shear Model depicting initial sub-horizontal shortening followed by overthrusting and superposed shear strain. c-d) Ductile Shear Model depicting initiation and continued deformation by shear.

Structures on this limb are consistent with initial shortening followed by extension as evident by the following relationships. S_{1sp} planes are initially the sites of shortening and dissolution and eventually become the sites of zonal shear and discrete slip resulting in the extension of the limb. Discrete S_{1sp} planes contain slickensides which indicate offset directions consistent with bedding offsets along these mini normal-faults. Ductile and brittle shear fabrics within S_{1sp} zones are also consistent with a superposed oblique shortening resulting in limb extension. The initial position of S_{1sp} planes within the modification strain ellipse is such that these planes would be favorably oriented to serve as planes of shear as modification progresses.

In summary, the observed structures and successions are consistent with the modification of preexisting folds by simple shear due to overthrusting.

DUCTILE SHEARING MODEL:

Initial deformation of unfolded layering by oblique shearing is depicted in Figure 39c. The progressive rotation of the fold limbs within this strain field is depicted in Figure 39d. The rotation of the overturned limb from a compressional to extensional field is consistent with the observed structures. The compressional structures observed on the shallow limb can also be accounted for since this limb remains in the compressional field of deformation. The observed kinematics of location L12 are consistent with the ductile shearing model.

Chilhowee (Location L20):

MODIFIED DUCTILE SHEAR MODEL:

The overturned beds along L20 (Figure 23) represent the overturned limb of a second order F_2 fold on the steeply dipping NW limb of the major anticline. The succession of mesoscopic structures are useful in that they record a sequence of strains recorded on this limb. The nearest observed thrust lies ~150m to the SE and dips 32° towards the SE. The thrust is inferred to be an important local structure controlling the orientation of the superposed strain field.

The structures on this overturned limb appear to record a succession of strains initiating with a first stage layer-parallel compression and first stage extension, followed by a superposed stage of compression and possibly extension once again. Initial layer-parallel shortening is recorded by the presence of strong S_{1p} fabrics which are at a high angle to bedding. Refraction of cleavage supports the inference of limb rotation and folding during this initial shortening. This shortening was then followed by extension and the boudinage of carbonate units. Boudin formation is post-S_1 and fold-related as evident by the deflection of cleavage into boudin necks and the parallelism of boudin axes and the determined fold axis. These structures record the rotation of this limb from the compressional strain field into the extensional field as shown in Figure 40a.

Subsequent shortening of this limb is recorded by the folding and contractional faulting of these boudined units. This switch in strain fields back to compression can only occur with a change in the local strain field. These changes are consistent with the rotation and superposition of simple shear on the existing fold limb (see Figure 40b). Continued rotation of this limb would result in its rotation into the extensional field. The presence of S* extension crenulations within slaty units also record a post-S_1 extensional stage, but the lack of crosscutting relationships prevents the determination of their relative timing other than post-S_1.

In summary, the observed structures record limb compression, followed by limb extension, followed by a second limb compression. This succession of structural development is consistent with the modification of preexisting folds by simple shear due to overthrusting and the modified ductile shear model.

DUCTILE SHEARING MODEL:

The ductile shearing model cannot account for the succession of structures observed. Once the limb rotates from the compressional strain field to the extensional field it cannot, in this model, rotate back into a compressional

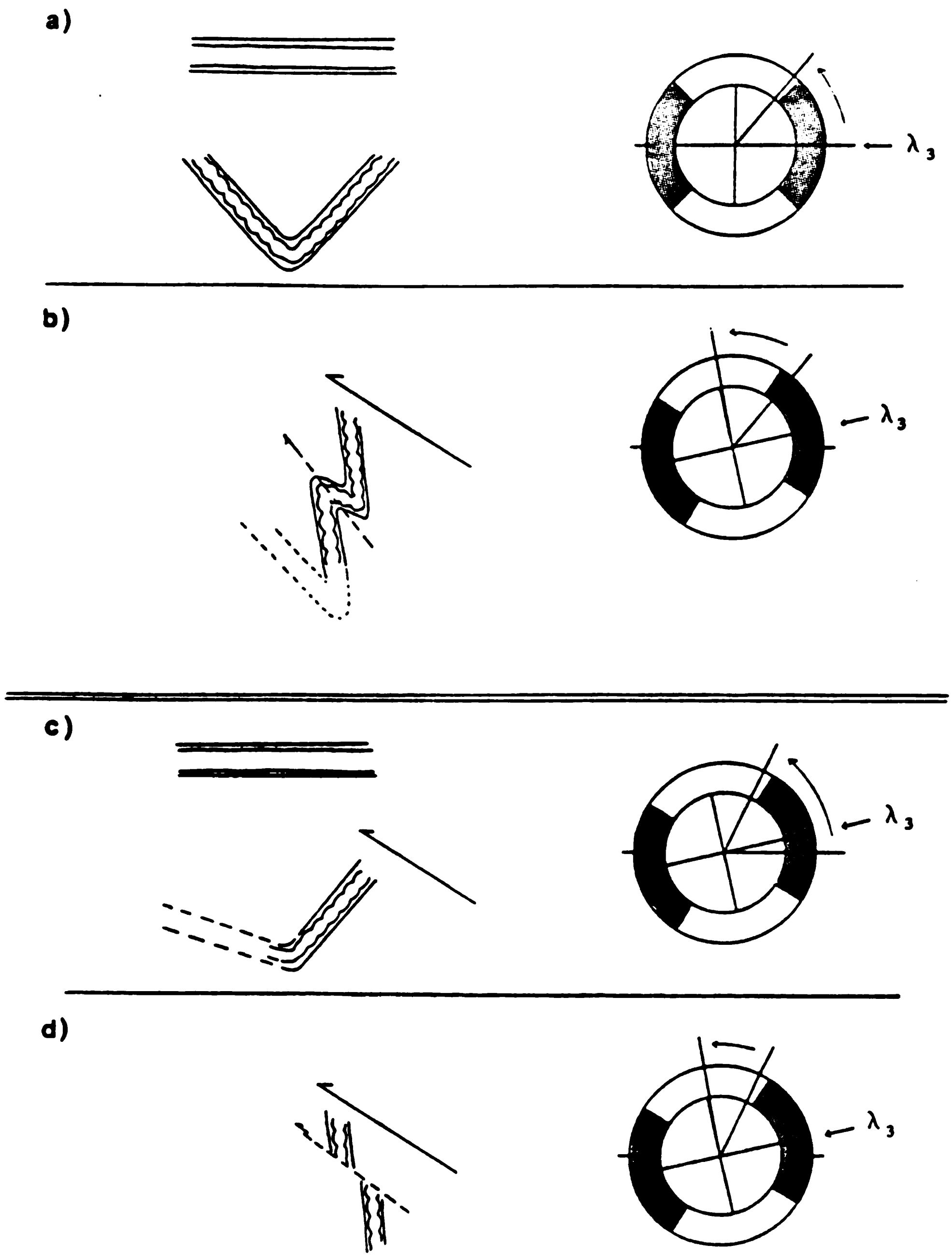

Figure 40. Evaluation of models for location L20:
a-b) Modified Ductile Shear Model depicting initial sub-horizontal shortening followed by overthrusting and superposed shear strain.
c-d) Ductile Shear Model depicting initiation and continued deformation by shear, (note: second stage compression not predicted).

field (see Figure 40c,d). The model cannot account for the superposed compressional strain recorded by the folding and faulting of the boudined units. The predicted kinematics are inconsistent with the observed succession of structures.

Chilhowee (Location L10):

The lack of local thrust or shear planes precludes the inference of the local strain field related to a modification event. In general, the folds present at location L10 appear to represent highly flattened or sheared F_1 folds. The succession of the structures on the main fold shown in Figure 17 indicate the rotation of both limbs from initial compressional fields to extensional fields. Large amounts of extension are recorded by the formation of both microscopic and mesoscopic extension crenulations. These extension crenulations may but do not necessarily indicate a deformation involving shear and may be explained by extreme flattening of the fold. Any attempt to determine possible kinematics for this fold would be highly speculative and is not attempted. The observed structures appear to be consistent with deformation by either model.

Summary of F_2 Kinematics:

The observed meso-and microscopic structures are consistent with the modification of preexisting folds. The derived kinematics are most consistent with the modification of preexisting folds by a component of simple shear due to overthrusting. The derived kinematics in all but one location (L20) are also consistent with formation by ductile shearing. Because of the inability of the ductile shearing model to account for the observed structures at L20, the model is rejected at that locality. It is suggested that on the mesoscopic scale the overthrust model better describes the observed deformation within the Miller Cove Sheet than does the ductile shearing model.

Discussion:

It is conceivable that on the macroscopic scale the ductile shearing model may better describe the observed deformation, while on the mesoscopic scale the modified ductile shear model can better account for the observed deformation. The formation of macroscopic folds, such as the anticline which fills the MCS, may have formed by a process of regional ductile shear. The formation of higher order (i.e., mesoscopic) folds on this anticline may have accompanied this initial folding event. The subsequent development of imbricates or contractional faults along the limbs of this macroscopic fold may have resulted in the local modification of these early-formed mesoscopic folds.

The late faults, in addition to cutting through existing structures, modify those structures in the footwall by a process involving simple shear. Ductile shear may have operated on the macroscopic scale, while a modified ductile shear acted as a secondary deformational process on preexisting structures on the mesoscopic scale.

CONCLUSIONS:

DISCUSSION:

Mesoscopic structures within the Miller Cove Thrust sheet of the Southern Appalachian Blue Ridge Province record the effects of superposed simple shear upon preexisting folds as a result of overthrusting. The succession of structures record a complex progressive deformation involving both folding and thrusting which is inconsistent with formation by a rigid ramp-flat thrust system.

Consistently observed throughout the study area is evidence for a progressive or superposed deformation. These include the modification of folds from F_1 to F_2 structures, and the superposition of incremental strains. Incremental strains are recorded by the complex succession of extensional and compressional structures and the superposition of shear across spaced cleavage.

The geometric interrelations of structures within the Miller Cove sheet suggest a progressive deformation that may be related to the changing strain fields accompanying the development of thrust or shear zones during an initial folding event. Refolding is proposed to be the result of a superposed non-coaxial strain (i.e., simple shear) in which the maximum and minimum strain axes rotate about the intermediate axis as the deformation progresses from layer-parallel shortening to simple shear. Modification in the form of footwall deformation is then a function of simple shear which decreases with distance from the thrust.

MODEL EVALUATION:

The "Rigid-Ramping Model" is rejected based on the results of other studies within the area and the inability of the model to predict the complex Taconic deformation reported in this study. The observed structures are inconsistent with those predicted by the rigid ramping model.

The derived kinematics are also, to some degree, inconsistent with the "Ductile Shearing Model". The ductile shearing model is rejected as the mechanism of deformation operating on the mesoscopic scale. This model may be more applicable to the macroscopic deformation of the area. Unfortunately, the evaluation of the macroscopic deformation is restricted by the superposed Alleghenian deformation which obscures regional Taconic relationships.

Observed structural successions are consistent with the "Modified Ductile Shear Model" involving the modification of footwall structures by the superposition of a simple shear or transpressive deformation due to overthrusting.
A transition exists from upright/open to inclined or overturned/close folds as a function of distance from local thrusts.

A variation in cleavage style exists across modified folds which reflects the superposed strain. Observed microfabrics are interpreted to record the reuse of preexisting spaced cleavage during fold modification. Superposed limb extension was accomplished by the reuse of spaced cleavage as planes of shear to facilitate limb extension. Superposed or progressive limb shortening was accomplished by the decrease in cleavage spacing (i.e., an increase in the density of dissolution planes). While the results do not provide a unique solution they are consistent with the modified ductile shear model of deformation.

CONCLUSIONS:

In summary, the following conclusions about the study area are drawn:

1) The polyphase deformation recorded within rocks of the Miller Cove sheet are consistent with their formation by the modification of preexisting folds by simple shear due to local overthrusting. A transition from <u>unmodified</u> upright/open F_1 folds with axial planar cleavage to <u>modified</u> overturned/close F_2 folds with fanned and modified spaced cleavage is present along the Cove Creek transect (location L300).

2) The variability of spaced cleavage is proposed to be the result of fold modification.

   (a) The superposed extension of fold limbs was accomplished by slip and shear along cleavage. The superposed shortening was accomplished by a decrease in cleavage spacing.

   (b) Brittle slip or shear along spaced cleavage is evident by the presence of shear microfabrics such as micro-faulted grains and micro pull-apart structures. Ductile shear zones along cleavage are evident by the presence of deformed quartz grain and calcite porphyroblast fabric.

(c) The nature of bedding offsets across spaced cleavage is a function of limb orientation with respect to the superposed strain field describing the modification (i.e., simple shear).

3) The NNE trend of F_2 fold axes observed along the Chilhowee transect are proposed to be a result of the rotation of F_1 fold axes from their initial ENE positions towards the direction of thrust movement due to simple shear. These rotations are assumed to be associated with the higher strains common to the base of thrust sheets.

General conclusions which might also be drawn include:

1) The modification of preexisting structures by simple shear due to overthrusting (i.e., footwall deformation) can be an important component of thrust or nappe sheet deformation. Determination of these heterogeneous strains (i.e., increasing simple shear near thrusts) by the construction of simple shear gradients might aid in any attempt to unfold a section and should lead to more properly balanced sections.

2) The offset of layering across crenulation cleavage can in some cases, occur by a process involving large components of shear in contrast to the conclusions of Gray (1979).

APPENDIX A

GRAIN ASPECT RATIO MEASUREMENTS:

Grain aspect ratios were determined using the general R_f/Phi techniques outlined by Lisle (1984). Ellipticities of the markers were determined and plotted with respect to a given reference line (cleavage where possible).

Microphotographs or photo-mosaics were prepared from oriented thin sections. Axial ratios were determined by the measurement of axial lengths of the sub-elliptical markers or estimation of axial lengths of the equivalent area ellipse for irregular shaped markers as used in Dunnet (1969). The axis coordinates were digitized with respect to a given reference line on the plane. Axial ratios and orientations were calculated, using a modified version of the computer program "RFPHI", and R_f/Phi plots generated. Data are summarized in Table A2.

The following parameters were calculated using the given equations (from Lisle, 1984):

Axial Ratio: R_f =(long axis length) /(short axis length)

Harmonic Mean:

$$R_h = N / (R_{f1}^{-1} + R_{f2}^{-1} + \ldots + R_{fN}^{-1})$$

EQN A-1

where N = number of markers in data group

Vector Mean:

$$PHI = \tfrac{1}{2} \arctan \{[\Sigma \sin 2(Phi)] / [\Sigma \cos 2(Phi)]\}$$ EQN A-2

Fluctuation: EQN A-3

$$F = \mathrm{Tan}^{-1} \left\{ \frac{[R_s(R_i - 1)]}{[(R_i^2 R_s^2 - 1)(R_s^2 - R_i^2)]^{1/2}} \right\}$$

where: R_i and R_s are initial and strained axial ratios determined by graphical solution as outlined in Lisle (1984).

Symmetry:

$$I_{sym} = 1 - [(n_a - n_b) - (n_c - n_d)] / N$$ EQN A-4

where : $n_{a,b,c,d}$ are the number of markers in each quadrant defined by R_h and PHI. Symmetry is then based on comparisons to the critical values given in Table A1.

TABLE A1. Critical values of I_{sym} used in the symmetry test. The values shown are the 5% (10%) points of the I_{sym} distribution.

Rs	Sample Size N: 20	35	60	100	200
1.5	0.3 (0.4)	0.51 (0.63)	0.60 (0.67)	0.74 (0.78)	0.82 (0.85)
2.0	0.5 (0.5)	0.63 (0.63)	0.73 (0.77)	0.80 (0.82)	0.86 (0.88)
3.0	0.5 (0.6)	0.63 (0.63)	0.73 (0.77)	0.80 (0.82)	0.87 (0.88)
5.0	0.5 (0.6)	0.63 (0.63)	0.73 (0.77)	0.82 (0.82)	0.87 (0.88)
10.0	0.6 (0.6)	0.63 (0.63)	0.73 (0.77)	0.82 (0.84)	0.87 (0.89)

TABLE A2. Grain aspect ratio parameters for noted samples.

Sample #	R_m (mean)	σ (w/ respect to S_1)	F	I_{sym}
L300-3QTZ				
A (xz)	1.7	7°	132°	.95
B "	1.8	11°	105°	.79
C "	1.7	-2°	161°	.82
L300-1QZT				
A (xz)	1.7	14°	115°	.82
B "	1.8	-.6°	151°	.78
C "	1.6	8°	124°	.96
L300-3POR				
A (xz)	1.4	-37°	135°	.81
B "	1.9	-18°	40°	.83
C "	1.4	-40°	140°	.80
XY	1.3	-26°	177°	.75
ZY	1.6	-1°	92°	.96
L300-1POR				
A (xz)	1.6	29°	97°	.94
B "	1.6	11°	82°	.92
C "	1.4	17°	165°	.67
L12-6QTZ				
A (xz)	1.7	-18°	127°	.94
B "	2.4	-8°	65°	.72
C "	1.7	-9°	160°	.98
L12-12QTZ				
A (xz)	1.5	-19°	160°	.96
B "	1.7	6°	132°	.84

ERROR ANALYSIS (Aspect Ratio Measurements):

Strain values were determined, and limited in consideration, to the reference frame of the microphotograph and the values evaluated relative to the trace of cleavage on that plane. Since the datum (cleavage trace) is present on the photographs, the evaluation of errors can be limited to the accuracy in measuring axis lengths and orientations relative to cleavage. The estimated maximum errors are given below:

A. Orientation of sample in field $\pm 2°$

B. Transfer of orientation to sample

goniometer measurements $\pm ½°$

stereonet determinations $\pm 1°$

(NOTE: Errors A and B do not contribute to measurements limited in scope to the reference frame of the microphotos since datum present on photos.)

- -

C. Orientation of cleavage trace on microphotograph $\pm 2°$

D. Orientation of axis orientation $\pm 2°$

E. Determination of axis length ± 0.05 units

Total estimated error in determination of λ_1 orientation $\pm 4°$

APPENDIX B

REMOVAL OF SHEAR STRAINS:

Sanderson (1979) and Lloyd & Whalley (1986) have shown that the transition in fold style from upright/open to inclined/close is indicative of fold modification by simple shear. The transition of upright/open to inclined/close folds, as well as the succession of structures along profile L300 on the Cove Creek transect are consistent with fold modification by simple shear. Sanderson (1979) suggests that a positive correlation between decreasing axial plane dips and interlimb angles is also indicative of a simple shear modification. A positive correlation between APD and ILA exists along L300 as shown in Figure B1.

The kinematic question addressed in this appendix is whether these folds formed by a continuous proccess of simple shear (i.e., ductile shear model) or if they formed by a combination of layer-parallel shortening followed by the superposition of simple shear (i.e., modified ductile shear model). It is here demonstrated that both models can account for the observed deformation with predicted bulk simple shear strains of $y = \tilde{}2.0$ predicted.

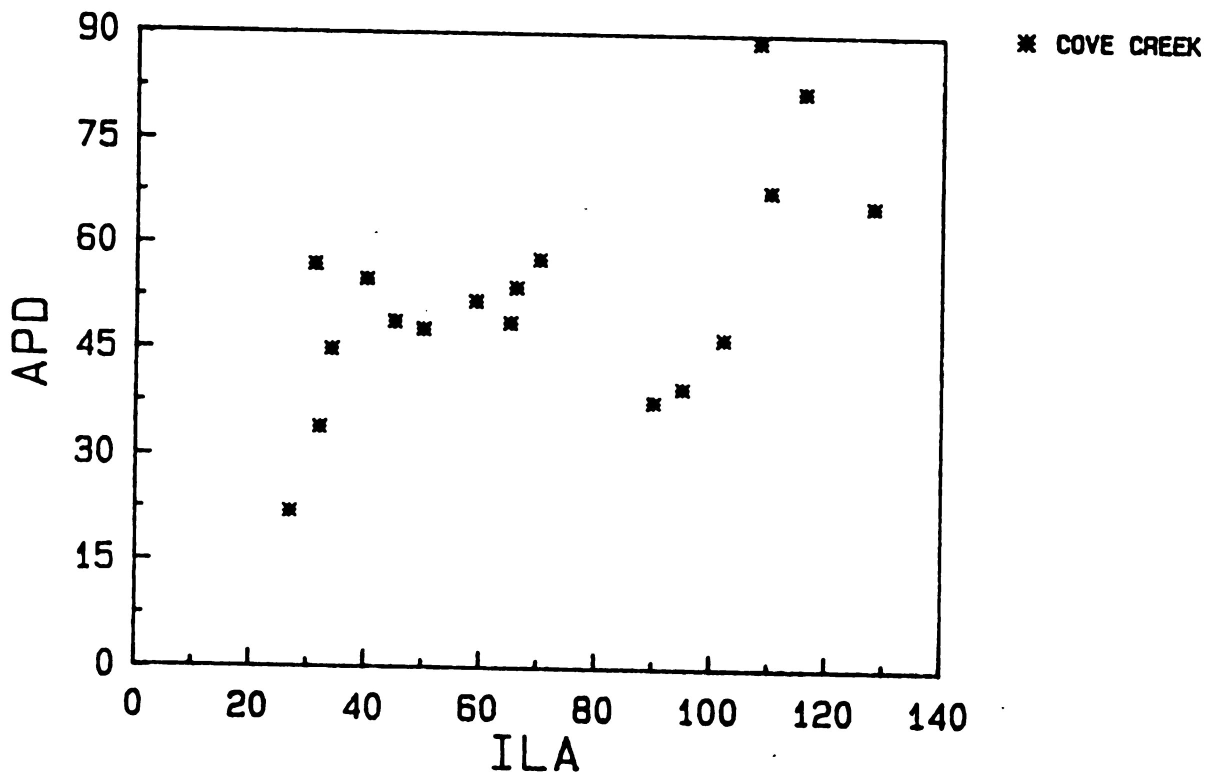

Figure B1. Scatter plot of Axial Plane Dip vs Interlimb Angle for mesoscopic folds along profile L300, Cove Creek.

This appendix is divided into two sections. The first concerns the determination of a shear gradient for location L300 and the removal of those shear strains to produce a premodification profile. In the second section, the premodification profile is used to determine the average values of bulk shear strain necessary to account for the observed shortening of the layering across the entire profile for each model.

A) SHEAR STRAIN GRADIENT & PREMODIFICATION PROFILE:

Shear strains were determined assuming that both the layering and axial planes acted as passive material planes during the simple shear deformation. The rotation of lines or planes within a shear zone are governed by the following equation:

$$y = \cot \theta' - \cot \theta \qquad \text{EQN B-1}$$

where:

y = shear strain

θ' = deformed orientation of the line within shear zone

θ = initial orientation of line

The shear strain applied to a passive marker can be determined knowing its deformed orientation and its initial orientation. The deformed orientations of axial planes are easily determined from the profile (Figure B2) or calculated

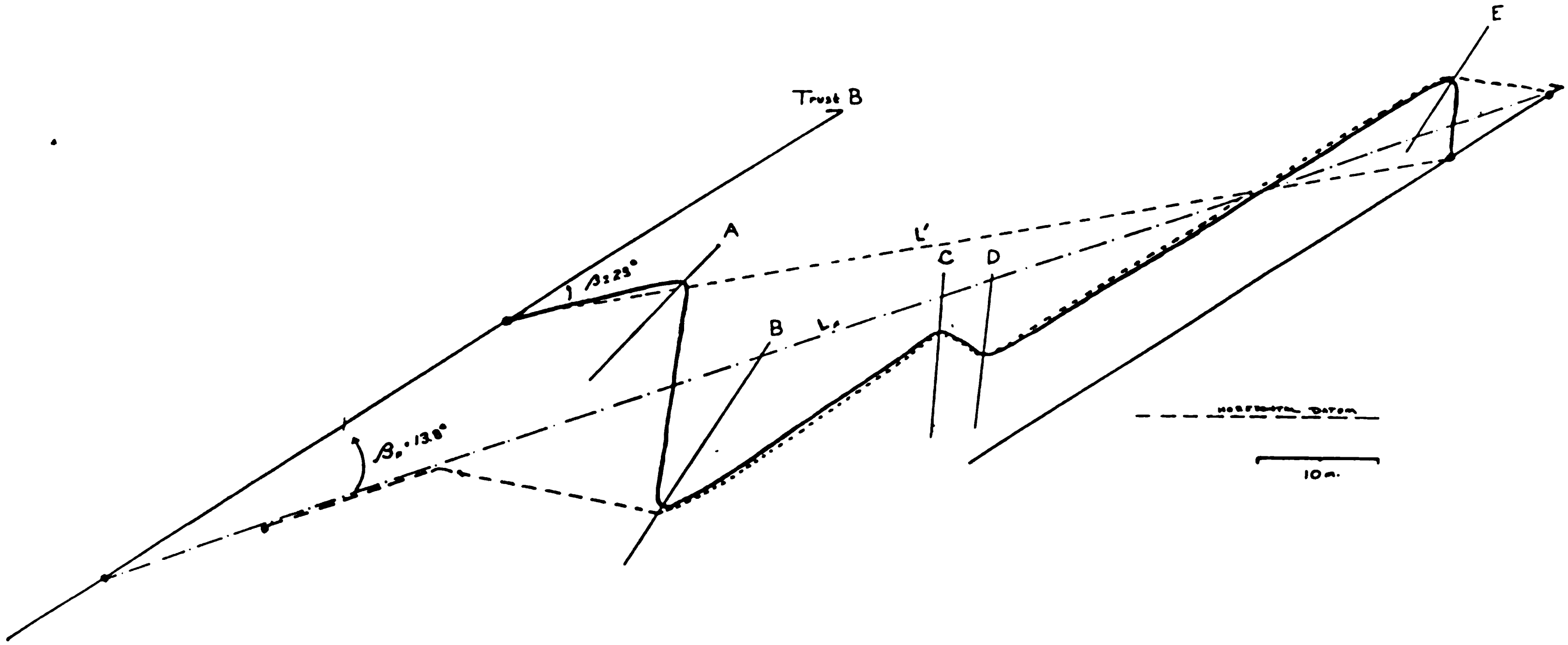

Figure B2. True structural profile of a marker bed in profile L300, Cove Creek. Pre- and post-modification limb positions depicted.

from orientation data. The initial orientations of the axial planes prior to modification are assumed to be vertical. This assumption is based on presence of near vertical axial planes in unmodified folds in the profile. A shear strain gradient (Figure B3) was calculated for the profile using the orientations of axial planes in the profile and EQN B-1 (see Figure B2 and Table B1).

This gradient was then used to determine the average shear strain which has effected each limb of the folds in the profile. These values were determined by locating the midpoint of each limb on the gradient curve and graphically solving for the associated shear strain. The initial orientations of the limbs were then solved for using EQN B-1, the deformed orientations of each limb, and the determined shear strain values. These shear strains were then removed by rotation of the limbs back to undeformed orientations and are depicted in the premodification profile in Figure B2.

The resultant premodification profile is characterized by open asymmetric folds, similar to kink or drag folds. The ILAs of these folds range between 121° to 149° and average ~135°. Because this method assumes that all shortening is taken up in the rotation of layering there is no change in the length of these limbs accounted for during unfolding. The space problem resulting from this assumption is demonstrated along the SE edge of the premodification profile, where the layering does not extend to the shear

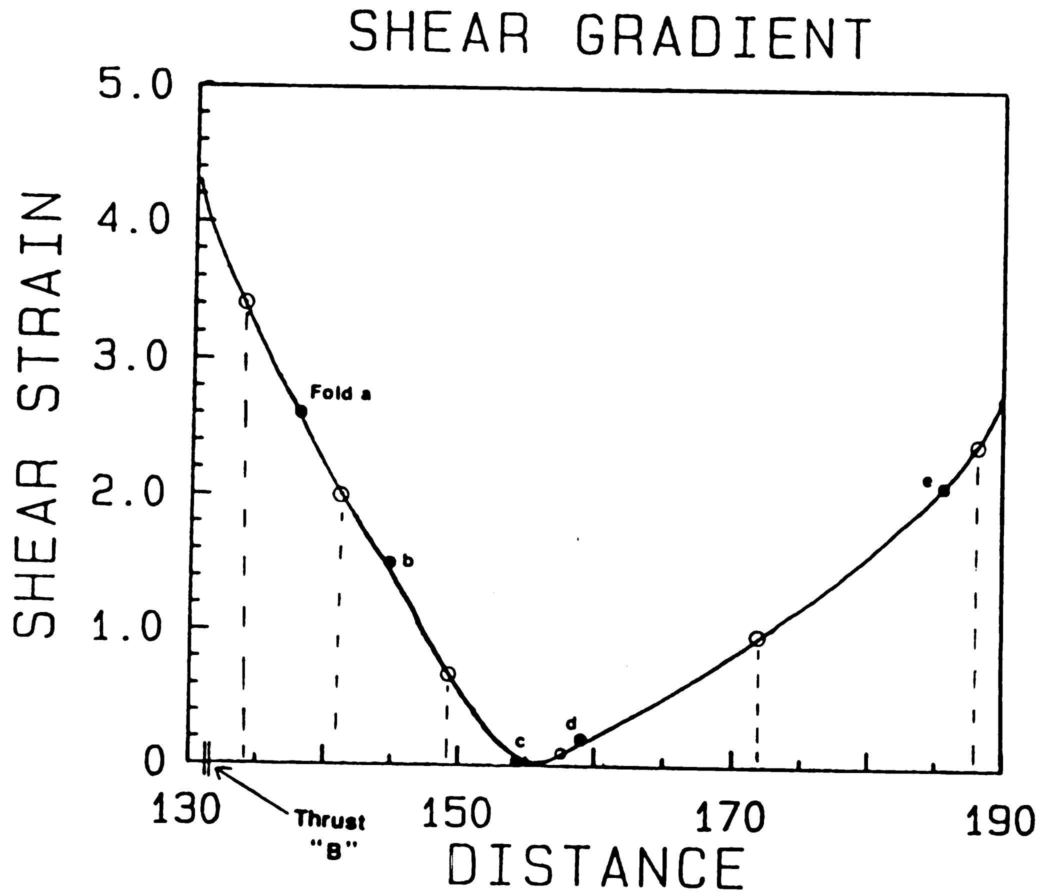

Figure B3. Shear strain gradient plot derived by assuming initially vertical axial planes (location L300).

TABLE B1. Calculated parameters for the determination and removal of shear strain along the Cove Creek L300 profile.

L300: Fold	APD: apd	β	β'	y	LIMB: β	β'	y	ILA'	ILAo
A	49	58	17	2.6	158	170	3.4	73	149
					50	139	2.0		
B	57	58	25	1.5	50	139	2.0	47	136
					3	3.2	0.7		
C	89	58	57	.03	3	3.2	0.7	117	121
					120	124	0.1		
D	82	58	50	0.2	120	124	0.1	119	123
					1	1.1	1.0		
E	52	58	20	2.1	1	1.1	1.0	49	143
					0	144	2.2		

<u>NOTE</u>:

Approximate thrust dips = ~32°
Therefore:

$$\beta = (\text{dip}°) - 32°$$

zone boundary. This suggests additional layer parallel shortening of the limbs took place during modification. This shortening is proposed to be reflected in the decrease in cleavage spacing on limbs undergoing superposed shortening during modification as noted in the text.

B) BULK SHEAR STRAIN ESTIMATES:

The rotation of the layering within the shear zone during modification can be used to determine the shear strain transmitted along the shear planes marked by the thrusts.

1. Modified ductile shear model:

The deformed orientation and deformed length of the layering can be measured off the profile. This was done using the projected intersection of layering and thrust planes as end points of the post-modification line. The undeformed orientation of the layering has been determined by the following method and calculations are summarized on p.149.

The shortening determined by the change in length of the premodification line (L_f) and the post-modification line (L') can be used to determine the initial orientation assuming simple shear deformation from:

$$e = [L' - L_f]/ L_f \qquad \text{EQN B-2}$$

$$\beta = \mathrm{Sin}^{-1}[(1+e)\mathrm{Sin}\ \beta']$$

and

$$\gamma = \cot\ \beta' - \cot \beta$$

The calculated angle is $\beta = 13.8°$ and resultant shear strain is $\gamma = -1.70$.

2. Ductile Shear Model:

Applying a similar method, the shear strains needed to form these final folds by the ductile shearing of undeformed oblique layering can also be calculated. The best estimate of initial length of the layering is the sum of the limb segments measured from the premodification profile constructed above. While early layer-parallel shortening cannot be determined, the lengths from the premodification profile will provide a best estimate. The initial orientation of layering, with respect to the shear zone, can be calculated from EQN B-1, B-2, and:

$$e = [L' - L_{uf}]/ L_{uf} \qquad \text{EQN B-3}$$

The calculated initial orientation of layering with respect to the shear zone is $\beta = 11.0°$, with an associated shear strain of $\gamma = -2.43$. Calculations are summarized on p.149.

CALCULATING BULK SHEAR STRAIN (from Figure B2 and Table B1):

From Profile: (lengths of layering)

$L' = 80.0m$ (final modified length)

$L_f = 130.0m$ (initial folded length)

$L_{uf} = 142.5m$ (initial unfolded length)

Incremental shortenings:

$e = (L' - L_f)/L_{uf} = -0.39$

$e = (L_f - L_{uf})/L_{uf} = -0.09$

$e = (L' - L_{uf})/L_{uf} = -0.44$

Angles:

where $\beta = [(1+e)\sin\beta_0]\sin^{-1}$

$\beta_{L'} = 23°$

$\beta_{Lof} = 13.8°$

$\beta_{Louf} = 11.0°$

AVERAGE BULK SHEAR STRAIN:

$\gamma_{L-Lof} = -1.97$ (MODIFIED DUCTILE SHEAR MODEL)

$\gamma_{L-Louf} = -2.43$ (DUCTILE SHEAR MODEL)

DISCUSSION:

The determined values of $y = 1.7$ and 2.4 as average or bulk shear strains are geologically reasonable for both models of deformation. These strain values are for the upright shallowly dipping limb of the macroscopic anticline of the Miller Cove sheet. Similar values ($y \leq 3.0$) are reported by Ramsey et al., (1983) for the upright limb of the Morcles nappe. Higher strain values ($y \geq 6.0$) are reported for the overturned limb near the base of the Morcles nappe and might be similarly expected near the base of the Miller Cove sheet. It is proposed these higher strains are in fact recorded by the rotation of folds axes (Figure 7) and tightness of folds (Figure 11) reported along the Chilhowee transect on the overturned limb of the Miller Cove anticline.

In summary, both the ductile shear and modified ductile shear models can account for the observed deformation on the upright limb of the macroscopic anticline assuming shear strain values of $y = \tilde{}2.0$. These strain values are geologically reasonable and consistent with values observed in other studies. For further discussion of the formation of asymmetric folds by various mechanisms, including pure and simple shear, the reader is referred to Gosh (1966).

APPENDIX C

ESTIMATING LOAD COMPONENT:

The estimate of increase in load on the footwall is calculated by determining the % increase in volume of a column of overthrusted material in the hangingwall for a given point on the fault surface. The % increase in load is a function of the distance which the hangingwall wedge is displaced up the fault plane. The following assumptions are made:

1) a homogeneous density for the column of material on the scale of wedge thickness), likewise for overburden (when considered);
2) fault dip $\beta \approx 30°$, (similar to observed values)

The **% Increase in Load (%IL)** is given by:

(NEW VOLUME OF COLUMN * INITIAL VOLUME) ÷ INITIAL VOLUME

If the radius of the column is assumed to be infinitely small then the change in volume is reduced to a change in length of the column and the problem simplified (see Figure C1 and below for equations):

$$\%IL = 100 * \{[(\pi R^2)(H') - (\pi R^2)(H)]/(\pi R^2)(H)\} \qquad \text{EQN C-1}$$

simplifying:

$$\%IL = 100 * [(\pi R^2)(H' - H)]/[(\pi R^2)(H)]$$

$$\%IL = 100 * (H' - H)/(H) \qquad \text{EQN C-2}$$

where:

$H = (\sin \beta)(X_L)$

$H' = (\sin \beta)(X_L + D)$

and:

X = point for which load calculated (midpoint on ramp of given length)

X_L = ½ ramp length

H = initial column height

H' = new column height

D = fault displacement

O = thickness (height) of overburden or roof material

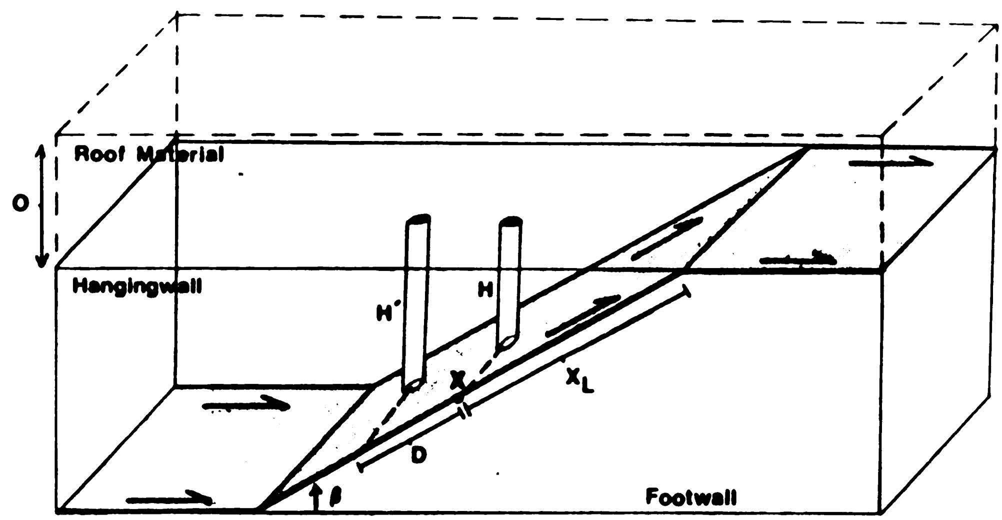

Figure C1. Parameters for determination of ramp load.

Table C1. Percent increase in load for varying amounts of offset along ramps of various lengths.

Fault Displacement	% Increase in Load (on variable ramp lengths)				
	2000m	1000m	100m	30m	100m + 500m roof
5m	0.3%	0.5%	5.0%	17.0%	0.5%
10m	0.5%	1.0%	10.0%	33.0%	0.9%
15m	0.8%	1.5%	15.0%	50.0%	1.4%
25m	1.3%	2.5%	25.0%	83.0%	2.3%
50m	2.5%	5.0%	50.0%	167%	4.5%

LIST OF REFERENCES

LIST OF REFERENCES

Borradaile, G.J., 1981, Particulate flow of rock and the formation of cleavage: Tectonophysics, v. 72, p.305-321.

Boyer, S.E., and Elliot, D., 1982, Thrust Systems: Bull. Am. Ass. Petrol. Geol., v. 66, p. 1196-1230.

Cambray, F.W., and Welland, M., 1985, Southward verging structures and coaxial refolding in the Benton Uplift, Ouachita Mountains: A result of southward directed thrusting: GSA Abstracts with Programs, v. 17, no. 7, p. 538.

Choukroune, P., Gapais, D., and Merle, O., 1987, Shear criteria and structural symmetry: Journal of Structural Geology, v. 9, no.5/6, p. 525-534.

Cook, F.A., Albaugh, D.S., Brown,L.d., Kaufman S., Oliver, J.E., and Hatcher, R.D., 1979, Thin-skinned tectonics in the crystalline southern Appalachians; COCORP seismic-reflection profiling of the Blue Ridge and Piedmont: Geology, v. 7, p.563-567.

Ellen, S.D., 1976, A theory of concentric, kink, and sinusoidal folding and of monoclinal flexuring of compressible, elastic multilayers; Part I, Introduction, The development of folds in layered chert of the Fransiscan assemblege near San Fransisco, California,Tectonophysics, v. 32, 1976, p. 295-320.

Gosh, S.K., 1966, Experimental tests of buckling folds in relation to strain ellipsoids in simple shear deformations: Tectonophysics, v. 3, p. 169-185.

Gray, D.R., 1979, Microstructure of crenulation cleavages; an indicator of cleavage origin: Am. Jour. Sci., v. 279, p. 97-128.

Hadley, J.B., and Nelson, A.E.. 1971, Geologic map of the Knoxville quadrangle, North Carolina, Tennessee, and South Carolina: U.S. Geol. Survey Map I-654, scale 1:250,00.

Harland, W.B., 1971, Tectonic transpression in Caledonian Spitsbergen, Geol. Mag., v. 108, p. 27-42.

Harris, L.D., 1970, Details of thin-skinned tectonics in parts of Valley and Ridge and Cumberland Plateau Provinces of the Southern Appalachians: in Fisher, G.W., Pettijohn, F.J., Reed, J.C., and Weaver, K., eds., Studies of Appalachian Geology: New York, NY, John Wiley and Sons, p. 161-173.

Hobbs, B.E., Means, W.D., and Williams, P.F., 1976, "An Outline of Structural Geology", 571 p., Wiley Int'l,NY.

Holcombe, R.J., 1973, Mesoscopic and microscopic analysis of deformation near Ducktown Tennessee: Stanford Univ., Palo Alto, CA, PhD. dissert., p. 225.

King, P.B., 1964, Geology of the central Great Smoky Mountains, Tennessee and North Carolina: U.S. Geol. Survey Prof. Paper 349-c, 148 p.

______, Neuman, R.B., and Hadley, J.B., 1968, Geology of the Great Smoky Mountains National Park, Tennessee and North Carolina, U.S. Geol. Survey Prof. Paper 587, 23 p.

Kish, S.A., Mohr, D.W., Merschat, C.E., and Wiener, L.S., 1975, Guide to the geology of the Blue Ridge south of the Great Smoky Mountains, North Carolina: North Carolina Div. Mineral Resources, Carolina Geol. Soc. Guidebook, 49 p.

Knipe, R.J., and White, S.H., 1979, Deformation in low grade shear zones in the Old Red Sandstone, S.W. Wales: Jour. Structural Geol., v. 1, no. 1, p. 53-66.

Lisle, R.J., 1984, Geological strain analysis; a manual for the Rf/Phi method, Permagon Press, New York, NY, 99 p.

Lister, G.S., and Snoke, A.W., 1984, S-C mylonites: Journal of Structural Geology, v. 6, no. 6, p. 617-638.

Livingston, J.E., 1977, Structural analysis of the Great Smoky thrust sheet along the Little Tennessee River, Tennessee: The Univ. of Tennessee, Knoxville, Dept. of Geol. Sci., M.S. thesis, 107 p.

Lloyd, G.E, and Whalley, J.S., 1986, The modification of chevron folds by simple shear: examples from north Cornwall and Devon, Jour. Structural Geol., v. 143, p. 89-94.

Milici, R.C., 1970, The Allegheny structural front and its regional tectonic implications: American Journal of Science, v. 268, p. 127-141.

Neuman, R.B. and Nelson, W.H., 1965, Geology of the western Great Smoky Mountains, Tennessee: U.S. Geol. Survey Prof. Paper 349-D, 81 p.

Platt, J.P., 1984, Secondary cleavages in ductile shear zones: Jour. Structural Geol., v. 6, no. 4, p. 439-442.

_______, and Vissers, R.L.M., 1980, Extensional structures in anisotropic rocks, Jour. Structural Geol., v. 2, no. 4, p. 397-410.

Powell, C. McA, 1979, A morphological classification of rock cleavage: Tectonophysics, v. 58, p. 21-34.

Ramberg, I.B., and Johnson, A.M., 1976, A theory of concentric, kink, and sinusoidal folding and of monoclinal flexuring of compressible, elastic multilayers; Part V. Asymmetric folding in the interbedded chert and shale of the Fransiscan complex, San Fransisco Bay area, California, Tectonophysics, v. 32, p. 295-320.

Ramsay, J.G., 1967, "Folding and Fracturing of Rocks", McGraw-Hill, New York, NY,

__________, Casey, M., and Kligfield, R., 1983, Role of shear in development of the Helvetic fold-thrust belt of Switzerland, Geology, v. 11, p. 439-442.

Rattey, P.R., and Sanderson, D.J., 1982, Patterns of folding within nappes and thrust sheet: Examples from the Variscan of southwest England; Tectonophysics, v. 88, p. 247-267.

Rich, J.L., 1934, Mechanics of low-angle overthrust faulting as illustrated by Cumberland thrust block, Virginia, Kentucky, and Tennessee: AAPG Bulletin v. 18, no. 12, p. 1584-1596.

Sanderson, D.J., 1979, The transition from upright to recumbant folding in the Varsican fold belt of southwest England: a model based on the kinematics of simple shear, Jour. Structural Geol., v. 1, no. 3, p. 171-180.

__________, 1973, The development of fold axes oblique to the regional trend, Tectonophysics, 16: p. 55-70.

__________, and Marchini, W.R.D., 1984, Transpression: Jour. Structural Geol., v. 6, no. 5, p. 449-458.

Segall, P., and Simpson, C., 1986, Nucleation of ductile shear zones on dilatant fractures: Geology, v. 14, p.56-59.

Simpson, C., and Schmid, S., 1983, An evaluation of criteria to deduce the sense od movement in sheared rocks: Geological Society of America Bulletin, v. 94, p. 1281-1288.

Sorby, H.C., 1880, On the structure and origin of noncalcareous rocks: Geologic Society of London Journal, v. 36, p. 46-92.

Williams, G.D., 1978, Rotation of contemporary folds into the X direction during overthrust processes in Laksefjord, Finnmark, Tectonophysics, 48: p. 29-40.

Williams, P.F., 1972, The development of metamorphic layering and cleavage in low grade metamorphic rocks at Bermagui, Australia: American Journal of Science, v. 272, p. 1-47.

Witherspoon, W., 1981, Structure of the Blue Ridge Thrust Front, Tennessee, Southern Appalachians: Univ. of Tennessee, Dept. of Geol. Sciences, PhD. dissert., 165 p.

Wojtal, S.F., 1983, Finite deformation in thrust sheets and their material properties: Johns Hopkins University, Dept. of Geological Sciences, PhD. dissert., 313 p.

Wright, T.O. and Platt, L.B., 1982, Pressure dissolution and cleavage in the Martinsburg shale: Am. J. Sci., 282, p. 122-135.